

Final report of the BAYREB project

Bayesian characterisation of buildings for optimal energy retrofit decisions

Simon Rouchier, Ph.D.



Projet financé par l'Agence Nationale de la Recherche
Plan d'action 2015 – Défi 6 – CES 22
Réf. ANR-15-CE22-0003



[HTTPS://LOCIE.GITHUB.IO/BAYREB/](https://locie.github.io/bayreb/)

June 2020

Contents

1	State of the art of building energy performance assessment	5
1.1	Why assessing the energy performance	5
1.2	Assessing the performance with in-situ measurements	7
1.2.1	Characterisation of unoccupied buildings	9
1.2.2	Characterisation of occupied buildings	12
1.3	The BAYREB project	16
1.3.1	Objective: characterisation before refurbishment	16
1.3.2	Statistical learning and inverse problems in building physics	16
1.3.3	Layout of this report	17
2	Calibration of heat transfer models and Bayesian inference	19
2.1	The objectives of thermal model calibration	19
2.2	Model calibration formulation and workflow	21
2.3	Modelling	24
2.3.1	Linear regression	24
2.3.2	State-space models	25
2.3.3	Gaussian Processes and Latent Force Models	28
2.3.4	Checking for structural identifiability	29
2.4	Calibration and inference	30
2.4.1	Ordinary least square estimation for linear regression	31
2.4.2	Maximum likelihood estimation	31
2.4.3	Bayesian inference	32
2.5	Validation and diagnosis	36
2.5.1	Parameter confidence regions	37
2.5.2	Residual analysis	39
2.5.3	Cross-validation	40

3	Testing the limits of building energy performance assessment with numerical benchmarking	43
3.1	Numerical model assessment methodology for physical interpretability	43
3.1.1	A numerical assessment framework for physical interpretability	44
3.1.2	Model assessment and comparison : a quantitative indicator	46
3.2	Repeatability of parameter estimation in variable weather conditions	49
3.2.1	Weather conditions influence: state of the art	49
3.2.2	The reference model undergoes variable weather conditions	50
3.2.3	Decrease in variability of R_{eq} estimation with experiment duration	55
3.2.4	Influential weather variables on an R_{eq} estimation	56
3.3	Decomposition of heat losses in a building	60
3.3.1	Model assessment framework for heat transfer decomposition	60
3.3.2	Estimation of the heat losses through ventilation	69
4	Practical applications	75
4.1	Energy signature: performance assessment with little information	75
4.1.1	The model	76
4.1.2	The data: commercial buildings	77
4.1.3	Model definition and training	79
4.1.4	Further questions	80
4.2	Linear regression: identifying what influences the energy balance	82
4.2.1	The data: ORNL test house	83
4.2.2	The model	86
4.2.3	Training	86
4.3	Stochastic state-space models: dynamic parameter estimation	91
4.3.1	Questioning and case study	91
4.3.2	Results and discussion	95
4.3.3	Summary	101
4.4	Latent force models: performance prediction of occupied buildings	101
4.4.1	Case study: twin houses	102
4.4.2	Performance assessment despite unmeasured influences	103
4.5	Real time parameter estimation with Sequential Monte Carlo	104
4.5.1	Case study: Round Robin Test Box	105
4.5.2	The SMC algorithm	108
4.5.3	Results	110
4.6	Separating transmission and air infiltration heat losses	110
4.6.1	Some theory on ventilation and heat loss	112
4.6.2	Case study: Gainsborough house	116
4.6.3	Using wind data to separate HTR from H_{inf}	116
4.6.4	Using CO ₂ data to estimate occupancy and air change rates	118
5	Summary and prospects of the project	123
5.1	Summary of the BAYREB project	123
5.2	Prospects	125
	Bibliography	137

1. Building energy performance assessment

1.1 Why assessing the energy performance

It is commonly known that the share of new buildings in the overall construction sector is very low. Most buildings are several decades old and often have poor energy performance, especially compared to recent standards for new constructions. The largest potential for energy savings in the building sector therefore lies in the renovation of the existing building stock. This was one of the motivations behind the second axis of the 6th societal challenge of the ANR call for projects: “du bâtiment au cadre de vie durable” (towards a sustainable built environment).

The renovation process of individual or collective buildings is generally solely based on their initial yearly energy consumption, and standard solutions are applied without any guarantee of performance. A condition for a cost-effective refurbishment, adapted to each specific building, is to perform detailed diagnostics of its performance prior to picking solutions: for instance, to estimate which proportion of the heat losses are caused by air leakage, by the envelope, or by a dysfunction of the heating systems. The first option to achieve such a detailed audit is to use an excessive amount of sensors, surveys and in-situ measurements, followed by lengthy interpretation of results in order to point the weaknesses of the building regarding energy efficiency. The second option is to implement inverse techniques, which are able to automatically learn from the data in order to construct a realistic representation of the characteristics of a building. The centre of the BAYREB project is the application of Bayesian inference as an inverse method for the energy audit of existing buildings.



In this document, the term of **diagnostics** essentially denotes the Energy Performance Diagnostics (DPE), which is an estimation of consumption and heat loss based on a regulatory calculation. The term of **characterisation** is then used to depict an estimation based on in-situ measurements, through model **calibration**. The term performance **assessment** here encompasses these two concepts of diagnosis and characterization. This section first describes the practice of diagnosis in France with a brief presentation of the DPE. Then, Sec. 1.2 deals with the research work that began in the 1980s and continues today to propose the energy characterisation of the building on the basis of static measurements (energy signature and co-heating methods) or dynamic measurements (QUB and ISABELE methods).

The European Energy Performance of Buildings Directive (EPBD) of 2002 introduced the first common methodology for calculating the integrated energy performance of buildings. In France, this led to the introduction of the Energy Performance Diagnosis (DPE), which has been mandatory since November 1, 2006 for all sales or rentals of new or existing properties.

The DPE describes the building or dwelling (surface area, orientation, walls, windows, materials, etc.), as well as its heating, domestic hot water production, cooling and ventilation equipment. It indicates, depending on the case, either the energy actually consumed (based on invoices, for individual dwellings built before 1948, collective and offices), or the estimated energy consumption for a standardised use of the building (3CL calculation method for individual dwellings built after 1948).

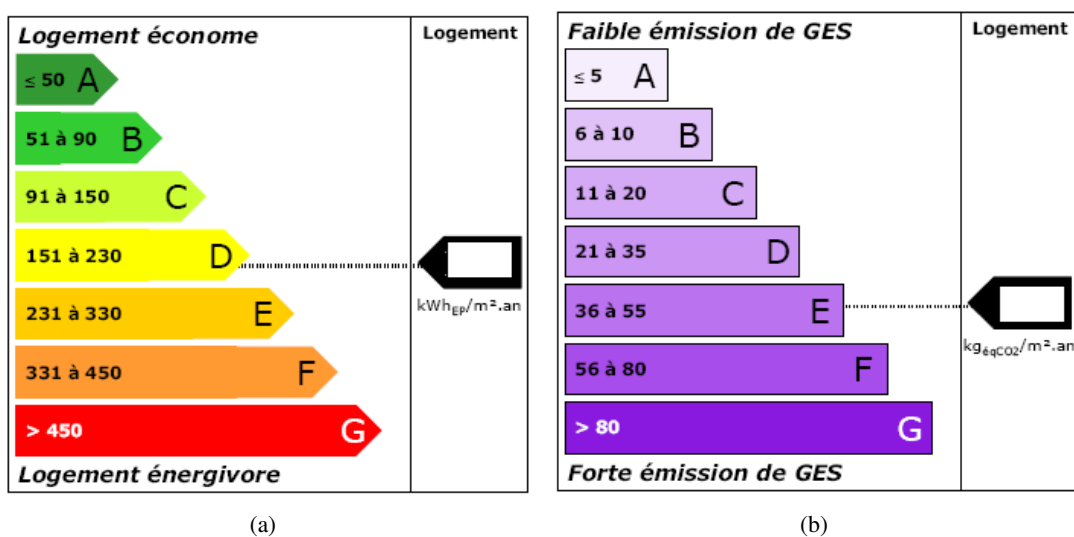


Figure 1.1: Regulatory environmental labels: energy label and climate label

One of the main elements of the DPE is the display of energy and climate labels, indicating the positioning of the dwelling with regard to its primary energy consumption and greenhouse gas emissions. It results in recommendations for energy improvements addressed to the owner, with estimations of the energy savings they represent and their payback time.

In theory, a rigorous and complete 3CL calculation establishes a detailed description of the consumption and losses of the dwelling: *U*-value of the glazed and opaque walls, losses due to thermal bridges and air change, environmental factors, inertia, intermittency factor, heating consumption, as well as the efficiency of distribution, emission, regulation and generation of heating, DHW and cooling.

The DPE as it is currently carried out in France has, however, limitations that justify the numerous research works on characterization, listed below.

- Even in its most detailed version, this calculation is purely theoretical and is based exclusively on the appraiser's knowledge of the building. However, buildings in need of rehabilitation are often the ones with the most unknowns due to ageing. A deterioration of the envelope can, for example, influence the *U*-value of the walls without being taken into account.
- The calculation does not take into account the actual behaviour of the occupants but assumes that of a typical family to evaluate the intrinsic performance of the building.
- This is not a dynamic thermal simulation in which the effects of inertia and solar gains would be precisely taken into account. Passive houses designed to rely on very little heating can therefore see their consumption largely overestimated compared to reality.
- Each element of the calculation is based on empirical coefficients derived from the properties

of typical components. For example, no measurements are taken to assess heat loss through air exchange due to the permeability of the envelope. These are evaluated on a purely theoretical basis.

The result of these approximations is that DPE only gives a vague idea of the theoretical performance of a building, without aiming at its actual performance. The recommendations it makes cannot be considered as specifically tailored to a particular building. In order to overcome these shortcomings, characterization methods were developed that aim to obtain a more or less detailed description of the actual performance of the building, based on measurements carried out in situ and a specified experimental protocol.

1.2 Assessing the performance with in-situ measurements

A great deal of work has been carried out since the 1980s aimed at estimating the actual performance of buildings on the basis of in situ measurements [Sub+88]. The objective of such an estimation can be, for example, to compare these real performances with those targeted at the time of design, to establish a predictive model of a building integrating its systems [BM11], or to establish a diagnosis prior to rehabilitation.

Several French ANR projects may be mentioned in relation to the topic of energy diagnostics and reliability of predictions. The ANR MEMOIRE¹ project has applied inverse methods as a means to identify intrinsic characteristics of a building. However, one of the difficulties identified in its outcome is the fact that scientific challenges remain to be raised before solutions could be submitted to professionals. The transition to the operational side demanded further investigations that had not yet been implemented. The ANR FIABILITE² project focused on the reliability of building simulation models and the impact of errors on their results. This is a key issue in the resolution of inverse problems, due to the high sensitivity of their solutions to inaccurate hypotheses. Though the FIABILITE project was not aimed at diagnostics, its findings are thus very relevant to the elaboration of a rigorous methodology for the energy audit. Later, the ANR COMIS³ project evaluated the real efficiency of innovative systems and their integration in buildings.

These projects show the relevance of a careful consideration of measurement data and simulation procedures in obtaining a reliable characterisation of the performance of equipment or of the envelope. Internationally, these concerns are addressed by several projects. Within the IEA EBC Annexes 58 and 71, full scale dynamic measurements and advanced statistical methods are used in order to come to a reliable performance characterisation. Within the PERFORMER European project⁴, methodologies were shown to assess thermal characteristics of a building: the ISABELE method (in situ assessment of the building envelope performance) by the CSTB and the QUB method (quick U-value of buildings) by Saint-Gobain.

A knowledge sharing effort was carried out within the IEA EBC 58 Annex, a project supported by the International Energy Agency's Energy in Buildings and Communities programme (IEA EBC), whose title was *Reliable Building Energy Performance Characterisation Based on Full Scale Dynamic Measurement*. Among other results, the project resulted on the one hand in an inventory of existing full-scale experimental test facilities [Jan16a] and recommendations for the implementation of an optimised measurement protocol [Jim16]; on the other hand in an inventory of

¹ANR MEMOIRE : Mesure Enrichie par la Modélisation pour une conception Intelligente en Rénovation Energétique. Programme ANR HABISOL, édition 2010

²ANR FIABILITE : Fiabilité des prévisions des performances énergétiques des bâtiments. Programme ANR HABISOL, édition 2010

³ANR COMIS : Evaluation des systèmes innovants intégrés à des bâtiments performants. Appel à projets générique 2014

⁴PERFORMER: Portable, Exhaustive, Reliable, Flexible and Optimized approach to Monitoring and Evaluation of building energy performance. 7 th Framework Programme (FP7) <http://performer-project.eu>

existing data analysis methods [Jan16b] and guidelines for their statistical interpretation [Mad16].

Annex 58 has led to an important structuring of research at the global level on the subject of characterization from dynamic measurements. However, the work carried out in this area has had its limitations due to its experimental nature: the tests were carried out under laboratory conditions in unoccupied test cells. However, the behaviour of the users of a building is an important factor in its performance. For this reason, the Annex 58 project was then continued in the form of Annex 71 (*Building Energy Performance Assessment Based on In-situ Measurements*) with a special focus on buildings observed in their actual conditions of use.

	Méthodes statiques Information faible	Méthodes dynamiques Information importante
Méthodes sans occupation Instrumentation intrusive	Co-heating	QUB ISABELE
Méthodes avec occupation Instrumentation non intrusive	Signature énergétique Régression linéaire	« Calibrage Bayésien »

Figure 1.2: Classification of methods

The methods for building performance assessment by in-situ measurements are hereby classified into two categories shown by Fig. 1.2:

- Methods feasible only in unoccupied premises, in which extensive instrumentation may be deployed for imposing heating loads and recording the building's behaviour.
- Methods that can be implemented in occupied buildings, using non-intrusive measurements. This category of methods is essentially represented in the literature by the principle of the energy signature, which compensates for the uncertainties linked to the occupation by a long measurement time, resulting in a very macroscopic and uninformative description of the performance.

Among these two categories, we also distinguish between so-called static methods and dynamic methods. The first are based on an energy balance of the building averaged over a sufficiently long period (from several weeks to several months) so that data may be aggregated in a sampling time where each point is a steady state of the building. The second category uses dynamic models of the observed thermal behaviour of the building, and allows much shorter measurement periods.

The trend today is to use dynamic measurements [Jan16b], backed by grey box models [BM11] to identify an increasing number of parameters of the building. This research paves the way for an informed selection of renovation scenarios in case of characterization of an older building. On the other hand, the intrusiveness of these methods poses a problem with regard to the objective of characterizing occupied building. Since the behaviour of the occupants represents a very influential unknown factor, it is generally overcome by considering only periods without occupancy of the building, and therefore preferably short periods. A new method, analysing measurements taken in occupied sites, should avoid any intrusiveness of the instrumentation. This is the objective of the BAYREB project, and this specification has also been identified as the motivation for IEA EBC 71 as a continuation of Annex 58.

The following sections show an overview of the main characterisation methods displayed by Fig. 1.2.

1.2.1 Characterisation of unoccupied buildings

The co-heating test

The co-heating test is a quasi-stationary protocol based on linear regression analysis of aggregated measurements of building performance. The method has undergone several developments in the literature since its first proposal [Sub+88]. A history and detailed description is given by [BR14], a summary of which is given here.

The method is based on the heat balance of an unoccupied room maintained at a constant temperature by electric heaters whose consumption is recorded. Indoor conditions (temperature and humidity) and outdoor conditions (wind, temperature, sunshine) are measured continuously during the test.



Figure 1.3: Setup of a co-heating test [BR14]

This is a quasi-static method, because an attempt is made to maintain a constant indoor temperature for the duration of the test. The aim is to overcome the effects of inertia of the building (thermal capacity of the envelope and the indoor air) and to write down its heat balance in a simplified form:

$$\sum \Phi + gAI_{sol} = \text{HLC} \Delta\theta_{ie} \quad (1.1)$$

where $\sum \Phi$ is the total heat input from heating devices, $\Delta\theta_{ie}$ is the indoor-outdoor temperature difference, and I_{sol} the global solar irradiance. By linear regression of this model on averaged measurements, two parameters may be estimated: the global heat loss coefficient HLC, and a solar aperture coefficient gA .

Some pre-processing of the measurements is necessary before the regression. An indoor temperature representative of the whole building must be reconstructed from the installed set of sensors. The data collected at the beginning of the test, corresponding to the "warm-up" of the building, should not be used since the model is based on a static balance. The points used for regression are then measurements averaged over a certain time interval, e.g. hourly or daily.

In its simplest version, the co-heating test allows estimating the real HLC coefficient of the building, as well as the solar aperture coefficient if solar gains are not neglected in the procedure. The disaggregation of HLC in several terms, in order to separate the respective part of static and air exchange losses, requires additional measurements: blower door or tracer gas.

A full description of the different test configurations developed over the years can be found in [BR14]. This family of characterization methods has two drawbacks that prevent its application in real conditions for the diagnosis of existing buildings :

- The regression is based on a static heat balance of the building aggregated into a single thermal zone.
- The experimental protocol is set up so that inertia effects can be neglected.

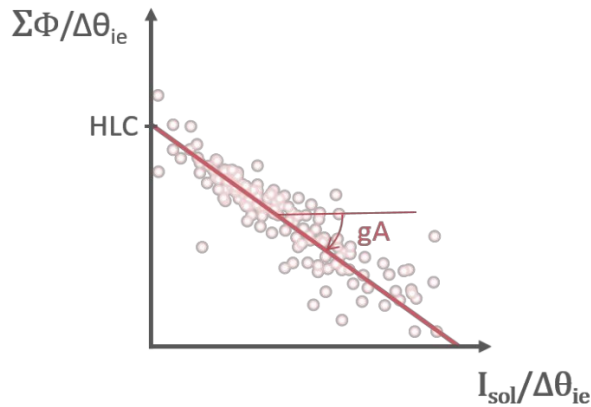


Figure 1.4: Linear regression on co-heating measurements [BR14]

The result of the regression is therefore a reduced number of parameters, which does not allow the adjusted model to be used for predictive purposes, nor does it allow the identification of specific pathologies in the building that would require rehabilitation.

The experimental protocol is based on intrusive instrumentation set up in an unoccupied room, albeit for a measurement time reduced to a few days. The applicability of this protocol in real conditions therefore remains restricted.

The QUB method

The QUB method (Quick U-Value of Buildings) was developed by the Saint-Gobain group in order to reduce the measurement time required by the co-heating test [MPR12]. The thermal properties estimated by the method are the HLC and the apparent heat capacity of the building. Its principle is illustrated by Fig. 1.5

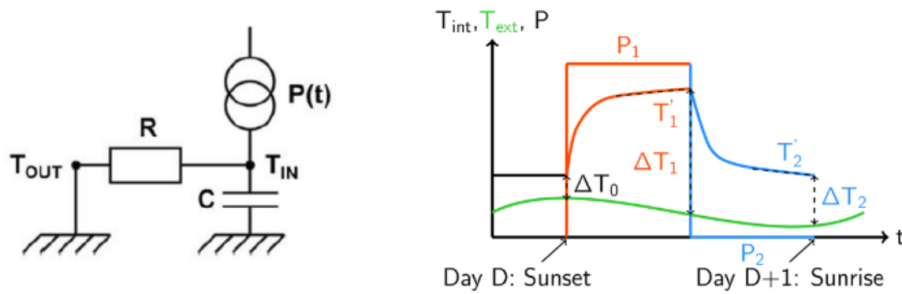


Figure 1.5: Principe of the QUB method

The method is based on a dynamic RC model with one resistance and capacity (left of the figure). Heating input is applied inside the building in three steps: an initialization period to reach a uniform indoor temperature; a step of constant high heating power P_1 ; a second step of lower power P_2 . These two steps are of equal duration. The indoor temperature of the building is recorded during this test. The analysis of the measurements consists in noting the slope of the evolution of the indoor temperature at the end of each time period (noted T'_1 and T'_2 on the diagram). Assuming that this evolution is then linear, the coefficient H_{QUB} and a thermal capacity indicator C_{QUB} are then deduced [Alz+18]. The hypotheses of the test are similar to those of the co-heating test: unoccupied building and homogeneous indoor temperature. Measurements are made at night in order to neglect solar gains and assume a constant outdoor temperature.

The duration of the test, which is shorter than a co-heating test, is determined by the initialization

period and by that of the two heating periods. In the fastest version of the test, the various articles where the QUB method is analysed [Meu+17; Sou+17] report H_{QUB} coefficients estimated with a precision of 10% based on two 4-hour or 6-hour slots. A decomposition of the time constants of the building [GA19] describes this duration as sufficient to observe the time constants that are prevalent on the behaviour of the building, despite the existence of much longer time constants. The QUB test was applied to several test buildings to illustrate the results. Two published examples are: the Energy House experimental house at the University of Salford [Alz+18; Meu+17]; a detached house in Nottingham [Sou+17].

The ISABELE method

The ISABELE method (In-situ assessment of building enveloppe performance) [BB14; SB14] assesses the energy performance of a new building right after construction. It was developed by the CSTB institute, and contributed to the PERFORMER european project.

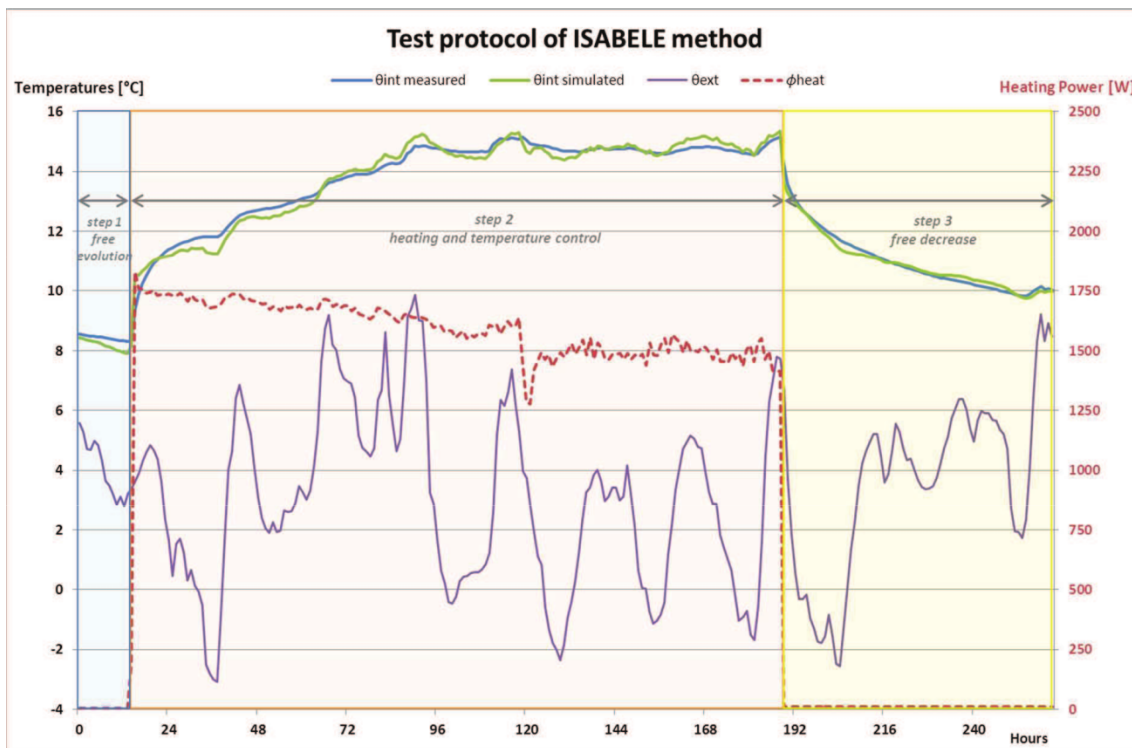


Figure 1.6: Settings of the ISABELE method

The method was developed to characterize the thermal properties of the envelope prior to the occupancy of the building. This requires the shortest possible instrumentation time to collect the necessary data. The experimental protocol is close to that of the QUB method, with the difference that a temperature setpoint is imposed for a given period of time and that the evolution of external conditions, especially solar irradiance, is also monitored. The data are then used to calibrate an RC model providing the desired properties. The model is used to simulate the experimental conditions, and its parameters are determined by fitting its outputs to the observations. The method for minimizing the gap between predictions and measurements is, depending on the case, the Nelder-Mead method [BB14] or Bayesian inference resolved by the MCMC algorithm [SB14].

The choice of any RC model makes it possible to attempt the simultaneous estimation of parameters governing various phenomena: the respective influences of transfers via opaque and glazed walls, air renewal and radiation. The article [BB14] thus addresses this problem of choosing

the right model for the description of the building for the identification of its properties, also described by [bacher_estimation_2011].

1.2.2 Characterisation of occupied buildings

The assessment of the intrinsic energy performance of an occupied building, independently from its operating conditions, remains a challenge. The main reason for this is the complexity and variety of phenomena which influence its energy balance, when it is operated by real occupants.

While the experimental protocols of the QUB and ISABELE protocols allow controlling the thermal loads, those of an occupied building are the sum of several contributions which are not always known: heating appliances, metabolic heat of the occupants, solar gains, heat losses of electrical appliances, heat losses of the DHW network, etc. In addition, the available consumption measurements (gas and electricity meters) cover other uses than space heating only, which has to be extracted from them. On the other hand, the heat losses through the envelope are also uncertain: the dwellings adjacent to the monitored thermal zone should be instrumented as well, in order to follow the heat exchanges between them; the losses through ventilation and leaks in the envelope are to be taken into account... Under these conditions, it is difficult to isolate the heat loss coefficient of the walls alone.

Static methods, such as the energy signature and other linear regression methods, require aggregated data which does not call for a detailed modelling of heat transfer phenomena. On the other side of the complexity spectrum, the characterisation of occupied buildings with dynamic methods was proposed with the so-called Bayesian calibration, described below.

Energy signature

Energy signature models are the simplest possible representation of a building as a static grey box model, where parameters are identified by analyzing consumption measurements rather than through detailed modeling (such as 3CL calculations or dynamic thermal simulation). So-called energy signature methods are therefore the first proposals for describing the intrinsic performance of a dwelling on the basis of measurements.

The energy signature of a building is a simplified model of its energy consumption profile (all energies combined) as a function of the outdoor temperature. Over a sufficiently long measurement period, the daily averages of heating power Φ_h and outdoor temperature T_e are compared in order to obtain by regression a profile approximating the following model:

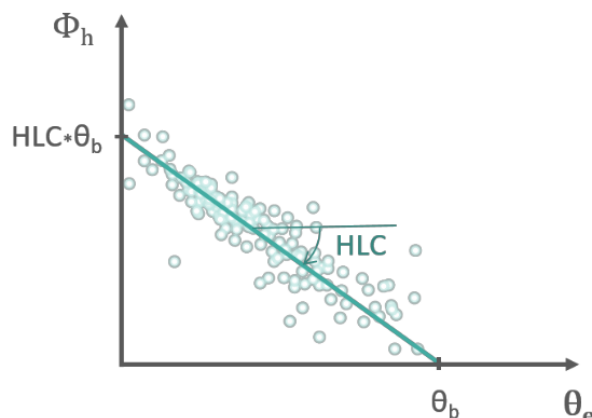


Figure 1.7: Principle of the energy signature

$$\Phi_h = \alpha + \text{HLC} (T_b - T_e) \quad \text{si } T_e \leq T_b \quad (1.2)$$

$$\Phi_h = 0 \quad \text{si } T_e > T_b \quad (1.3)$$

where the α coefficient is the baseline consumption of the building (DHW, lighting...) and T_b is the heating base temperature, as function of the indoor temperature set point and the solar gains. The building is thus described by three parameters (α, HLC, T_b). A similar model may be used to describe a cooling load above a second threshold temperature.

The PRISM method [Fel86] is a typical example of an energy signature model. The measurements required by the PRISM method can be collected without any intrusive instrumentation. However, because of the simplicity of the formulation, these measurements must cover a sufficiently long period of time for a clear trend to emerge. Since this is a static model using only averaged daily values, it does not provide a detailed description of the heat loss types in a building. It has however other uses, as summarised in this non-exhaustive list :

- [Fel86] uses the method to calculate a single indicator of normalized annual energy consumption (NAC). This indicator describes the intrinsic performance of the building, decoupling it from the influence of weather. It is therefore used to assess the actual performance gain between before and after renovation, regardless of outdoor conditions.
- [RR92] proposed a generalisation of the PRISM method, including the effects of occupancy. For a given building, the parameters (α, HLC, T_b) are identified in two different sets, corresponding respectively to occupied and unoccupied conditions. The number of days of occupancy of an office building appears as additional data. Due to this additional complexity, a statistical analysis of the results is proposed in order to quantify the uncertainty on the identified parameters and on the NAC indicator.
- [Ham87] illustrates the limitations of the method for the estimation of building parameters (energy audit): the results of the method should be limited to the prediction of consumptions on large time scales.
- [Flo92] supports this observation, and attributes the estimation error of building parameters to insufficient consideration of solar gains. The author links the uncertainty in the estimation of the heat loss coefficient to correlations between meteorological data (sunshine and outdoor temperature).
- [SAO09] also find that the values found for the heat loss coefficient vary little when there is little sunshine in cold climates.

The general observation is that static energy signature models can only be used as a basis for physical interpretation of the building parameters with great caution. They do not make it possible to disaggregate the different sources of heat loss (static losses, equipment efficiency, air change) since the time scale of their observations is at least one day. However, they have the benefit of not using intrusive instrumentation and allow interpreting measurements made in occupied buildings.

Bayesian calibration

Dynamic models allow reducing the measurement time needed to learn the thermal properties of buildings, and observing the effects of inertia not covered by static models. On the other hand, in order to be able to learn parameters calibration on measured data, it is essential that all the influential phenomena are represented by the selected model, on a time scale corresponding to the chosen level of detail. This implies, for example, that if a model is based on a time discretization of 10 minutes, then the internal heat sources and consumption readings must be known with the same precision. This requirement naturally poses a problem in occupied premises, where the behaviour of the occupants (presence, interaction with the envelope) must therefore be supplied to the model or evaluated by it.

In order to perform an informative calibration in occupied premises, a recent lead followed by several research teams is the use of hybrid systems incorporating statistical models (black box model) in the description of heat transfers (grey box model). Gaussian processes [Ras04; Sol16] (GP) are, for example, a type of non-parametric models used to represent random phenomena that are not explicitly described in the building thermal model. This allows them to be used for parameter prediction and estimation despite the presence of significant uncertainties and unobserved phenomena.

- Bayesian model calibration refers to using a GP as a surrogate model to reproduce a reference model, then training a second GP as the discrepancy function between this model and observations, then evaluating the posterior distribution of calibration parameters. In this context GPs have static inputs and are not dynamic models.
- Gaussian processes can also simulate dynamical systems through a state-space representation [Sol16]. Once included as a non-measured input into a state-space This opens the way to Latent Force Models (LFM). LFM can be seen as hybrid models that contain a first-principles physical model part and a non-parametric GP model part. They are used for learning and stochastic control in physical systems which contain unknown input signals. These unknown signals are modeled as Gaussian processes (GP) with certain parametrized covariance structures [SAL18]. To the author's knowledge, the only application of this method to building energy is [Gho+15].

The first approach mentioned above was originally proposed by [KO01], in what they call the Bayesian approach to the calibration of computer models.

$$z_i = \zeta(\mathbf{x}_i) + e_i = \rho \eta(\mathbf{x}_i, \theta) + \delta(\mathbf{x}_i) + e_i \quad (1.4)$$

where \mathbf{x}_i is a series of known model inputs, z_i are observations, $\zeta(\mathbf{x}_i)$ is the true value of the real process, $\eta(\mathbf{x}_i, \theta)$ is a computer model output with parameter θ , $\delta(\mathbf{x}_i)$ is the discrepancy function and $e_i \sim N(0, \lambda)$ are the observation errors. In [KO01], GP are used to represent prior information about both $\eta(\cdot, \cdot)$ and $\delta(\cdot)$. ρ and λ are hyperparameters, to be added to the list of hyperparameters of the covariance functions into a global hyperparameter vector ϕ .

Before attempting prediction of the true phenomenon using the calibrated code, the first step is to derive the posterior distribution of the parameters θ , β (parameters of the GP mean functions) and ϕ . Hyperparameters are estimated in two stages: $\eta(\cdot, \cdot)$ is estimated from a series of code outputs, and $\delta(\cdot)$ is estimated from observations. [KO01] restrict their study to having analytical, tractable posterior distributions that do not require methods such as MCMC. Therefore they fix the value of some hyperparameters to make these functions tractable, and have to resort to some simplifications.

The same approach was done by [AAC12] (see Fig. 1.8) who investigated the question of the identifiability of calibration parameters θ . Their formulation is very similar to [KO01]:

$$y^e(\mathbf{x}) = y^m(\mathbf{x}, \theta^*) + \delta(\mathbf{x}) + \varepsilon \quad (1.5)$$

A series of computer model runs is used to train a first GP on simulation data. Then, the discrepancy function is modeled by fitting another GP based on simulation data, experimental data and the prior for the calibration parameters.

To the author's knowledge, the first application of this method to buildings was [HCA12]. They followed the formulation of Bayesian calibration developed by [KO01] and used three sets of data as input: (1) monthly gas consumption values as observations $y(x)$, (2) computer outputs from exploring the space of calibration parameters $\eta(x, \theta)$, and (3) the prior PDF of calibration parameters $p(\theta)$. The model outputs $\eta(x, \theta)$ and the bias term $\delta(x)$ are both modeled as GPs. Calibration parameters are for instance: infiltration rate, indoor temperature, U -values, etc. With very little data, results of [HCA12] are posterior PDFs which are very close to the priors.

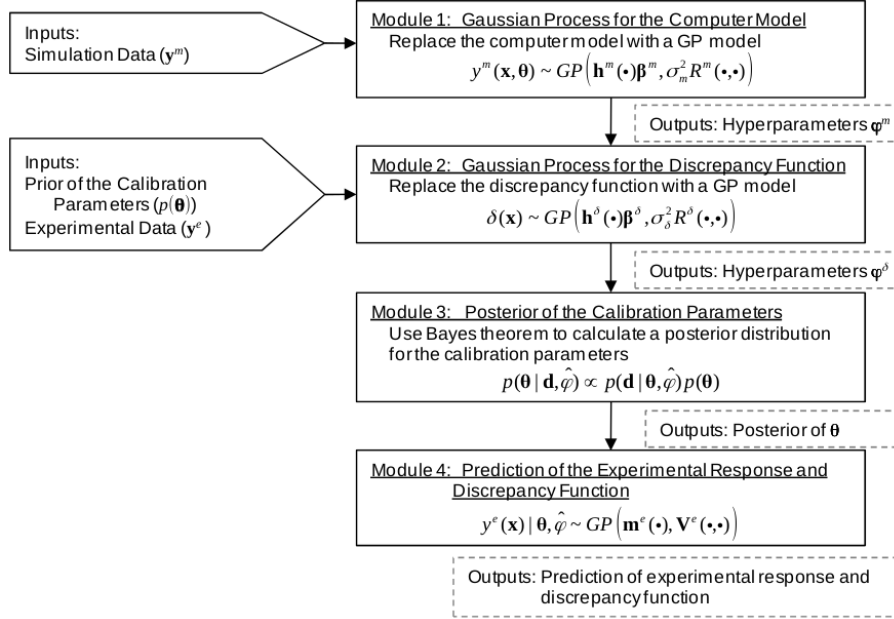


Figure 1.8: Modular Bayesian approach from [AAC12]

GP learning scales poorly with the amount of data, which restricts its applicability to lower observation time steps. [KCP17] studied the influence of time resolution on the predictive accuracy and showed the advantage of higher resolutions. More recently, [Cho+17] used the NUTS algorithm for the MCMC sampling in order to accelerate learning. In [CM18], they give a summary of publications using Bayesian calibration in building energy. In [MS18], a hybrid model is implemented. A zero mean GP is trained to learn the error between the grey-box model and the reference data (Fig. 1.9). As in the previous references, both models are added to obtain the final predicted output. They are trained in sequence: the GB model has some inputs \mathbf{u}_{GB} and is trained first (Fig. 1.10); then the GP has some other inputs \mathbf{u}_{GP} and is trained on the GB model's prediction error. Results are the hyperparameters of the GP.

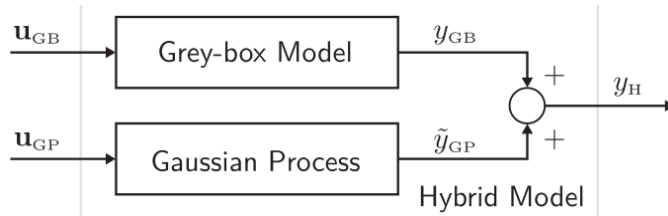


Figure 1.9: Diagram of the hybrid model from [MS18]

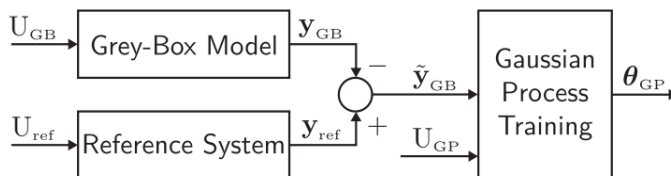


Figure 1.10: Training procedure of the hybrid model from [MS18]

Models trained by this method are said to have very good prediction performance, since the GP predicts the inadequacy of the GB as a function of new inputs, not included in the physical model. However, the method may not be fit for the interpretation of physical parameters. Indeed, since the GB model is first trained independently from the GP, it is biased and its parameter estimates are not interpretable.

1.3 The BAYREB project

1.3.1 Objective: characterisation before refurbishment

The BAYREB project belongs to the general field of the energy refurbishment of buildings. It aims at providing decision makers and renovation experts with decision support tools for the renovation process regarding energy efficiency. The project is part of a workflow based on stochastic methods that will support the decision process in a twofold manner:

- Using in situ sensor measurements, aided with Bayesian inference and a prior model of the building, to evaluate its real energy performance, diagnose envelope properties and eventual pathologies, while providing confidence intervals for all inferred data;
- Using the acquired knowledge of the true state of the building, and its uncertainty, as a basis for the elaboration of optimal renovation solutions.

The project focuses mostly on the first stage of this process: proposing a method for a detailed and robust energy audit.

The renovation process of individual or collective buildings is generally solely based on their initial yearly energy consumption, and standard solutions are applied without any guarantee of performance. A condition for a cost-effective refurbishment, adapted to each specific building, is to perform detailed diagnostics of its performance prior to picking solutions: for instance, to estimate which proportion of the heat losses are caused by air leakage, by the envelope, or by a dysfunction of the heating systems. The first option to achieve such a detailed audit is to use an excessive amount of sensors, surveys and in-situ measurements, followed by lengthy interpretation of results in order to point the weaknesses of the building regarding energy efficiency. The second option is to implement inverse techniques, which are able to automatically learn from the data in order to construct a realistic representation of the characteristics of a building.

The target of the BAYREB project is to use in-situ measurements (temperature, humidity, CO₂) to acquire the knowledge justifying the choice of the most suitable rehabilitation solution. The characterization of the properties of the envelope via in situ instrumentation is already proposed by the methods described above (section 1.2). However, these methods are not all applicable to pre-renovation diagnosis because their experimental protocol is not feasible in occupied premises, and/or their results are too aggregated to evaluate the effects of different renovation solutions.

The challenges of the project are therefore twofold:

- First, the behaviour of the building must be monitored **in its normal conditions of use**, with no ability to set controlled boundary conditions, and measured with sensors of limited type and accuracy. This potentially leads to high measurement uncertainties and poorer data sets.
- Secondly, we wish to disaggregate the different sources of heat loss, in order to enable the renovation decision. The model calibrated by the inverse problem must therefore have a sufficient level of detail.

1.3.2 Statistical learning and inverse problems in building physics

According to the definition of [BW98], inverse techniques are a suite of methods which promise to provide better experiments and improved understanding of physical processes. Inverse problem theory can be summed up as the science of training models using measurements. The target of such

a training is either to learn physical properties of a system by indirect measurements, or setting up a predictive model that can reproduce past observations.

In the last couple of decades, building physics researchers have benefitted from elements of statistical learning and time series analysis to improve their ability to construct knowledge from data. What is referred to here as inverse problems are actually a very broad field that encompasses any study where data is gathered and mined for information.

- **Material and component characterisation:** many material properties are not directly observable and must be estimated by indirect measurements. Inverse heat transfer theory [Bec85] was developed as a way to quantify heat exchange and thermal properties from temperature sensors only, and has translated well into building physics: for instance, the characterisation of heat and moisture transfer properties of materials is an inverse problem under investigation [Ber+16; KK96; Rou+15; Rou+17] because of how time consuming traditional hygric characterisation methods are.
- **Building energy performance assessment,** from the original energy signature models [Fel86; RR92] to co-heating tests [BR14], is an inverse problem. It can be used to formally estimate the energy savings after retrofit measures [HZ12; Zha+15] or to point out faults in system or envelope performance [HCA12].
- **Model predictive control** [HGP12] requires models describing the thermal behaviour of the building, as well as the internal and external influences on its performance. Inverse problems thus include the identification of building energy performance models, weather forecast models [DL14; Old+12], occupancy behaviour models [DH15; DA09], that are reliable and computationally efficient.

These scientific challenges are gaining visibility due to the increasing availability of data (smart meters, building management systems...), the increasing popularity of data mining methods, and the available computational power to address them.

Many engineers and researchers however lack the tools for a critical analysis of their results. This caution is particularly important as the dimensionality of the problem (i.e. the number of unknown parameters) increases. When data are available and a model is written to get a better understanding of it, it is very tempting to simply run an optimisation algorithm and assume that the calibrated model has become a sensible representation of reality. If the parameter estimation problem has a relatively low complexity (i.e. few parameters and sufficient measurements), it can be solved without difficulty. In these cases, authors often do not carry a thorough analysis of results, their reliability and ranges of uncertainty. However, it is highly interesting to attempt extracting the most possible information from given data, or to lower the experimental cost required by a given estimation target. System identification then becomes a more demanding task, which cannot be done without proof of reliability of its results. One should not overlook the mathematical challenges of inverse problems which, when added to measurement uncertainty and modelling approximations, can easily result in erroneous inferences.

In order to answer the questioning presented above, the project started with a significant literature review on the applications of inverse problems and statistical learning in building sciences, which was published in [Rou18].

1.3.3 Layout of this report

This report presents the methodology followed by the BAYREB project in order to meet its objectives: addressing the scientific challenges towards a detailed estimation of an occupied building's thermal properties, using only a non-intrusive measurement procedure.

Chapter 1 presented a state of the art of building energy performance assessment, and an overview of several recent research projects on the topic.

Chapter 2 describes the entire workflow of characterisation and the choices made to answer

the project's questioning: which sensor information is required, what type of model has been selected, what algorithms were used to calibrate them, and what criteria were used to evaluate the validity of results.

Chapter 3 introduces the numerical benchmark that has been developed to study the identifiability of the heat transfer properties of buildings. It is a virtual test environment that allows recreating variations of a reference building and weather data, in order to assess the interpretability and robustness of calibration results.

Chapter 4 includes all results of the project regarding applications to real data processing, either measured in unoccupied experimental test cells, or in real occupied buildings. Each case aims at answering one of the main questions of the project: how to ensure the reproducibility of results, how to perform real-time parameter estimation, how to separate air change related heat loss from transmission heat loss, etc.

Chapter 5 introduces some of the outlooks of the project.

2. Modelling, calibration and inference

This chapter introduces all the numerical methods used in the BAYREB project to solve the inverse problem of the energy characterisation of buildings in real conditions of use. It does not constitute a complete review of the models and algorithms developed in the literature, but focuses on the methods selected for the project, and justifies these choices. Due to the ill-posed nature of inverse problems and the need to process their results with caution, emphasis will be placed on the validation stages of modelling and calibration.

2.1 The objectives of thermal model calibration

Before describing and justifying the choices of methods for modelling and inference, let us start by laying down the definitions and hypotheses behind what we seek to estimate: the energy performance of the building envelopes, which cannot be directly measured.

Fig. 2.1 shows a schematic outlook of heat gains and losses in a heated space. The temperature variation, on the right side of the diagram, comes from the imbalance between all heat gains (Φ_{in} , red lines) and all heat losses (Φ_{out} , blue lines).

$$C \frac{\partial T}{\partial t} = \Phi_{in} - \Phi_{out} \quad (2.1)$$

The term of heat loss may be broken down as such:

$$\Phi_{out} = H_{tr}^e(T_i - T_e) + H_{tr}^s(T_i - T_s) + \sum_j H_{tr}^{adj,j}(T_i - T_{adj,j}) + \Phi_{inf} + \Phi_v \quad (2.2)$$

- The first term $H_{tr}^e(T_i - T_e)$ denotes heat loss by direct transmission from the heated room at temperature T_i to the outside at temperature T_e . The H_{tr}^e coefficient includes the heat transmissivity of opaque walls, glazing and thermal bridges.
- The second term $H_{tr}^s(T_i - T_g)$ denotes heat loss towards the ground at temperature T_g .
- The third term encompasses heat exchange with all adjacent rooms. This mainly concerns unheated spaces, which may have a significant temperature difference with the thermal zone under consideration.

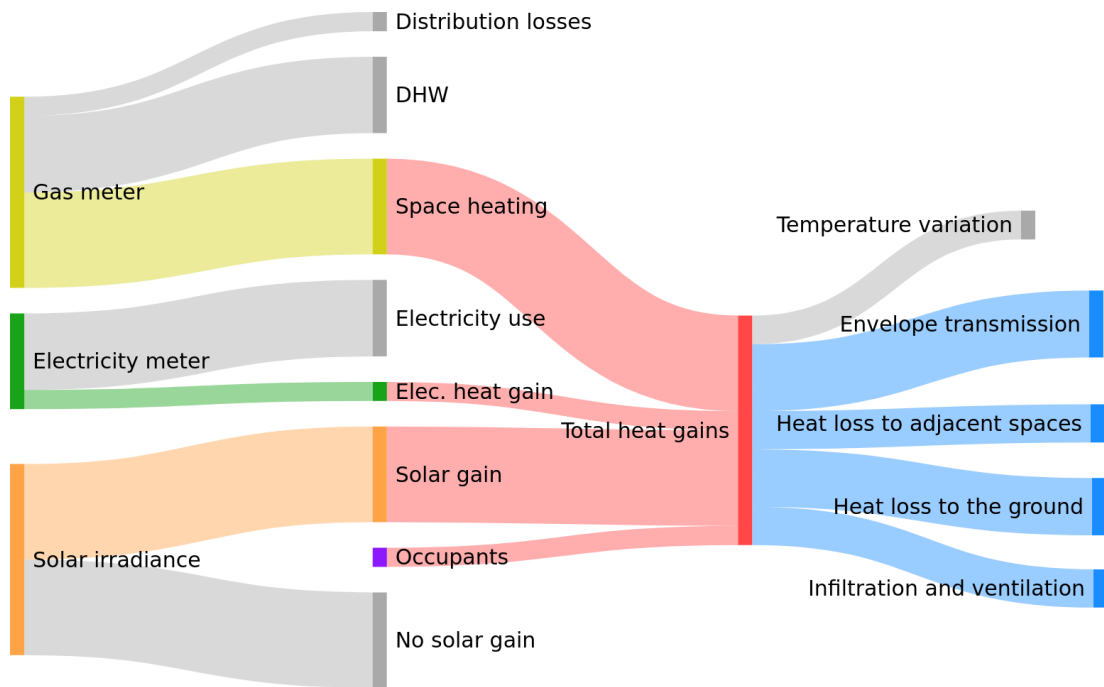


Figure 2.1: Decomposition of heat gains and losses in a heated zone.

- Φ_{inf} et Φ_{ven} respectivement dénotent la perte de chaleur par infiltration ou par ventilation mécanique.

The objective of the project is to characterise the envelope of a building by estimating the terms of this decomposition, and to find out if non-intrusive measurements are sufficiently informative to disaggregate them.

The first three terms of this decomposition may be aggregated in order to define two global indicators of the heat performance of the envelope: the Heat Loss Coefficient (HLC) and Heat Transfer Coefficient (HTC).

$$\Phi_{out} = \underbrace{\text{HTC} (T - T_e) + \Phi_{inf} + \Phi_v}_{\text{HLC}(T - T_e)} \quad (2.3)$$

$$\text{HLC} = \text{HTC} + \Phi_{inf} / (T - T_e) \quad (2.4)$$

The HTC describes all heat transmission through the envelope, and the HLC also includes the effect of air infiltration. Controlled mechanical ventilation is not included in these coefficients, but may as well be considered as part of the heat gains.

One of the main questionings of the project already arises from Eq. 2.2: is it possible to estimate separate heat transfer coefficients using only measurements that may be recorded without disturbing the normal operation of the building?

The second challenge posed by the specifications of the project arises from the difficulty of knowing the actual total heat gains Φ_{in} in Eq. 2.1. The red part of Fig. 2.1 illustrates the diversity of heat sources inside a thermal zone.

- The energy consumption dedicated to space heating is only a part of a meter reading (e.g. gas) which includes production and distribution losses, and often also cover the production of domestic hot water (DHW).

- The heat gain from electrical appliances, cooking, lighting and other uses, is difficult to estimate. It is a certain percentage, subject to fluctuations, of the electricity meter readings.
- The solar gains are usually significant, and a fraction of the total solar irradiance which depends on the orientation of the room relative to the position of the sun, shadings, type of glazing, etc.
- The metabolic heat gain from occupant depends on their presence. It may have an impact on the total heat balance of well insulated buildings.

There are therefore two obstacles to the disaggregation of heat loss coefficients. First, the coefficients we use to describe the envelope performance are not directly observable. Second, the system under consideration is under a series of excitations, some of which are unknown or difficult to monitor. In order to meet the project's requirements, careful and documented choices will have to be made regarding the types of measurements to perform, the structure of models used to simulate the building, the training algorithms used to calibrate these models, and the criteria used to assess the validity of their results.

2.2 Model calibration formulation and workflow

Calibrating a model means finding the settings or set of parameters with which its output best matches a series of observations, called a training dataset. This data usually originates from measurements (in either experimental test cells or real buildings), but may also have been produced by a complex reference model that we wish to approximate by a simplified one.

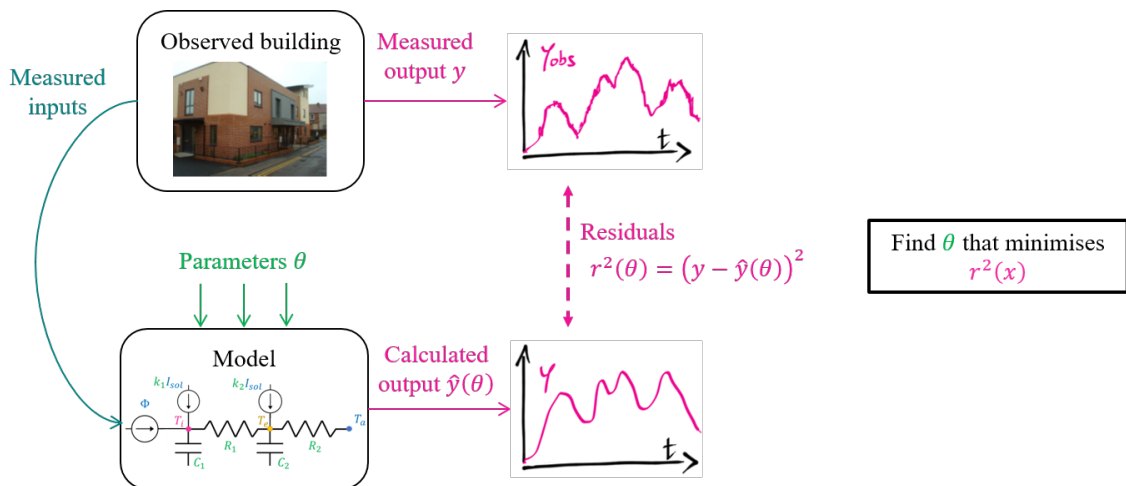


Figure 2.2: Model calibration in a nutshell

The general principle of solving a system identification problem is to describe an observed phenomenon by a model allowing its simulation. Fig. 2.2 illustrates the principle of model calibration. Measurements $\mathbf{z} = (\mathbf{u}, \mathbf{y})$ are carried in an experimental setup: a building is probed for the quantities from which we wish to estimate its energy performance (indoor temperature, meter readings, climate, etc.) A model is defined as a mapping between some of the measurements set as input \mathbf{u} (boundary conditions, weather data) and some as output \mathbf{y} . The model equations are parameterised by a finite set of variables θ . Parameter estimation is the process of assessing θ from a discrete set of N data points $\mathbf{y}_{1:N} = \{\mathbf{y}_k, k \in 1 \dots N\}$.

The output of the ideal, undisturbed physical system is noted \mathbf{y}^* , which is the hypothetical outcome of an ideal, non-intrusive sensor. Under the hypothesis of additive measurement noise

$\varepsilon(t)$, the observed output sequence is:

$$\mathbf{y}_k = \mathbf{y}_k^* + \varepsilon_k \quad (2.5)$$

The most common situation is that of additive white gaussian noise, i.e. $\varepsilon_k \sim \mathcal{N}(0, \sigma)$ is a sequence of independent and identically distributed (i.i.d.) variables, where the k index denotes data points and the measurement uncertainty σ may or may not be known.

The aim of the inverse problem is to approximate the system with a mathematical formulation of the outputs $\hat{\mathbf{y}}(t, \theta)$ that will allow the estimation of θ . Ideally, the model is unbiased: it accurately describes the behaviour of the system, so that there exists a true value θ^* of the parameter vector for which the output $\hat{\mathbf{y}}$ reproduces the undisturbed value of observed variables.

$$\mathbf{y}^*(t) = \hat{\mathbf{y}}(t, \theta^*) \quad (2.6)$$

Eq. 2.6 is written in continuous time: the discrete system output from Eq. 2.5 is the series of values taken by the continuous process $\mathbf{y}^*(t)$ at the time coordinates $\{t_k, k \in 1 \dots N\}$. In the following, the continuous and discrete notations of each variable may be used alternatively.

In practice, θ^* will never be reached exactly, but rather approached by an estimator $\hat{\theta}$, which may hold different values according to the criteria it follows. The hypothesis of an unbiased model $\hat{\mathbf{y}}$ (Eq. 2.6) states that there exists a parameter value θ^* for which the model output is separated from the observations \mathbf{y} only by a zero mean, Gaussian distributed measurement noise. It means that the model perfectly reproduces the physical reality, and the only perceptible error is due to the imperfection of sensors. This is exceedingly idealistic because all models are wrong to some extent. Building energy simulation is a multi-physics, multi-scale topic that cannot accurately portray all phenomena of heat and mass transfer: forward problems are always simplified to some extent. The identification procedure is a series of experimental and numerical steps along which lay several sources of errors [MJP11b]: the forward problem is an approximation of the modelled physical process, with a given spatial discretisation; a hypothesis on the model may be excessively simplifying or the parametrization of a function may be wrong; the intrusiveness of a sensor may be overlooked; measurements are affected by noise and depend on sensor calibration, etc.

The most intuitive way to calibrate a model is to minimize an indicator such as the sum of squared residuals with an optimisation algorithm, in order to find the value of θ that makes the model most closely match the data. Modelling approximations are problematic because inverse problems are typically ill-posed [BW98]: their solution is highly sensitive to noise in the measured data and approximation errors. A global optimum of the inverse problem may then be found with unrealistic physical values for the material properties as a consequence of seemingly moderate errors made when setting up the problem. In order to address these issues, a probabilistic framework is used to describe all steps of the procedure while accounting for all known sources of uncertainty. The observations, model outputs and parameter values are all defined in terms of probability distributions rather than single values.

In order to ensure, as much as possible, that the parameters returned by the model calibration procedure are physically interpretable, a workflow was developed in the project and shown on Fig. 2.3. This workflow sums up the important steps that be followed before and after applying the training algorithm itself, and the various tests to be performed to prevent hasty conclusions. The steps are summarized below, and detailed in the following sections.

Data acquisition and processing

Measurements are an insight of the real behaviour of a building, and are the basis for training models to reproduce it. The required types of monitoring depend on the characterisation target and on the specific energy uses of the building under study. Other important characteristics of the

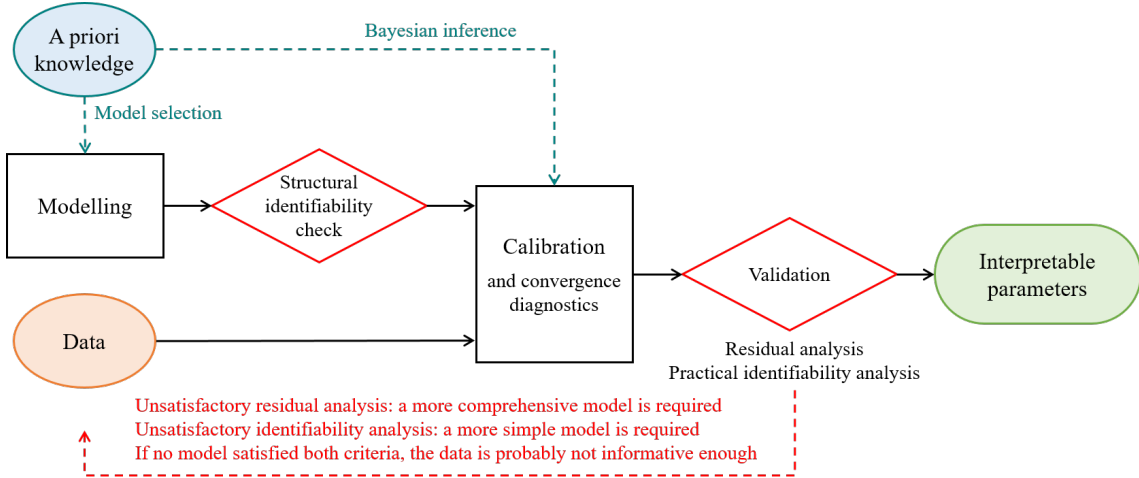


Figure 2.3: Proposed workflow for model selection, calibration and validation

data are: the type and accuracy of sensors used for a given measurement, the acquisition time step, the spatial granularity of observation. Data pre-processing, which includes handling irregular or incomplete data, is also a requirement for reliable training results. An example of processed dataset is shown on Fig. 2.4.

	ti	te	Qh	Qi	isoldif	isol	WindDirection	WindSpeed	m_vent	T_vent
2018-12-21 00:00:00	21.0601	2.2	3320	0	0.0	0.0	239.0	2.2	0.066667	7.25
2018-12-21 00:10:00	21.0780	2.1	3310	0	0.0	0.0	253.0	2.1	0.066667	7.25
2018-12-21 00:20:00	20.6715	1.6	1100	0	0.0	0.0	237.0	2.8	0.066667	6.90
2018-12-21 00:30:00	20.0508	0.6	590	0	0.0	0.0	217.0	2.6	0.066667	6.65
2018-12-21 00:40:00	19.8456	0.5	580	0	0.0	0.0	236.0	2.0	0.066667	6.35

Figure 2.4: Insight of the header of a data file

Modelling

Selecting an appropriate model structure is essential to the learning procedure. The complexity of the model is a compromise between realism and parsimony: it should at least describe all the most significant processes occurring in the system, and should not allow any redundancy in the input-output relationship. Among several models, equally capable of reproducing a dataset, the best choice is usually the most simple one [HTF01].

Before being fitted by statistical learning, a numerical model should pass a test of **structural identifiability**, which will detect an eventual redundancy in its formulation or its parameters. This step is described below in Sec. 2.3 along with the choices of models used within the BAYREB project.

Calibration

Calibration refers to the search for the parameters of a model, with which it outputs the best possible fit with a given training dataset. The most intuitive way to solve the problem for the optimal model parameters is to minimize a measure of model adequacy, such as the sum of squared residuals between its output and the observations, with an optimisation algorithm. The output of

this procedure is the mean value and covariance matrix of the estimated parameters.

The training algorithms used within the project will be described in Sec. 2.4. They include deterministic training by maximum likelihood estimation, and Bayesian inference, which allows letting some prior knowledge of the system influence the results.

Validation of the calibrated model

The ill-posed nature of inverse problems makes their results particularly sensitive to the various sources of uncertainty that punctuate the overall solving procedure: measurement uncertainties modelling assumptions, discretisation approximations, intrusiveness of sensors, etc. [MJP11a]. Before the estimated parameters may be physically interpreted, some precautions should be taken. Sec. 2.5 will describe the two main validation tests which are necessary conditions for parameter interpretability:

- **Residuals analysis** checks that the deviation between the predictions of a calibrated model and measurements is close to white noise. If this is not the case, the model is insufficient to explain all the phenomena generating the observations: its complexity should be increased.
- **Practical identifiability** analysis of parameters assesses whether their estimates are bounded. Otherwise, there is a need to reduce the complexity of the model or increase the observation period.

These tests are described in [Rou18] and in Sec. 2.5 below.

2.3 Modelling

Only the model structures used within the BAYREB project are presented here. A more thorough list of options is available in [Rou18].

2.3.1 Linear regression

Linear regression has already been mentioned earlier, as it includes some of the methods introduced in Sec. 1.2, especially the co-heating test and the energy signature models.

As an example of how the energy balance of a building may be formulated as a linear regression problem, let us start from Eq. 2.1 and reformulate it under the following assumptions:

- Steady-state conditions $\partial T / \partial t$ of a single-zone building.
- The only heat gains to the building are from heating Φ_h and solar gain $\Phi_s = g_A I_{sol}$, where g_A is a solar aperture coefficient.
- The heat loss through all parts of the envelope is assembled into a global heat loss coefficient HLC.

Under these very convenient assumptions, the energy balance of a heated zone may be approached by:

$$\Phi_h = \text{HLC} (T_i - T_e) - g_A I_{sol} \quad (2.7)$$

where Φ_h , $(T_i - T_e)$ and I_{sol} are measured data. In order for the steady-state assumption to hold, each data point of these series must be representative of an equilibrium state of the building, which means that higher-resolution time series data should be averaged on a long enough time step size.

The goal of linear regression analysis is to determine a linear relationship between a dependent variable y and one or several independent variables x .

$$y = \theta_0 + \theta_1 x_1 + \theta_2 x_2 \quad (2.8)$$

In the above example, the model output y is the measured heating power Φ_h , and the inputs x_1 and x_2 are the other measured series $(T_i - T_e)$ and I_{sol} . By fitting this model, for instance with the

ordinary least squares method, one may estimate the θ_1 and θ_2 coefficients, which respectively represent HLC and g_A in our example. Eq. 2.8 may additionally include a constant intercept θ_0 .

Linear regression models have several limitations: they cannot represent non-linear phenomena, such as radiative heat exchange between walls; they don't allow identifying the parameters driving dynamical phenomena; they impose a fixed structure to the energy balance equation. Despite these limitations, they can however be very useful as a first insight into the heat balance of a building: they allow a quick assessment of which types of measurements have an impact on the global balance (see Sec. 4.2) and guide the choice of more detailed models. Moreover, if a large enough amount of data is available, the estimates of some coefficients such as the HLC often turn out to be quite reliable.

2.3.2 State-space models

State-space models (SSM), which include the simplified resistor-capacitor (RC) model structures, are a popular choice for either parameter estimation or system identification. When written as a set of Stochastic Differential Equations, they allow accounting for modelling approximations [BM11; JPH08; KMJ04; MH95] and offer a more reproducible parameter estimation than deterministic models that overlook modelling errors [RRO18].

The formulation of SSM with an example

Consider the example of a simple building represented by a 2-resistor, 2-capacitor model structure (2R2C) as shown by Fig. 2.5. The equations of this model are:

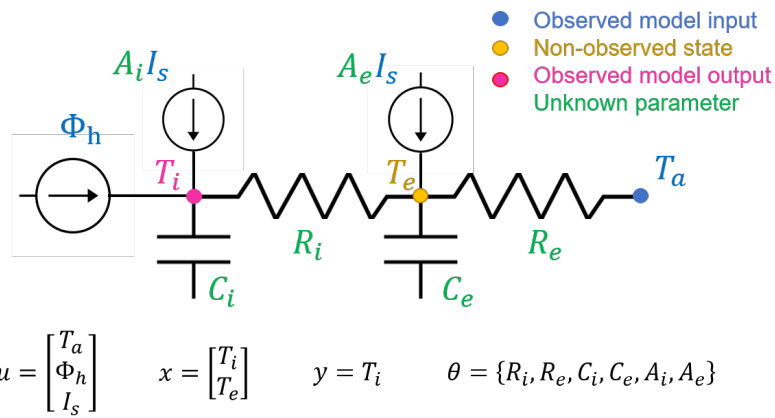


Figure 2.5: Model with 2 resistors and 2 capacitors

$$C_i dT_i = \frac{1}{R_i} (T_e - T_i) dt + \Phi dt + A_i I_s dt + \sigma_i d\omega_i \quad (2.9)$$

$$C_e dT_e = \frac{1}{R_e} (T_i - T_e) dt + \frac{1}{R_e} (T_a - T_e) dt + A_e I_s dt + \sigma_e d\omega_e \quad (2.10)$$

where T_i , T_e and T_a are the indoor, envelope and ambient (outdoor) temperatures. The envelope temperature is associated with the thermal mass of the opaque surfaces, and does not represent a specific coordinate within the envelope. The model has two states T_e (unobserved) and T_i (observed); Φ_h (W) is the indoor heating power; I_s (W/m^2) is the global horizontal solar irradiance. R_i (K/W) is the thermal resistance between the indoor air temperature and the envelope, R_e the resistance between the envelope and the ambient air. C_i and C_e (J/K) are the heat capacities of the interior and the envelope, respectively, and A_i and A_e (m^2) are their solar gain coefficients. $\{\omega_i\}$ and $\{\omega_e\}$ are

standard Wiener processes. σ_i^2 and σ_e^2 are their variances. This process noise is a way to account for modelling approximations, unrecognized inputs or noise-corrupted input measurements.

Despite its simplicity, this model structure is able to reproduce the thermal behaviour of a simple unoccupied building [RRO18]. Eq. 2.9 and 2.10 can be written in matrix form:

$$d \begin{bmatrix} T_i \\ T_e \end{bmatrix} = \begin{pmatrix} -\frac{1}{R_i C_i} & \frac{1}{R_i C_i} \\ \frac{1}{R_i C_e} & -\frac{1}{R_i C_e} - \frac{1}{R_e C_e} \end{pmatrix} \begin{bmatrix} T_i \\ T_e \end{bmatrix} dt + \begin{pmatrix} 0 & \frac{1}{C_i} & \frac{k_1}{C_i} \\ \frac{1}{R_e C_e} & 0 & \frac{k_2}{C_e} \end{pmatrix} \begin{bmatrix} T_a \\ \Phi_h \\ I_s \end{bmatrix} dt + \sigma d\omega \quad (2.11)$$

which is the state equation in the following stochastic state-space model, written in continuous-discrete form:

$$dx(t) = A_\theta x(t) dt + B_\theta u(t) dt + \sigma_\theta d\omega \quad (2.12)$$

$$y_t = C_\theta x_t + \varepsilon_t \quad (2.13)$$

A state-space model is a set of two equations: the first one, the state equation (Eq. 2.12), results from the physical formulation of the system. Its matrices A_θ , B_θ and σ_θ are given the θ subscript to indicate that they depend on a parameter θ , which is the set of unknown values to be estimated: resistances, capacities, solar gain factors and variances of the Wiener processes. The state vector x includes the temperatures T_i and T_e calculated by the model, and $u = [T_a, \Phi_h, I_s]$ is the input vector including boundary conditions and excitations. The second equation, Eq. 2.13, is the observation equation. It indicates that the measured quantity y_t may be different from the output of the state equation. In our case, the observed temperature is only the first component of the state vector, and is encumbered with some measurement error ε_t . In this equation, time is noted as a subscript to indicate that observations come in a discrete sequence.

Discretisation

The stochastic model described by Eq. 2.12 must be discretized in order to specify its evolution between discrete time coordinates. Let us denote the sample interval length Δt and assume that the inputs $u(t)$ are constant during each interval. Eq. 2.12 and 2.13 can be discretized into the following discrete linear system of equations:

$$x_t = F_\theta x_{t-1} + G_\theta u_t + w_t \quad (2.14)$$

$$y_t = C_\theta x_t + v_t \quad (2.15)$$

where x_t denotes the vector of states at the time coordinate t , and y_t denotes the observations. The F_θ and G_θ matrices of the discrete equation result from the matrices of the continuous equation 2.12 using the usual state-space discretization method. Their coefficients are functions of θ and of the time step size Δt . Similarly, the process noise in discrete time $w_t \sim \mathcal{N}(0, Q_d)$ has a covariance matrix Q_d that can be calculated from the covariance matrix of the process noise in continuous time σ . The observation error v_t has a covariance R , which depends on the variance of ε_t and the time step size.

The discretization equations are given here, and are available with more detail in [MH95; Rou18]:

$$F_\theta = \exp(A_\theta \Delta t) \quad (2.16)$$

$$G_\theta = A_\theta^{-1} (F_\theta - I) B_\theta \quad (2.17)$$

$$Q = \int_0^{\Delta t} \exp(A_\theta \Delta t) \sigma \exp(A_\theta^T \Delta t) dt \quad (2.18)$$

$$R = \frac{1}{\Delta t} \text{var}(\varepsilon_t) \quad (2.19)$$

where A , B and C are the matrices of the continuous linear system 2.12 and 2.13.

The Kalman filter equations

Given a state transition probability $p(\mathbf{x}_t | \theta, \mathbf{x}_{t-1}, \mathbf{u}_t)$ (Eq. 2.14) and an observation probability $p(\mathbf{y}_t | \mathbf{x}_t)$ (Eq. 2.15), a Kalman filter produces $p(\mathbf{x}_t | \mathbf{y}_{1:T}, \theta)$, the probability distribution function of each state \mathbf{x}_t given measurements and parameter values, and the marginal likelihood function $L_y(\theta) = p(\mathbf{y}_{1:T} | \theta)$. Its algorithm has been described by many authors including [MH95; Rou18] and is shortly recalled here.

Filtering produces $p(\mathbf{x}_t | \mathbf{y}_{1:N}, \theta)$, the probability distribution function of each state \mathbf{x}_t given measurements and parameter values. In the following, definitions adapted from [SS16a] are used: $\mathbf{x}_{t|s}$ is the expected state at time t given observations up to time s . $\mathbf{P}_{t|s}$ is the variance of the state \mathbf{x}_t , i.e. the mean-squared error.

$$\mathbf{x}_{t|s} = E(\mathbf{x}_t | \mathbf{y}_{1:s}, \theta) \quad (2.20)$$

$$\mathbf{P}_{t|s} = \text{Var}(\mathbf{x}_t | \mathbf{y}_{1:s}, \theta) = E[(\mathbf{x}_t - \mathbf{x}_{t|s})(\mathbf{x}_t - \mathbf{x}_{t|s})^T | \mathbf{y}_{1:s}, \theta] \quad (2.21)$$

The Kalman filter algorithm is described here and illustrated by Fig. 2.6:

- Set the initial states $\mathbf{x}_{0|0}$ and their covariance $\mathbf{P}_{0|0}$
- for $t = 1 \dots T$:
 1. **Prediction step:** given the previous state $\mathbf{x}_{t|t}$ and its covariance $\mathbf{P}_{t|t}$, the model estimates the one-step ahead prediction.

$$\mathbf{x}_{t+1|t} = \mathbf{F}_\theta \mathbf{x}_{t|t} + \mathbf{G}_\theta \mathbf{u}_{t+1} \quad (2.22)$$

$$\mathbf{P}_{t+1|t} = \mathbf{F}_\theta \mathbf{x}_{t|t} \mathbf{F}_\theta^T + \mathbf{Q} \quad (2.23)$$

2. **Innovations** (prediction error) $\boldsymbol{\varepsilon}_{t+1}$ and their covariances Σ_{t+1} are then calculated, along with the Kalman gain \mathbf{K}_{t+1} , by comparing **measurements** \mathbf{y}_{t+1} (see Fig. 2.6) with the one-step ahead prediction $\mathbf{x}_{t+1|t}$:

$$\boldsymbol{\varepsilon}_{t+1} = \mathbf{y}_{t+1} - \mathbf{H}_\theta \mathbf{x}_{t+1|t} \quad (2.24)$$

$$\Sigma_{t+1} = \mathbf{H}_\theta \mathbf{P}_{t+1|t} \mathbf{H}_\theta^T + \mathbf{R} \quad (2.25)$$

$$\mathbf{K}_{t+1} = \mathbf{P}_{t+1|t} \mathbf{H}_\theta^T \Sigma_{t+1}^{-1} \quad (2.26)$$

3. **Updating step:** the new states at time $t + 1$ are updated, as a compromise between the one-step ahead prediction and the measurement.

$$\mathbf{x}_{t+1|t+1} = \mathbf{x}_{t+1|t} + \mathbf{K}_{t+1} \boldsymbol{\varepsilon}_{t+1} \quad (2.27)$$

$$\mathbf{P}_{t+1|t+1} = (\mathbf{I} - \mathbf{K}_{t+1} \mathbf{H}_\theta) \mathbf{P}_{t+1|t} \quad (2.28)$$

- The total (negative) log-likelihood can be calculated up to a normalizing constant:

$$-\ln L_y(\theta) = \frac{1}{2} \sum_{t=1}^T \ln |\Sigma_t(\theta)| + \frac{1}{2} \sum_{t=1}^T \boldsymbol{\varepsilon}_t(\theta)^T \Sigma_t(\theta)^{-1} \boldsymbol{\varepsilon}_t(\theta) \quad (2.29)$$

Roughly speaking, the Kalman filter applies Bayes' rule at each time step: the updated state $p(\mathbf{x}_t | \mathbf{y}_{1:t}) = \mathcal{N}(\mathbf{x}_{t|t}, \mathbf{P}_{t|t})$ is a posterior distribution, obtained from a compromise between a prior output of the model $p(\mathbf{x}_t | \mathbf{y}_{1:t-1}) = \mathcal{N}(\mathbf{x}_{t|t-1}, \mathbf{P}_{t|t-1})$ and the evidence brought by measurements \mathbf{y}_t . Their relative weight is expressed by the Kalman gain \mathbf{K}_t that measures the relative confidence we put in both the model and the measurements.

This standard Kalman filter algorithm works for linear systems only. Non-linear systems require another filter, such as the Extended Kalman Filter (used by [KMJ04]), the Unscented Kalman Filter [WM00], or the particle filter.

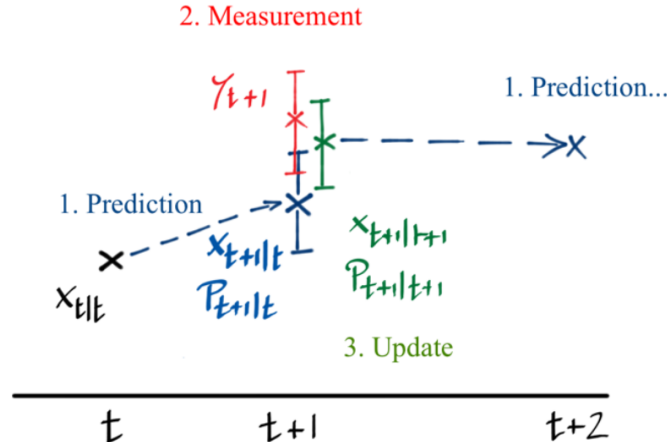


Figure 2.6: Schematic view of one iteration of the Kalman filter

2.3.3 Gaussian Processes and Latent Force Models

Gaussian Processes (GP) are a type of non-parametric models used in machine learning applications [Ras04]. In time series analysis, Gaussian Processes are used for learning input-output mapping, e.g. $y = f(t)$ where the time t is the input of the function. The dissertation [Sol16] provides insights on the connection between temporal GP models and stochastic differential equations describing the evolution of the process over the temporal domain. Covariance functions can be represented in terms of a dynamical model (the GP prior) and measurement model of the form:

$$d\mathbf{f}_t = \mathbf{A}_g \mathbf{f}_t dt + \mathbf{Q}_g^{1/2} d\mathbf{w}_t \quad (2.30)$$

$$y_k = \mathbf{C}_g \mathbf{f}_k + \mathbf{v}_k \quad (2.31)$$

where $\mathbf{f}_t = (f_1(t), \dots, f_m(t))$ contains p stochastic processes. The system is defined by the state matrix \mathbf{A}_g , the scaling matrix \mathbf{Q}_g and the initial state covariance matrix $\mathbf{P}_0 = \text{var}(\mathbf{f}_0)$; the model (2.30-2.31) is a special case of the model (2.12-2.13) with no input vector.

Latent Force models (LFM) can be seen as hybrid models that contain a first-principle physical model part and a non-parametric GP model part. They are used for learning and stochastic control in physical systems which contain unknown input signals. These unknown signals are modeled as GP's with certain parameterized covariance structures. The Latent Force Model is obtained by combining the physical state-space (2.14-2.15) and the Gaussian process state-space (2.30-2.31) [SAL18]:

$$d\mathbf{x}_t = (\mathbf{A}_p \mathbf{x}_t + \mathbf{B}_l \mathbf{C}_g \mathbf{f}_t + \mathbf{B}_p \mathbf{u}_t) dt + \mathbf{Q}_p^{1/2} d\mathbf{w}_t \quad (2.32)$$

$$d\mathbf{f}_t = \mathbf{A}_g \mathbf{f}_t dt + \mathbf{Q}_g^{1/2} d\mathbf{w}_t \quad (2.33)$$

$$\mathbf{y}_k = \mathbf{C}_p \mathbf{x}_k + \mathbf{v}_k \quad (2.34)$$

where $\mathbf{B}_l \in \mathbb{R}^{p \times q}$ is the input matrix for the latent forces.

Gaussian processes can therefore be used to include uncertain or unobserved phenomena into the physical equations of an RC model: training a purely RC model may be sufficient to predict a system observed in controlled, well-known conditions. However, all the phenomena and boundary conditions are seldom known or measured, which can bring a bias to the physical interpretation and the prediction of the estimated model. In this case, a Latent Force Model can be used to model these unknown input signals (latent forces). An example of LFM application to building energy performance assessment is [Gho+15].

2.3.4 Checking for structural identifiability

The usual definition of identifiability originates from [BÅ70]. This notion was originally predominantly developed to help understanding complex biological systems, each of which is modelled by a specific set of differential equations with unobservable parameters. The question of identifiability is whether the input-output relation of the system may be explained by a unique parameter combination θ .

$$y(\theta) = y(\tilde{\theta}) \Rightarrow \theta = \tilde{\theta} \quad (2.35)$$

Two conditions are required for the parameter estimates to be identifiable: the model structure must allow for parameters to be theoretically distinguishable from one another, with no redundancy; the data must be informative so that parameter uncertainty is not prohibitively high after identification. These conditions are respectively denoted **structural and practical identifiability**.

Structural identifiability relates the possibility of finding parameter estimates to the structure of the model, independently from measurements. Let us illustrate this question in the particular case of linear, time invariant systems. This includes RC models for buildings where not all temperature nodes are observed. It was shown by [GG76] that two sets of parameter values are indistinguishable if and only if they both yield the same impulse responses and transfer functions.

Linear models

The first way to check for structural identifiability of a linear state-space model such as Eq. 2.12 and 2.13 is to take a Laplace transform of the system and check whether the same input-output relation implies an unique parameter set [WP97]. This analysis is illustrated here with the 2R2C model example (Fig. 2.5). The system can be written in Laplace form as:

$$s\mathbf{X}(s) = \mathbf{AX}(s) + \mathbf{BU}(s) \quad (2.36)$$

$$\mathbf{Y}(s) = \mathbf{CU}(s) \quad (2.37)$$

The transfer function of this system is then a $[1 \times 2]$ matrix:

$$\mathbf{H}(s, \theta) = \frac{\mathbf{Y}(s)}{\mathbf{U}(s)} = \mathbf{C}(s\mathbf{I}_2 - \mathbf{A})^{-1} \mathbf{B} \quad (2.38)$$

$$= \frac{1}{s^2 + \frac{C_iR_i + C_eR_i + C_eR_e}{C_iC_eR_iR_e}s + \frac{1}{C_iC_eR_iR_e}} \begin{bmatrix} \frac{1}{C_iC_eR_iR_e} & \frac{1}{C_e}s + \frac{R_i + R_e}{C_iC_eR_iR_e} \end{bmatrix} \quad (2.39)$$

Note that this derivation can be done manually due to the simplicity of the 2R2C model. In case of a more complicated linear model, a symbolic computation software is preferable.

The system is structurally identifiable iff the unicity of transfer function implies the unicity of parameters:

$$\mathbf{H}(s, \theta) = \mathbf{H}(s, \tilde{\theta}) \Rightarrow \theta = \tilde{\theta} \quad (2.40)$$

This is solved by checking for unicity of each term of the transfer function for two parameter sets θ and $\tilde{\theta}$:

$$\frac{C_iR_i + C_eR_i + C_eR_e}{C_iC_eR_iR_e} = \frac{\tilde{C}_i\tilde{R}_i + \tilde{C}_e\tilde{R}_i + \tilde{C}_e\tilde{R}_e}{\tilde{C}_i\tilde{C}_e\tilde{R}_i\tilde{R}_e} \quad (2.41)$$

$$\frac{1}{C_iC_eR_iR_e} = \frac{1}{\tilde{C}_i\tilde{C}_e\tilde{R}_i\tilde{R}_e} \quad (2.42)$$

$$\frac{1}{C_e} = \frac{1}{\tilde{C}_e} \quad (2.43)$$

$$\frac{R_i + R_e}{C_iC_eR_iR_e} = \frac{\tilde{R}_i + \tilde{R}_e}{\tilde{C}_i\tilde{C}_e\tilde{R}_i\tilde{R}_e} \quad (2.44)$$

One can quickly check that the unicity of two transfer functions $\mathbf{H}(s, \theta)$ and $\mathbf{H}(s, \tilde{\theta})$ indeed implies the equality of each individual parameter: the condition of structural identifiability is satisfied.

A second method for structural identifiability analysis of linear models is to express impulse response with its Markov parameters. This was done by [ASK12] for the identification of a multi-zone thermal model, as a preliminary step to study the impact of experimental data quality. A more complete description of this method is available in [Rou18].

Non-linear models

The issue of structural identifiability however applies to all classes of models, and not only RC networks. The identifiability of non-linear models is analysed from the same theoretical basis [BÅ70; GG76]: proving that the input-output relation of the model can only be explained by a single set of parameters. Recent overview articles [GMJ17; Rau+14] provide a list of *a priori* structural identifiability analysis methods. Particularly, [GMJ17] give a particularly clear explanation of the following alternatives, and apply them linear and non-linear models close to those used in building simulation.

- The Taylor series expansion approach was theorised by [Poh78]. It relies on the uniqueness of the coefficients of a Taylor series expansion of the output with respect to time. This philosophy is therefore similar to the impulse response method, except that the model is dealt with in continuous time. There exists an order of differentiation for this series expansion, which coefficients form a non-linear algebraic system of equations in the parameters and from which the structural identifiability may be pronounced. Its solvability is checked by the rank of the Jacobian matrix. As underlined by [Sed01], the order of differentiation in this method is not bound, which can lead to highly complex calculations as the models grow large. The author circumvents the exponential complexity by the use of differential algebra for the series expansion. For this purpose, [Sed01] developed an algorithm available on Maple and later [KAJ12] on Mathematica.
- Based on the differential algebra theory, a global identifiability analysis can be performed for dynamic models described by polynomial or rational equations [Rau+14]. The characteristic set of the differential ideal from the model structure can be used to define a normalized exhaustive summary of the model, which is in essence an implicit description of its input-output behaviour. Showing the injectivity of the exhaustive summary proves the identifiability of the model. Later, [PAD03] developed an algorithm made available by [Bel+07] as the DAISY algorithm. Its easiness of use makes it an interesting tool although it quickly becomes prohibitive for large systems.

To the author's knowledge, there has however been no application of these methods to the field of building energy simulation. A comparative study has however been applied to civil engineering problems by [CCS15].

2.4 Calibration and inference

Let us assume that the first two steps of the procedure have been completed: data have been recorded and processed, and a model structure has been selected and checked for structural identifiability.

Model calibration is seen here as the process of training a model to reproduce some given data. In the following, we will mostly use this term to denote the search for the optimal parameters with which model predictions best fit observations. The expression **model training** describes the same process, but implies that the main use for the trained model will be to forecast predictions beyond the period of observation. Model calibration is a way to allow performing **statistical inference**, i.e. deducing properties of underlying probability distributions behind the data generating process (the building) and its properties, and making decisions. The term of **statistical learning** encompasses data mining, inference and prediction [HTF01].

2.4.1 Ordinary least square estimation for linear regression

As mentioned above, the first criterion on which we may judge model adequacy is the residual sum of squares (RSS) between and observation (column) vector $\mathbf{y}^T = (y_1, y_2, \dots, y_N)$ and the output of the model $\hat{y}_\theta(\mathbf{X}) = \hat{y}(x_i, \theta)$ that was chosen to reproduce it as a function of an input matrix \mathbf{X} and parameter θ .

$$\text{RSS}(\theta) = \sum_{i=1}^N (y_i - \hat{y}(x_i, \theta))^2 \quad (2.45)$$

The input matrix $\mathbf{X} = (X_1, X_2, \dots, X_p)$ has the shape $N \times p$ where N is the number of data points and p the number of input variables. Each of its columns X_j can be a series of N measurements by one sensor, or come from transformations of the original data. Each line $x_i = (x_{i1}, x_{i2}, \dots, x_{ip})$ is a vector of different types of measurements for the i th case.

The ordinary least square (OLS) estimator is the value of θ that minimizes RSS:

$$\hat{\theta} = \operatorname{argmin}_{\theta} \sum_{i=1}^N (y_i - \hat{y}(x_i, \theta))^2 \quad (2.46)$$

The minimum of the sum of squares is found by setting the gradient to zero. There is one gradient equation per parameter of the model:

$$\frac{\partial \text{RSS}}{\partial \theta_j} = -2 \sum_{i=1}^N (y_i - \hat{y}(x_i, \theta)) \frac{\partial \hat{y}(x_i, \theta)}{\partial \theta_j} = 0 \quad (2.47)$$

We will mostly apply ordinary least squares estimation to linear regression models, such as energy signature or co-heating methods. These models can be written in the following vector or matrix forms:

$$y_i = \theta_0 + \sum_{j=1}^p X_{ij} \theta_j + \varepsilon_i \quad (2.48)$$

$$\mathbf{y} = \mathbf{X}\theta + \boldsymbol{\varepsilon} \quad (2.49)$$

where $\varepsilon_i \sim \mathcal{N}(0, \sigma)$ is a series of unobserved, uncorrelated random variables which account for influences other than the explanatory variables x_i . The residual sum of squares (Eq. 2.45) for this type of model can be written as:

$$\text{RSS}(\theta) = (\mathbf{y} - \mathbf{X}\theta)^T (\mathbf{y} - \mathbf{X}\theta) \quad (2.50)$$

Solving the ordinary least-squares criterion (Eq. 2.47) then leads to a closed-form expression for the estimated value of the unknown parameter vector θ and its covariance matrix:

$$\hat{\theta} = (\mathbf{X}^T \mathbf{X})^{-1} \mathbf{X}^T \mathbf{y} \quad (2.51)$$

$$\text{cov } \hat{\theta} = \sigma^2 (\mathbf{X}^T \mathbf{X})^{-1} \quad (2.52)$$

2.4.2 Maximum likelihood estimation

Maximum likelihood estimation (MLE) is a method of estimating the parameters of a probability distribution by maximizing a likelihood function. An example of likelihood function is given by Eq. 2.29 as the outcome of the Kalman filter algorithm that iteratively predicts the next state of a state-space model. A state-space model is indeed a statistical model, as the states it predicts are defined by probability distributions, and the parameters θ are the parameters of these probability

distributions. The estimation of θ can be conducted through two statistical paradigms: maximum likelihood estimation, also referred below as the frequentist approach, and Bayesian inference (see Sec. 2.4.3).

The frequentist approach considers that parameter estimation will asymptotically converge towards the true values θ^* as the number of observations grow [BB04; Bet18]. This means that given a model that perfectly characterizes the system, its parameters will converge with certainty to the correct target values θ^* at a \sqrt{n} rate, \sqrt{n} being proportional to the width of the uncertainty band. So in theory, the larger the dataset, the narrower the estimation interval, hence the closer to the correct target values.

The assumption of asymptotic behaviour also means that refining the state of information will be done from the data only. Physical expectations on the parameter values or prior information bear no pertinent information compared to the observed data. Model calibration in a frequentist approach consists therefore in determining the probability density of the set of parameters θ from the data y only: $p(\theta|y)$. This measure is called the likelihood $L_y(\theta)$.

Given the asymptotic behaviour of the parameter estimation, the likelihood is often considered to have a Gaussian shape. The calibration procedure is then much simplified as it suffices to determine the only point around which the likelihood is maximum. Variances and covariances are then approximated thanks to the Gaussian-shape assumption. Model calibration is therefore simplified to a simple maximization numerical problem or to a minimization problem when the negative logarithmic likelihood is considered, which is numerically simpler to solve.

Among many existing methods, see reviews by [WP97] or [Tar05], steepest-descent methods are proven to be numerically effective. Starting from θ_k at iteration k and given a certain radius α around θ_k , the idea is to find the direction within said radius that gives the largest change in the likelihood. Finding the maximum of L therefore means finding the direction around θ_k that induces the largest growth in $L_y(\theta)$. The algorithm continues until no radius however small produces any improvement on L , which is where the maximum likelihood estimator $\hat{\theta}_{ML}$ is found. To avoid flat regions upon initialisation randomly far from the optimum, it is best to minimize $-\log L$ than to maximize L as it transforms a Gaussian-shaped objective into a nicer paraboloid shaped objective (Mosegaard and Tarantola, 2002).

Descent methods are proven to be effective because they use the derivatives of around θ_k to find the steepest direction. The first and second derivatives may be given analytically as in the Newton methods, or may be numerically estimated as in the quasi-Newton methods. The BFGS algorithm, standing for Broyden, Fletcher, Goldfarb, and Shanno its discoverers, is a popular quasi-Newton method when the derivatives to the second order of the objective function L are not known. The BFGS algorithm has in this context superlinear convergence rate, i.e. faster than a linear convergence, which is a desirable property for finding in a reasonable number of iterations an acceptable estimation of the optimum. The BFGS algorithm is implemented in Matlab, R and Python. For the latter, the CTSM-R library uses a BFGS algorithm for RC models structures estimation, as well as the pySIP library [RR19] that uses the SciPy library for its BFGS algorithm in the optimize.minimize function.

2.4.3 Bayesian inference

In Bayesian estimation, the unknown parameters are treated as random variables with a certain prior distribution $p(\theta)$, which represents the prior belief before looking at the data. Then, all the information available in the data is summarized in the likelihood function $p(y_{1:N}|\theta)$. The prior belief and the data information are combined in the Bayes' theorem to compute the posterior distribution:

$$p(\theta|y_{1:N}) = \frac{p(y_{1:N}|\theta)p(\theta)}{p(y_{1:N})} \propto p(y_{1:N}|\theta)p(\theta) \quad (2.53)$$

where $p(\theta|y_{1:N})$ is a constant which does not need to be computed and ensures that $p(\theta|y_{1:N})$ is a probability density function.

When it is not possible or not computationally efficient to sample directly from the posterior distribution, Markov Chain simulation is used to stochastically explore the typical set (Gelman et al. (2013)). Markov chains used in Markov Chains Monte Carlo (MCMC) methods are designed so that their stationary distribution is the posterior distribution. If the chain is long enough, the state history of the chain provides samples from the typical set $\{\theta_1, \dots, \theta_N\}$

Metropolis-Hastings

Algorithm 1 Metropolis Hastings algorithm

```

1: for  $n = 1 \dots N$  do
2:   Draw a new value from a proposal distribution  $g$ 
3:    $\theta' \leftarrow g(\theta'| \theta_{n-1})$ 
4:   Compute the marginal likelihood using a Kalman filter (for linear models):
5:    $(p(\mathbf{x}_{1:T} | \theta, \mathbf{y}_{1:T}), L_y(\theta')) \leftarrow \text{KALMANFILTER}(\theta')$ 
6:   Accept or reject the proposal:
7:    $\alpha \sim U(0, 1)$ 
8:   if  $\alpha \leq \frac{L_y(\theta') p(\theta') g(\theta_{n-1} | \theta')}{L_y(\theta_{n-1}) p(\theta_{n-1}) g(\theta' | \theta_{n-1})}$  then
9:      $\theta_n \leftarrow \theta'$ 
10:    else
11:       $\theta_n \leftarrow \theta_{n-1}$ 
12:    end if
13:  end for

```

The Marginal Metropolis Hastings (MMH) algorithm is part of the family of Markov Chain Monte Carlo (MCMC) methods. It calculates a finite sequence of samples $\{\theta_n, n \in 1 \dots N\}$ approximating the posterior distribution. Algorithm 1 employs a Kalman filter to compute the states $p(\mathbf{x}_{1:T} | \theta, \mathbf{y}_{1:T})$ and likelihood $L_y(\theta)$ associated to each proposal for θ . If the state-space model is non-linear, this filter can be replaced by a particle filter: this approach is known as Particle Markov Chain Monte Carlo (PMCMC) [ADH10].

The choice of the proposal distribution g , and a good initialisation, are critical for the performance of the algorithm. A burn-in phase at the beginning of the Markov chain must be discarded as it does not reflect the posterior distribution. [RG18] construct the proposal distribution by using the gradient and Hessian of the posterior, calculated by differentiation of the Kalman filter equations. Alternatively, the Adaptive Metropolis Hastings algorithm is used by [RRO18].

Sequential Monte Carlo

We now consider the procedure for on-line parameter estimation. The target is to construct a sequence of posterior distributions $\{p(\theta|y_{1:t}), t \in 1 \dots T\}$, one for each observation point, that will allow us to visualize the information gained during the experiment in real time.

The SMC algorithm for parameter estimation is an adaptation of particle filtering for state variables. The foundation of this method is the Importance Sampling paradigm as described by [CGM07]: simulating samples under an instrumental distribution and then approximating the target distributions by weighting these samples using appropriately defined importance weights. The reader is referred to [CGM07] and [Kan+15] for a deeper explanation of SMC and its application to parameter estimation. The method used here is inspired from the Iterated Batch Importance Sampling algorithm [Cho02]. It is described in Fig. 2.7 and Algorithm 2.

The algorithm starts with the generation of a population of N_θ particles drawn from a prior distribution $p(\theta)$. Each parameter is assigned an initial state \mathbf{x}_0 and weight. At each time step

Algorithm 2 Sequential Monte Carlo algorithm

1: **Initialisation:** generate a population of N_θ particles, their states and weights
 2: **for all** $j \in \{1 \dots N_\theta\}$ **do**
 3: $\theta_0^{(j)} \sim p(\theta)$
 4: $\mathbf{x}_0^{(j)} \sim p(X_0)$
 5: $\omega_0^{(j)} = 1$
 6: **end for**
 7: **for** $t = 1 \dots T$ **do**
 8: **for all** $j \in \{1 \dots N_\theta\}$ **do**
 9: **Resampling**
 10: $\{a_j, j \in 1 \dots N_\theta\} \leftarrow \text{MULTINOMIAL}\left(\omega_{t-1}^{(j)}, j \in 1 \dots N_\theta\right)$
 11: **Rejuvenation** by a single MMH step with proposal distribution $\mathcal{N}(\hat{\mu}_{t-1}, \hat{\Sigma}_{t-1})$
 12: $(\theta_t^{(j)}, \mathbf{x}_{0:t-1}^{(j)}, L_{t-1}^{(j)}) \leftarrow \text{MMH}\left(\theta_{t-1}^{(a_j)}, \mathbf{x}_{0:t-1}^{(a_j)}, \mathbf{y}_{0:t-1}\right)$
 13: **Propagate and weight**
 14: $(\mathbf{x}_t^{(j)}, L_t^{(j)}) \leftarrow \text{KALMANFILTER}\left(\mathbf{x}_{t-1}^{(j)}, \theta_t^{(j)}, \mathbf{y}_t\right)$
 15: where $L_t^{(j)} = p(\mathbf{y}_t | \mathbf{x}_{t-1}^{(j)}, \theta_t^{(j)})$ is the incremental likelihood.
 16: $\omega_t^{(j)} = \omega_{t-1}^{(j)} \cdot L_t^{(j)}$
 17: **end for**
 18: Normalise weights
 19: $\omega_t^{(j)n} = \omega_t^{(j)} / \sum_{j=1}^{N_\theta} \omega_t^{(j)}$
 20: Calculate weighted mean and covariance of parameters
 21: $\hat{\mu}_t = \sum_{j=1}^{N_\theta} \omega_t^{(j)n} \theta_t^{(j)}$
 22: $\hat{\Sigma}_t = \sum_{j=1}^{N_\theta} \omega_t^{(j)n} (\theta_t^{(j)} - \hat{\mu}_t) (\theta_t^{(j)} - \hat{\mu}_t)^T$
 23: **end for**

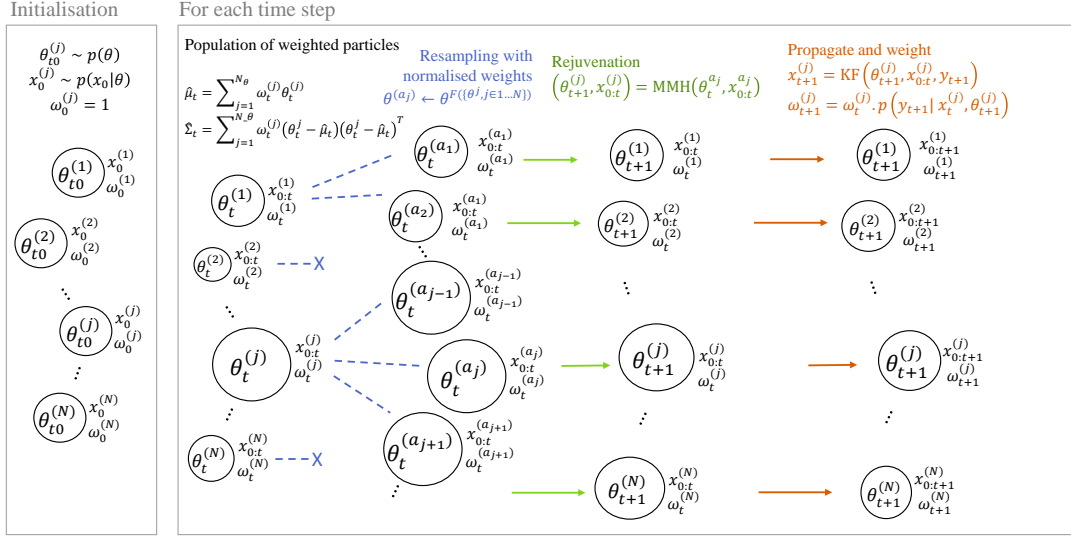


Figure 2.7: Principle of the SMC algorithm

t , a Kalman filter computes the states $\mathbf{x}_t^{(j)}$ and likelihood $L_t^{(j)}$ associated to each particle $\theta_t^{(j)}$. If the state-space model is non-linear, this filter can be replaced by a particle filter: this approach is known as the SMC² algorithm [CJP13]. By this operation, the population of particles is updated so that at each time t they are a properly weighted sample from $p(\theta|y_{1:t})$ [CJP13]. After several time steps, there is a risk that only a few of the initial N_θ particles are significantly more likely than the others and concentrate the majority of the total weight: a resampling step is then performed in order to generate a new population of particles from the most influential ones, and a MCMC rejuvenation step then restores the diversity of particles [Mur13].

Resampling does not occur every time a new observation becomes available, but only when required: this is measured by the effective number of particles that significantly contribute to the total weight of all particles [Mur13]. This operation decreases the number of unique particles, hence the subsequent rejuvenation step that restores diversity. The choice of $\mathcal{N}(\hat{\mu}_t, \hat{\Sigma}_t)$ as the proposal distribution for the MCMC rejuvenation step was proposed by [Cho02] and ensures a reasonable acceptance ratio while leaving $p(\theta|y_{1:t})$ invariant. The rejuvenation step makes the algorithm quite computationally expensive, since the total likelihood of all particles $p(y_{1:t}|\theta)$ must be recalculated every time resampling occurs. This problem is mitigated by the fact that particles can be resampled independently, making this effort parallelisable.

Hamiltonian Monte Carlo

The hamiltonian Monte Carlo algorithm suppresses the random walk behavior by borrowing an idea from physics. Metaphorically, the vector of parameters represents the position, \mathbf{q} , of a frictionless particle which follows a physical path determined by the curvature of the posterior distribution. In order to mimic this behavior, the algorithm introduces auxiliary momentum parameters, \mathbf{p} , to the

parameters of the posterior distribution, \mathbf{q} , with the joint probability distribution

$$\begin{aligned}\pi(\mathbf{q}, \mathbf{p}) &= \pi(\mathbf{p}|\mathbf{q})\pi(\mathbf{q}) \\ &= \exp[\log\pi(\mathbf{p}|\mathbf{q}) + \log\pi(\mathbf{q})] \\ &= \exp[-K(\mathbf{p}, \mathbf{q}) - V(\mathbf{q})] \\ &= \exp[-H(\mathbf{p}, \mathbf{q})]\end{aligned}\tag{2.54}$$

where $H(\mathbf{p}, \mathbf{q}) = K(\mathbf{p}, \mathbf{q}) + V(\mathbf{q})$ is the Hamiltonian function, $K(\mathbf{p}, \mathbf{q})$ the kinetic energy and $V(\mathbf{q})$ the potential energy. The value of the Hamiltonian represents the energy of the system (Betancourt 2017a).

A new state is generated by first sampling from the conditional distribution over the momentum:

$$\mathbf{p} \sim \pi(\mathbf{p}|\mathbf{q})\tag{2.55}$$

and then simulating the Hamiltonian dynamics for some time, t , with the Hamilton's equations

$$\frac{d\mathbf{q}}{dt} = +\frac{\partial H}{\partial \mathbf{p}} = \frac{\partial K}{\partial \mathbf{p}}\tag{2.56}$$

$$\frac{d\mathbf{p}}{dt} = -\frac{\partial H}{\partial \mathbf{q}} = -\frac{\partial K}{\partial \mathbf{q}} - \frac{\partial V}{\partial \mathbf{q}}\tag{2.57}$$

$$(2.58)$$

Hamilton's equations generate trajectories which conserve the value of the Hamiltonian, which means that every Hamiltonian trajectory is confined to an energy level set [Bet17]. The frictionless particle can move rapidly and even turn corners in the parameter space to preserve the energy of the trajectory [Gel+13]. Furthermore, the gradient of the logarithm of the posterior distribution, $\partial v/\partial \mathbf{q}$, guides the Markov chain along regions of high probability mass which provides an efficient exploration of the typical set. Unfortunately, it is seldom possible to generate Hamiltonian trajectories analytically, and the Hamilton's equations must instead be integrated numerically. This is possible via the *leapfrog* integrator [Rad12]

2.5 Validation and diagnosis



The present section is part of the article [Rou18] written by the author.

Let us suppose that the user has gathered measurement data $\mathbf{z} = (\mathbf{u}, \mathbf{y})$, chosen a numerical model and its parameterisation θ to depict the observed phenomena, checked for theoretical identifiability, and run a parameter estimation algorithm in either the least-squares or maximum likelihood framework, to obtain an estimate $\hat{\theta}$ and its covariance matrix $\text{cov}(\hat{\theta})$. Let us now address how the results of an inverse problem solved with one model type and one data set can be validated.

Once the parameter estimation is complete, several steps should be followed to make sure the results are usable. These steps are listed by [Mad16] for both model selection and validation, and fall within three categories.

- **Tests on the parameter estimates.** This is to make sure that the chosen model structure is appropriate and does not include redundant parameters. It is especially important in characterisation studies, where the parameter values are the sole target of the identification. Practical identifiability is a measure of the information truly gained by the model from the experiment, and helps identify how much each parameter has been updated by observations.

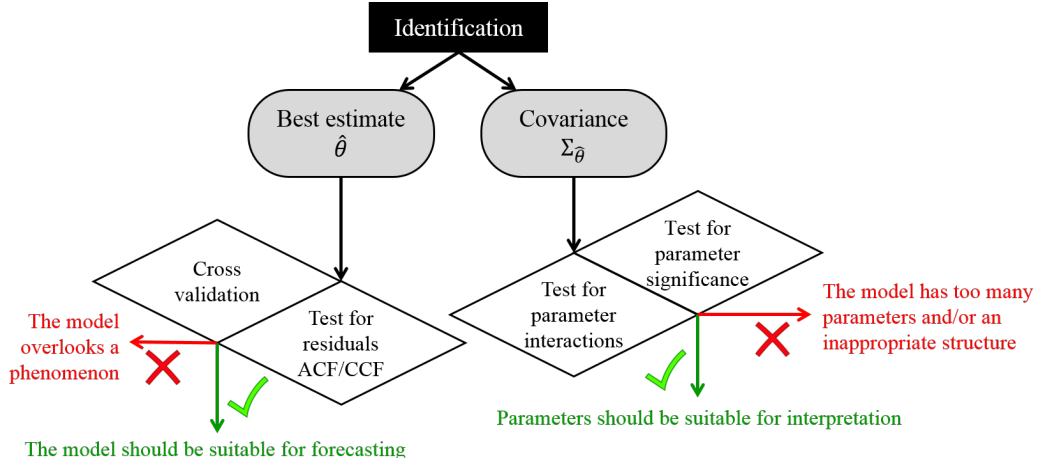


Figure 2.8: Validation steps

- **Tests on the model output** and residuals. This is to make sure that the model complexity is sufficient to replicate the observations, and can be trusted to simulate the reality with different initial and boundary conditions. It is especially important if the target of the system identification study is to establish a predictive model.
- **Out-of-sample validation** of the predicted output using a different dataset than the one used for training.

In addition to checking model validity, these steps allow establishing a diagnosis of which improvements can be brought to the model.

2.5.1 Parameter confidence regions

In this part, the analysis concerns mostly the covariance matrix of the estimate $\text{cov}(\hat{\theta})$, which can for instance be calculated by Eq. 2.52 in the least-squares estimation. The covariance matrix is related to the correlation matrix $\mathbf{R}_{\hat{\theta}}$ by:

$$\text{cov}(\hat{\theta}) = \sigma_{\hat{\theta}} \mathbf{R}_{\hat{\theta}} \sigma_{\hat{\theta}} \quad (2.59)$$

where $\sigma_{\hat{\theta}}$ is a diagonal square matrix containing the standard deviation $\sigma_{\hat{\theta}_i}$ of each individual parameter $\hat{\theta}_i$. The matrices $\mathbf{R}_{\hat{\theta}}$ and $\sigma_{\hat{\theta}}$ are the basis for testing for superfluous parameters in the model.

A preliminary sensitivity analysis performed before parameter estimation does not guarantee that the confidence intervals and regions of estimates are finite. Such an analysis is performed either globally (for Monte-Carlo and sampling-based methods) or locally near an initial guess value of the parameters. In either case, its outcome cannot precisely depict the uncertainty ranges of parameters near the estimate $\hat{\theta}$ obtained by the identification.

The first criterion for validating parameter estimates is their individual significance. A low influence of a parameter on the model output results in low values of the sensitivity matrix $\mathbf{S} = (\partial -\log L_y(t_i, \theta_j)/\partial \theta_j)$ or information matrix $\mathbf{F} = \mathbf{S}^T \mathbf{S}$, which translates into high values in the diagonal of the covariance matrix (Eq. 2.59). It is important to note that the calculation of the covariance matrix depends on the data: it only measures whether parameters are significant **in the conditions of the experiment**. The marginal significance of a parameter is evaluated by comparing its absolute value $|\hat{\theta}_i|$ with its standard deviation $\sigma_{\hat{\theta},i}$. It can be done by a simple comparison of both, or with a t-test for statistical significance: [Lju98; Mad07] use the value of the standard deviation $\sigma_{\hat{\theta},i}$ to test the hypothesis H_i that $\hat{\theta}_i$ is statistically significant, against the hypothesis H_0 that it is

not. Alternatively, the confidence interval of a single parameter can be approached by the value of its diagonal term in the covariance matrix.

The second criterion for validating parameters is the lack of serious correlations between estimates. The correlation matrix \mathbf{R}_θ has coefficients between -1 and 1, indicating pairwise coupled effects of parameters on the model output. A high correlation between two parameter estimates means that the model structure should be revised or that one of the parameters should be fixed to an assumed value. A statistically insignificant parameter may disturb the estimation of more important parameters it interacts with: it is generally stated that if a parameter is found to be either insignificant or strongly correlated with another, it should be removed from the model and the estimation should be conducted once more [Mad16; PG03].

Perhaps the most informative way to assess the practical identifiability of a model is the display of confidence regions and intervals for its parameter estimates. A likelihood-based method of setting these regions is described by [ME95; Rau+09] as the likelihood ratio test and is briefly summarised here. Suppose a model of p parameters θ which exhibit some interaction. We want to draw the confidence regions for a subset θ_1 of the parameters of length p_1 , with the remaining parameters denoted θ_2 , in order to see if this region is finite and the model identifiable. If the maximum likelihood estimator $\hat{\theta}_{ML}$ has been identified, the likelihood ratio function is defined by:

$$R(\theta_1) = \max_{\theta_2} \left[\frac{L_y(\theta_1, \theta_2)}{L_y(\hat{\theta})} \right] \quad (2.60)$$

A property of the likelihood ratio test is that $-2 \ln [R(\theta_1)]$ asymptotically follows a χ^2 distribution with p_1 degrees of freedom [ME95]. An approximate $100(1 - \alpha)\%$ likelihood-based confidence region for θ_1 is the set of all values such that:

$$-2 \ln [R(\theta_1)] < \Delta_{1-\alpha, p_1}^2 \quad (2.61)$$

where $\Delta_{1-\alpha, p_1}^2$ is the $1 - \alpha$ quantile of the χ^2 distribution with p_1 degrees of freedom. Note that this test can be performed after a deterministic parameter estimation, by using the sum of squared residuals instead of the likelihood function:

$$-2 \ln \left[\frac{L_y(\theta)}{L_y(\hat{\theta})} \right] = \frac{1}{\sigma^2} (r^2(\theta) - r^2(\hat{\theta})) \quad (2.62)$$

From this theory of asymptotic likelihood-based confidence regions, [Rau+09] proposed the definition of the profile likelihood function $\chi_{PL}^2(\theta_i)$ of a single parameter θ_i as an a posteriori way to check its structural and practical identifiability. This function is defined as the likelihood ratio in the particular case of a single explanatory parameter:

$$\chi_{PL}^2(\theta_i) = \max_{j \neq i} \left[\frac{L_y(\theta_i, \theta_j)}{L_y(\hat{\theta})} \right] \quad (2.63)$$

As written by [Rau+09]: structurally non-identifiable parameters are characterized by a flat profile likelihood. The profile likelihood of a practically non-identifiable parameter has a minimum, but is not exceeding a threshold $\Delta_{1-\alpha}$ for increasing and/or decreasing values of θ_i (here, $\Delta_{1-\alpha}$ is the $1 - \alpha$ quantile of the χ^2 distribution with one degree of freedom). As an example, the 95% confidence interval of a single parameter θ_i is the interval of values so that $\chi_{PL}^2(\theta_i)$ does not exceed the threshold $\Delta_{1-95\%} = 3.84$.

A comprehensive application of this theory in a building physics application was proposed recently by [DR17] to measure the identifiability of parameters of several RC models describing the thermal characteristics of a building component. Results reveal large differences in the practical

identifiability of models between winter and summer conditions: this underlines the importance of the richness of excitation data on the results of an inverse problem, independently from the model structure. Two-dimensional confidence regions can also be shown by applying Eq. 2.61 to pairwise parameter combinations: these regions can be plotted in the form of a correlation matrix enriched with precise confidence thresholds [Rau+09].

2.5.2 Residual analysis

The most straightforward way to check for the validity of a calibrated model is a visual comparison between measurements and simulations that takes into account both the measurements noise and the model input data uncertainties. The agreement between model and reality is stated to be good when a significant overlapping is observed between simulations and measurements uncertainty bands [PG03]. Note that this statement also holds for a white-box model where parameters are not the outcome of an inverse problem: the validation of such a model should meet these standards as well.

However, a more systematic analysis of the residuals is often preferable. Statistical tools to compare measurements and simulations can be used to assess the validity of the model after calibration. The following steps were recommended for all model validation procedures during the PASSYS project by [PMM91]. Let us focus on the definition of the residuals calculated from the calculation of any of the estimates $\hat{\theta}$ defined above:

$$r(t) = y(t) - \hat{y}(t, \hat{\theta}) \quad (2.64)$$

Residuals from an ideal unbiased model should behave like white noise, i.e. a stochastic process that approaches a stationary normal distribution with zero mean. In time series analysis, the stationarity of this stochastic process can be checked if its mean and variance do not vary over different time periods. Another method is to use the normalized autocorrelation function (ACF) of residuals:

$$\text{ACF}_r(\tau) = \frac{1}{\sigma_r^2} E[(r(t) - \mu_r)(r(t + \tau) - \mu_r)] \quad (2.65)$$

where μ_r and σ_r^2 are the mean and variance of the process (the residual). The ACF measures the average correlation between points separated by a lag τ within the time series. The ACF of a true white noise signal is zero for all lags other than zero. The whiteness test on the ACF is the first statistical test in residual analysis [PMM91]. The second test is the independence test described below.

The criterion of white noise residuals is very difficult to meet in practice [KSS13] as all models include hypotheses and approximations in addition to measurement uncertainty. Furthermore, numerically high values of the ACF do not precisely point out the source of model inadequacies. Enter the cross-correlation function (CCF):

$$\text{CCF}_{r,u}(\tau) = \frac{1}{\sigma_r \sigma_u} E[(r(t) - \mu_r)(u(t + \tau) - \mu_u)] \quad (2.66)$$

The CCF checks if the residuals are correlated with any of the input processes u . Should a significant cross-correlation with one of the inputs be found, then it is likely that this input is improperly accounted for in the model [Mad07]. Ideally, a correct model structure should not yield any cross-correlation between residual and input signals. Statistical tests to meet the independence criterion are described by [PMM91].

A strong residual ACF does not necessarily imply that an input is being overlooked. An example of model which checks the independence test (CCF) but fails the whiteness test (ACF) is shown by [KSS13]. The satisfying low values of the CCF suggest that no input is missing in the model. By

adding an error model to the model structure, the authors then saw the ACF fit within a reasonable bandwidth. According to [Lju98], the ACF obtained from a model missing an error model is less likely to meet the whiteness test. Other examples of residual analysis for model validation include:

- [JMA08] apply residual analysis to the validation of different ARX and ARMAX models in a numerical study: these models include error models.
- [RDS14] identify reduced-order models of buildings on reference simulations from a detailed physical model. The reduced-order models are described by stochastic differential equations. The authors analyse the cumulated periodograms (this is equivalent to analysing the ACF) to pick the necessary complexity of reduced models.
- [JK17] draw ACF and CCF profiles after estimation in a deterministic agent-based framework and found relatively high values for these functions.

The overall conclusion is that deterministic grey-box modelling is unlikely to meet the standards for the whiteness test of residuals. In a deterministic context, a good overlap between confidence regions of predictions and observations is often a sufficient criterion for judging that a model structure is appropriate.

2.5.3 Cross-validation

The result of an inverse problem is the set of parameters $\hat{\theta}$ with which a specific model \hat{y} offers the closest fit to the training data. The goal of system identification is however to build a model which accurately predicts the outcome of new input conditions. The generalization performance of a model relates to its prediction capability on independent test data [HTF01]. Estimating this prediction error is the first step towards the selection of the appropriate model complexity to represent the reality. A complex model will make more use of the training data than a simple model: its average training error will be lower, but the covariance of the parameter estimates $\text{cov}(\hat{\theta})$ will be higher, hence so will the variance of output predictions over the test dataset. There is a model complexity threshold over which decreasing the training error means increasing the generalization error: such a model is overfitted and has a poor prediction performance.

Expected prediction errors $E \left[(y - \hat{y}(u))^2 \right]$ can be decomposed into two main components: the squared bias and the variance [HTF01]. As a reminder, the hypothesis of additive Gaussian measurement noise still holds: $y(t) = y^*(t) + \varepsilon(t)$ with $\varepsilon \sim \mathcal{N}(0, \sigma)$.

$$\underbrace{E \left[(y - \hat{y}(u))^2 \right]}_{\text{Expected prediction error}} = \underbrace{(E[\hat{y}(u)] - y^*)^2}_{\text{Bias}^2} + \underbrace{E \left[(\hat{y}(u) - E[\hat{y}(u)])^2 \right]}_{\text{Variance}} + \sigma^2 \quad (2.67)$$

The squared bias is the deviation between the average estimation $E[\hat{y}(u)]$ and the real, noise-free value of the output y^* . This term should be equal to zero under the hypothesis of an unbiased model $y^*(t) = \hat{y}(t, \theta^*)$. This hypothesis is however very optimistic in practice and requires a model with a large number of degrees of freedom (parameters). The variance is the expected deviation of the prediction $\hat{y}(u)$ around its mean. It can be evaluated by propagating the parameter uncertainty $\text{cov}(\hat{\theta})$ into an output uncertainty. The last term is an irreducible error due to the measurement noise. Fig. 2.9 illustrates the bias-variance tradeoff in the search of the lowest prediction error.

Evaluating the exact prediction error requires a separate dataset from the one used for training purposes. Cross-validation is a convenient way to assess the generalization ability of a model by splitting the original dataset in several samples. The most intuitive approach is the holdout method which splits the original data in two sets (Fig. 2.10(a)): a training set used to fit the model (typically two thirds of the original data) and a test set for its validation. Alternatively, k -fold cross-validation (Fig. 2.10(b)) splits the original sample into k subsamples. $k - 1$ samples are used as training data while the remaining sample is used as validation data. The process is then repeated k times by using each subsample once for validation. This method can give estimates of the variability of the true

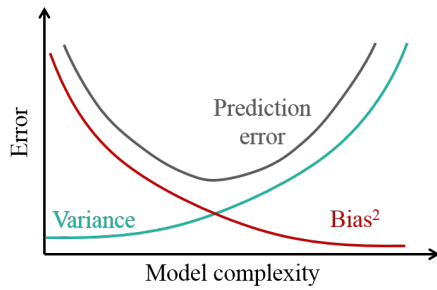


Figure 2.9: Bias-variance trade off

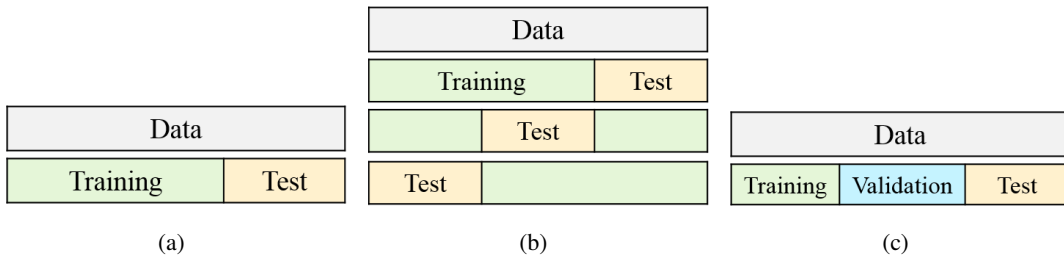


Figure 2.10: Splitting data for cross-validation

estimation error. In a data-rich situation, the best approach is to split the dataset into three parts [HTF01] as shown on Fig. 2.10(c): a training set used to fit the models; a validation set used to estimate prediction error for model selection; a test set to assess the generalization error of the selected model.

3. Numerical benchmark

 This chapter summarises the main parts of the Ph.D. thesis of Sarah Juricic.

3.1 Numerical model assessment methodology for physical interpretability

In the perspective of using stochastic RC models to infer thermal performance estimation of a building from nonintrusive measurements, it would be desirable to assess the extent to which RC models are physically interpretable. In literature, interpretability of a model is done case by case on the basis of expert knowledge of the tested building, such as in [BR14; CM18] or on a numerical simulated building energy model as in [DR17; Sen+20]. Extrapolating the validity of the models to other test cases is risky, all the more so as the data used in non intrusive measurements poorly informative and possibly biased. In addition, exploiting actual on-site measurements brings other issues which make inference of interpretability tricky: effect of initial conditions and thermal states of the building, including thermal inertia, duration possibly not as long as necessary, limited measurements although necessary for better knowledge of the building behaviour.

This section proposes therefore a numerical model assessment framework aiming at:

- creating a realistic building simulation environment to synthetically generate datasets for models to be trained,
- proposing an accurate target value of thermal performance of the building envelope and its components,
- assessing the physical interpretability of any model calibrated by a robust indicator,
- comparing in a common framework the interpretability of different models,
- providing the possibility to assess the interpretability of a model in variable configurations, as to verify repeatability of a calibration and to a certain extent generalisation of the results.

Section 3.1.1 first exposes the principles of the framework for model assessment while detailing how the proposed framework alleviates the issues attached to the realism of numerical simulations. Section 3.1.1 also details the case study simulated in the framework and in the end used to generate synthetic data. Section 3.1.2 describes how to assess a model with respect to the physical interpretability of its thermal performance estimation.

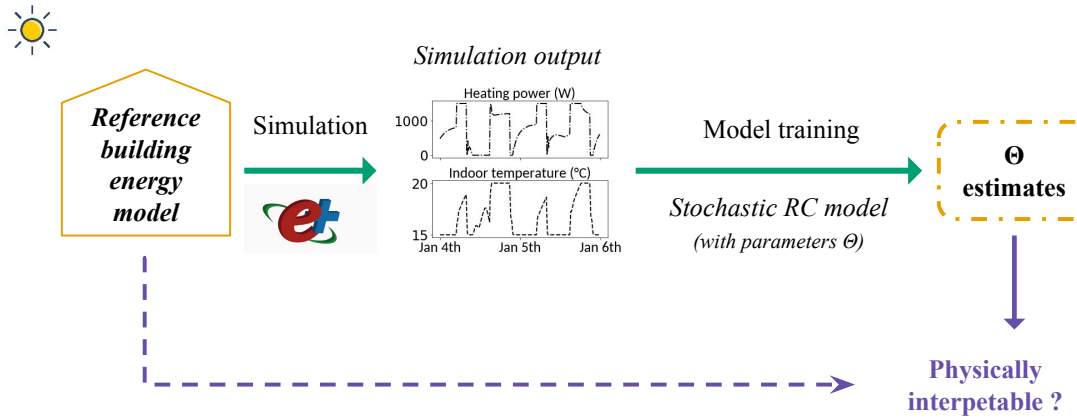


Figure 3.1: Principle of a numerical framework for model assessment: a numerical building energy comprehensive model generates synthetic data that serves as training data for an RC stochastic model. The calibration outcome is compared to the theoretical properties of the building of the numerical model.

3.1.1 A numerical assessment framework for physical interpretability

The objective of a numerical framework for model assessment is to act as a sort of test-bed: the framework should recreate a non intrusive experiment as close to reality as possible to provide realistic synthetic datasets that serve as training data for the model under study.

To be of use, benchmark studies should avoid common pitfalls that prevent the generalization of the results [Kre19]. The recommendations in [Kre19] are concededly intended for optimization algorithms but are still valid for the present application, with in particular the following pitfalls:

- relying on an unrealistic setup: ideal measurements (no systematic error, no measurement error),
- use the same model for data generation as for calibration (cf. the "inverse crime" from [KS07]),
- not generalisable to other building configurations and typologies.

Proposition for a numerical assessment framework

The proposed model assessment framework is shown in Figure 3.1. A comprehensive highly detailed building is modelled in the EnergyPlus software (see Section 3.1.1). It is defined with a number of physical properties (scalars), the quantity of interest, that the model under study estimates. From a given weather dataset, EnergyPlus performs a dynamic thermal simulation from which are extracted the output necessary to the calibration of the model under study, stochastic RC models in the present application.

Model calibration delivers either posterior distributions of the parameters (Bayesian approach) or parameter estimations with Gaussian error assumption (frequentist approach). Either way, the results can then be compared to the physical properties of the comprehensive model from where interpretability can be assessed. An assessment framework is detailed in section 3.1.2.

The basic procedure described in Figure 3.1 assesses the interpretability of one model, but only on the basis of synthetic data from a single building energy model. Let us here underline that the model "tested" should actually be the model that best fits the generated data in the sense of the validation workflow in section 2.5. Indeed, it makes no sense to calibrate and assess a model that would not pass the validation workflow. Instead, for a given synthetic dataset, an appropriate model is selected and then assessed. This does in any case not provide generalisable outcome as it remains

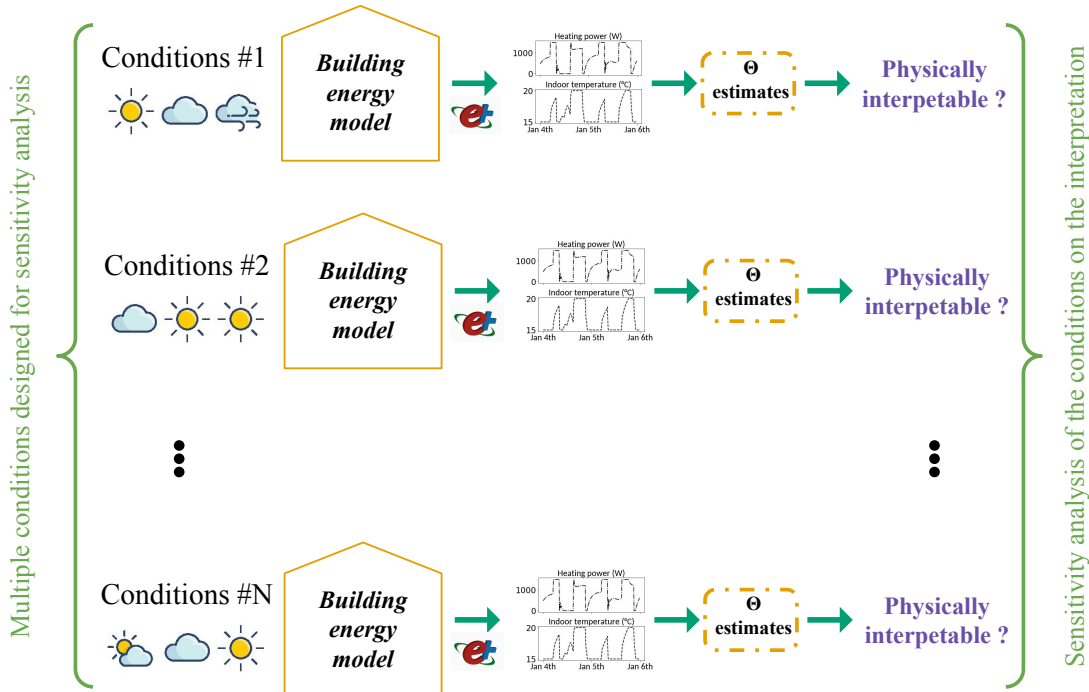


Figure 3.2: Building energy model simulations in variable conditions: the overall framework assesses to what extent a stochastic RC model is robust and coherent to variations of the numerical building energy model. Variable simulation conditions can be weather related for repeatability assessment (as illustrated here) or can be envelope related for physical meaning of the parameters of the RC model.

too case-specific.

The assessment therefore rather relies on a larger framework, where boundary conditions or physical properties of the envelope vary. The idea is illustrated in Figure 3.2. Each stochastic RC model is assessed for its physical interpretability from a coherent set of hundreds of datasets. The variations focus then either on the weather conditions or on the building envelope. The former allows a controlled repeatability assessment and the latter assesses in particular the individual physical interpretability of the model parameters. The model assessment framework has therefore better generalisation ability.

A comprehensive building energy model as reference

The model assessment framework relies on a comprehensive building energy computer model, from now on called *reference model*. The reference model needs to be as detailed as possible in order to depict realistic thermal dynamics.

Relying on a computer model is concededly arguable: it introduces itself a characterization error as it cannot produce data as realistic as actual data, because of discretization of the heat equation and simplifications of some phenomena. The validity of this work relies on the hypothesis that the reference model in EnergyPlus is yet detailed enough. It is indeed assumed that although not perfectly realistic, a reference model can be sufficiently detailed to study the aggregation of physical phenomena in RC models and to uncover biased results. Additionally, it does not constitute an "inverse crime", to quote [KS07], as the reference model is more detailed in its description of the building physics than the RC models tested.

The reference model is simulated with the simulation software EnergyPlus. The advantage

of using such software is that it has been proven to be reliable for accurate thermal simulation [Cra+01; NRE16] and it has already been used for the purpose of generating synthetic data in scientific literature including recently and among others [And+17; Fou+13; GRM17; LHS19]. In addition, as mentioned by [Tia+18], the EnergyPlus software has the advantage of using as input file a ASCII file, easily edited with many programming languages.

Various choices can be made for the reference model to account for heat and mass transfer modelling, solar irradiation, etc. The choices made for the reference model are therefore driven by the purpose of this study, i.e. thermal behaviour, but also on the need of reasonable simulation duration as hundreds of simulations are planned for model assessment.

In an effort to use a realistic case study, a multi-zone building energy model inspired by an actual building design has been chosen. The case study has a single storey. With two storeys or more, the issue of temperature discrepancy across the building would have been inevitable. A one-storey building will be less significantly prone to temperature stratification than higher case studies.

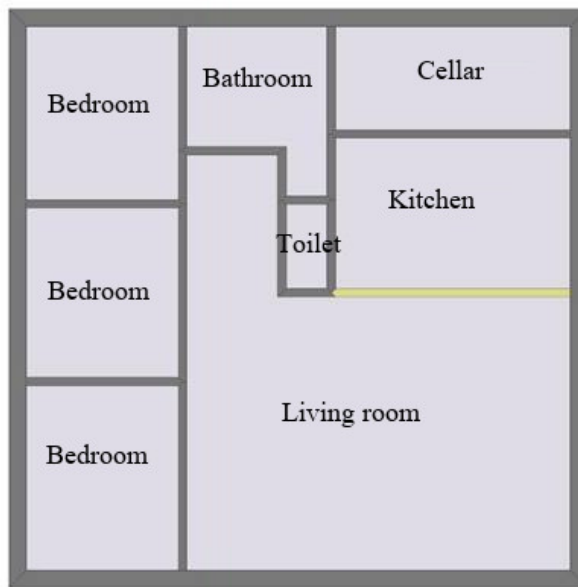


Figure 3.3: Floor plan of the case study used as multi-zone reference model in the application of the model assessment framework

The reference model is a multi-zone building of a one-storey house. Its floor plan is shown in Figure 3.3, where each room is modelled as an independent zone in EnergyPlus. It has unheated crawlspace and attics. The heated space is about $100 m^2$ and is equipped with convective heaters. The composition of the envelope and further details on the hypotheses for systems and ventilation are detailed in [juricic].

3.1.2 Model assessment and comparison : a quantitative indicator

The last step of model assessment consists in assessing how close the estimated thermal performance of the building is to the theoretical target value. As the theoretical thermal performance is accurately known, it is possible to quantify the closeness of the estimation to the target value.

In [Sen+20] for example, such comparison is made with error ε to the target value defined as in equation 3.1 and with a conditional indicator, whether or not the target value is included in the

confidence intervals (with a yes or no answer).

$$\varepsilon = (R_{\text{estimated}} - R_{\text{target}}) / R_{\text{target}} \times 100 (\%) \quad (3.1)$$

Applied in preliminary works [Jur+18; Jur+19], such indicators proved to be limited for model comparison at large scale. Indeed, it is rather inconvenient that the assessment is made by two different values, one of which is not even scalar. Furthermore, it does not properly reflect the desirability of the results, because it compares a single maximum likelihood estimator to the target value, without reflecting on acceptable margins and uncertainty.

Instead, an alternative quantitative indicator is proposed in this work as an attempt to better reflect on the desirability of both the results' accuracy and uncertainty. It is inspired by the Bayesian approach, where parameter estimations are continuous probability densities. It can be extended to the frequentist approach with the assumption of Gaussian distribution. Let us remind that the mode is the most probable value and that the credible set is the Bayesian conceptual version of the frequentist confidence intervals.

Accuracy of the estimation to the target value can then be categorized in the 4 following cases, illustrated in Figure 3.4:

- (1) accurate mode and narrow credible set : the target value falls in the 89 % credible set (or 95 % CS), the mode is close to the target value. This category shows high accuracy and low uncertainties of the estimation. Estimations in this category are the most satisfactory results;
- (2) accurate mode and large credible set : the target value falls in the credible set, but the uncertainties are large ;
- (3) inaccurate mode and large credible set : the target value falls close to the tails of the credible set, meaning that the mode is misleadingly far from the target value but that at least the uncertainties are representative of the informativeness of the data and the model ;
- (4) inaccurate mode and narrow credible set : the least satisfactory result. The model and/or the data give bias to the parameter estimation and the target value does not fall in the credible set, which will mislead the expert examining the data.

To make model assessment and comparison easier, these 4 categories need then to be translated into a metric, which needs to be high for category (1), moderate for categories (2, 3) and low for category (4).

Intuitively, the probability mass around the target value fits this objective. For a discrete probability function, the probability mass at the target value exactly would suffice, i.e. for $X : S \mapsto R$ a discrete random variable, the probability at the target value x is:

$$P(X = x) = P(\{s \in S : X(s) = x\}) \quad (3.2)$$

This work deals with continuous probability density functions and probability density of a continuous variable at the target value is exactly 0 by definition. Instead, the probability density of the volume around the target value is an option, i.e. the probability of random variable X of density f to be between limits a and b :

$$P(a < X \leq b) = \int_a^b f(x)dx \quad (3.3)$$

Figure 3.4 illustrates how a probability density is equivalent to calculating the integral of the posterior density function between a and b , i.e. the area under the curve between a and b being on either sides of the target value. The values taken by this metric are bound between 0 and 1, meeting then the criteria stated earlier. For a category (1) type of posterior distribution, the metric is close to

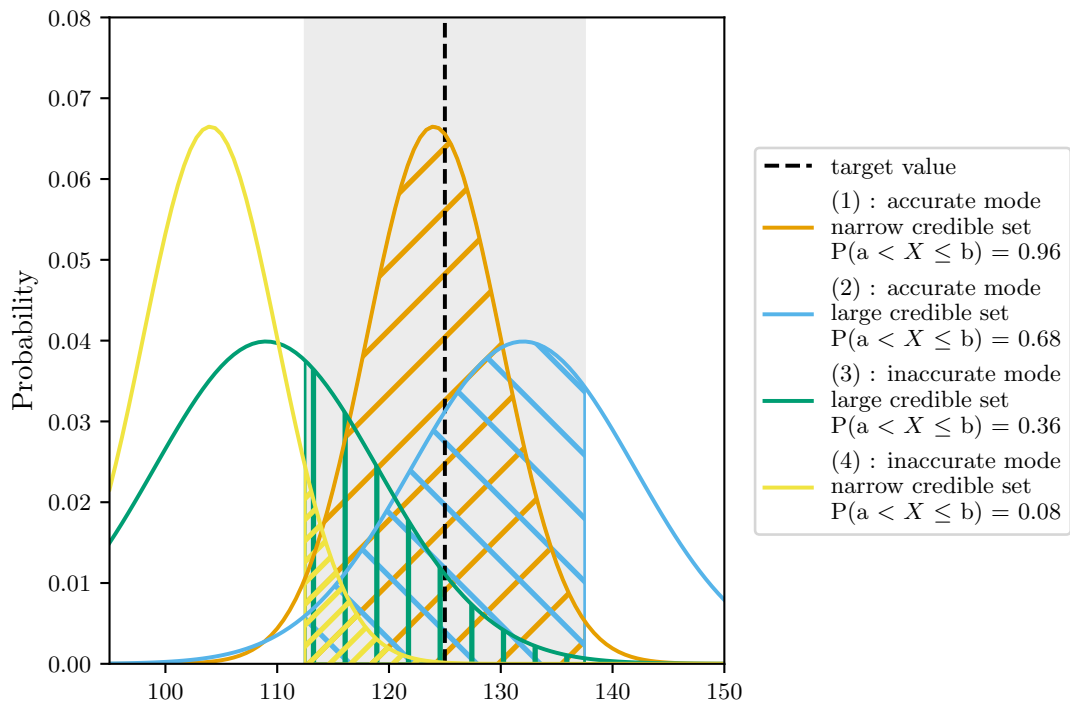


Figure 3.4: Illustration of 4 categories of posterior distributions (synthetic data). Limits a and b defined as for example $\text{target} \pm 10\%$ create a region of interest (in grey) around the target value (dotted black line). The probability of each density to be within these limits (hatched areas) defines a quantitative indicator that takes values between 0 and 1.

1, as in the illustration from Figure 3.4 $P(a < X \leq b) = 0.96$. For categories (2) and (3), the metric will show values around 0.5. Category (4) results are very unlikely and the metric tends to 0.

Another argument in favour of the probability density on $[a, b]$ is that the metric is standardized between 0 and 1 whatever the order of magnitude of the target value, therefore facilitating model assessment on any of its parameters. The interval $[a, b]$ is perfectly arbitrary. We propose to take as reference a 5 % acceptability error. The assessment metric becomes:

$$P(a < X \leq b) = \int_{a=target-5\%}^{b=target+5\%} f(x)dx \quad (3.4)$$

3.2 Repeatability of parameter estimation in variable weather conditions

The accuracy of thermal performance estimation is function of the information carried in the dataset: information carried in the input variables (heating, outdoor weather conditions) and the system response, indoor temperature. The dynamic nature of the indoor temperature is therefore driven by the heating and the outdoor weather conditions.

In a non intrusive experiment, the heating input is itself conditioned by the indoor temperature set point which remains user-friendly as to be non intrusive with respect to possible occupancy. The heating power is therefore not as informative as in a controlled experiment. The dynamic provided by the outdoor conditions probably play a larger role in the dynamics of indoor temperatures than in controlled experiments. As the effect of weather conditions grows larger, it is possible that the calibration results depend on the actual conditions during the experiment. Poorly informative heating input raises therefore the issue of weather dependency of the results. If then the results are dependent on the outdoor conditions, results are not repeatable.

3.2.1 Weather conditions influence: state of the art

Previous work on thermal performance estimation of the envelope in a non intrusive framework has focused on the study of a single wall performance or on the entire envelope of a building. [RI18] show how solar irradiation significantly defers stability and convergence of the estimation of the conductive thermal resistance of a wall R_c , i.e. the inverse of the HTC of the wall, using heat flow meters following the ISO 9869 standard [ISO14]. The authors suggest using flow meters on both sides of the walls to secure a robust and faster estimation of R_c .

[PGT18] propose an innovative method to exploit non intrusive data from heat flux and temperature meters to determine dynamic thermal characteristics of a wall. The use of 12,5 days data, although not justified, met acceptable accuracy on the results.

[GCG18] precisely study the duration of a heat flux meter test for estimating the U -value, again following the [ISO14], and compares its stability to the criteria given by the standard, in which is given that three conditions must be met simultaneously to end the test [GCG18]:

- the first condition is that the test must last 72 h or longer,
- the second condition is that the U -value obtained at the end of the test must not deviate more than 5 % from the value obtained 24 h earlier,
- the third condition is that the U -value obtained from the first N days and from the last N days must not deviate more than 5 %, with $N = 2/3 \cdot \text{total duration}$.

There seems to be no limitation to applying the last two conditions to other calibration techniques than the methods defined in the ISO, although [GBE18] mention that it has never been seen in literature and that it might be too conservative.

In an application of RC models on heat flux measurements, [GE18] and [GBE18] introduce the idea of stabilisation of the estimation : from short datasets, the estimates suffer from the prominent noise in the data. As the dataset grows, the values stabilise towards a final value. Applying the

criteria of the ISO 9869-1:2014 standard, they found that up to 10 days were necessary to reach stabilisation in autumn and winter season whereas longer periods were necessary in warmer seasons. The minimum length tested was 3 days, as demanded by the ISO standard, but authors found that shorter datasets sufficed in some cases with the use of a dynamic model.

At wall scale again, [RGM19] compared a dynamic model calibrated by Bayesian inference to the average and dynamic methods described in the ISO 9869-1:2014 standard and found that the temperature difference was more determinant than the length of the dataset, thus uncovering the major role played by uncontrolled boundary conditions.

[RDC99] point out the issue of data informativeness in a study where non intrusive measurements are used to assess building overall heat loss and overall ventilation rate of a large commercial building using a steady-state equation. They found that daily averaged data over a year combined with a multi-step regression technique, where multiple regressions are performed one after the other to estimate parameters one by one, achieved the best results. Parameter identification over a single season was less accurate: in winter and summer seasons, the combined variability of the outdoor temperature and the relative humidity was narrower than during the spring season. Large variability of these two weather variables yielded less correlated parameters and more accurate overall parameter identification.

[DR17] applied dynamic grey box modelling in a non intrusive framework to assess the thermal performance of a single wall based on heat flux measurements. The authors used two different data subsets of 10 days in winter (steady indoor temperature assumed at 20 °C) and 9 days in summer (free floating indoor and outdoor temperatures). They found that winter conditions with constant indoor temperatures were not appropriate to identify the parameters of interest, considering that temperatures are the main variables of the differential equations used for the exploitation of the data. Summer free floating conditions were then found to be more informative and led to identifiable and interpretable parameters. Let us remind here that identifiability relates to the unicity of the parameter estimation and interpretability to the ability to give the estimation a physical meaning. Both may be confounded if the model characterizes perfectly the system.

More recently, [Sen+19] studied the physical interpretation of ARX models, aiming for the estimation of the HTC via on-board monitoring, i.e. in a non intrusive measurement framework. Four different indoor temperature scenarii were tested through 20 days of synthetic data twice: once for training and once for validation. The building modelled in TRNSYS is a single-zone opaque box and the study focused on the estimation of the HTC in case of heat losses to the ground. There is no mention of the influence of the length of the dataset on the results, but in order to fit at best the available data, a model selection process is applied to check that the residuals can be considered as white noise and that the parameters of the ARX models are significant through a marginal t-test.

3.2.2 The reference model undergoes variable weather conditions

Using a numerical building energy model presents the advantage of knowing the exact thermal performance of the case study. The simulation environment allows to perform simulations under any weather conditions. This section presents different ways to consider such variations and why in the end stochastically generated weather data has been chosen. The section also describes the dataset selection and details on the calibration of the RC model.

Adaptations of the reference model methodology

The case study described in section 3.1 is used to produce synthetic datasets. Its thermal properties in this specific application are described in Table 3.1. To focus on the study of weather variability and avoid effect of heat losses through unheated adjacent spaces (attics and crawl space), the insulation thicknesses of horizontal walls has been set at 30 cm, which basically ensures very low heat transfers. At the same time, vertical walls have medium insulation and the air change rate is quite large.

Vertical insulation thickness	10 cm
Attic insulation thickness	30 cm
Ground floor slab insulation thickness	30 cm
Air change rate	1.0 h ⁻¹

Table 3.1: Thermal characteristics of the numerical building energy model used in this application

This case study configuration yields an overall theoretical thermal resistance $R_{eq}^* = 5.19 \times 10^{-3} \text{ K/W}$. This theoretical value is later on called **target value** R_{eq}^* , in opposition to the estimated values of the overall thermal resistance R_{eq} (without *), estimated from the "collected" data.

In essence, as illustrated by Figure 3.5(a), the case study is simulated with N different weather conditions datasets. As a result, there are N synthetic simulation outputs, from which indoor temperature and heating power are saved. Each synthetic dataset serves as training data for a stochastic RC model. Finally, an overall thermal resistance can be inferred from the estimated parameters of the RC model.

To explore adequate experiment duration under variable weather, each synthetic dataset gives data subsets of growing length, each serving as training data. As shown in Figure 3.5(b), starting at date \mathcal{D} , subsets of 2, 3, 5, 8, 11, 15 and 25 days are considered for model training.

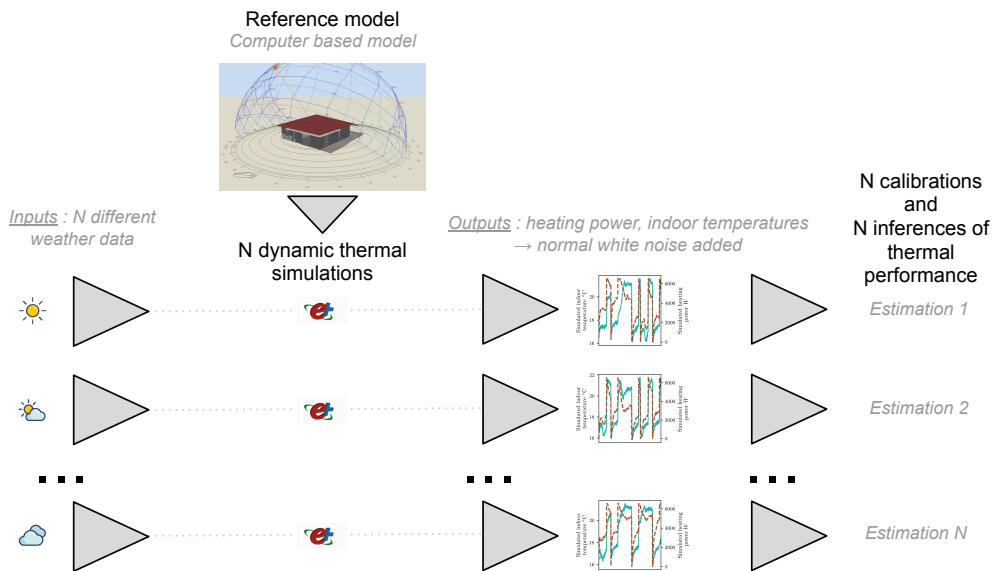
Weather variability in a numerical methodology

In application of the aforementioned methodology, the idea is to use various weather datasets to study how these boundary conditions influence the stability of overall heat transfers estimation. This section first shows how simulations with actual weather data were insufficient in deeply understanding the relationship between weather and R_{eq} estimation and then presents a set of 2000 stochastically generated weather files, built for sensitivity analysis. This set will prove to be an informative alternative to actual weather data.

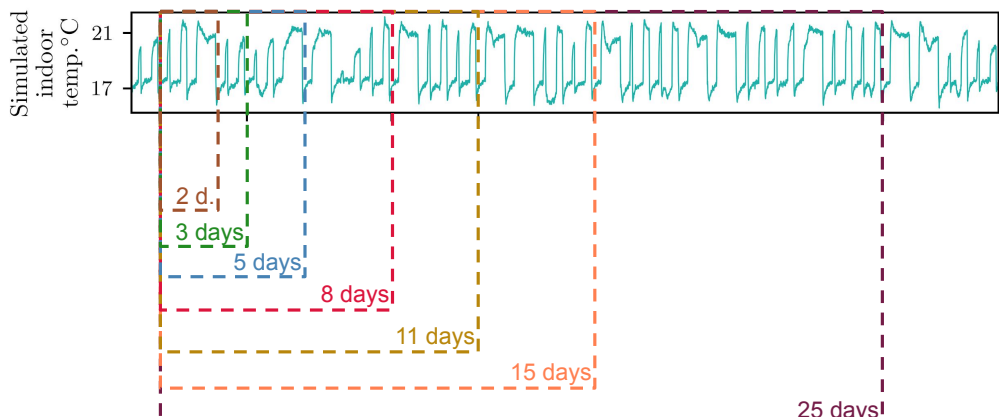
This study proposes to use synthetic weather data from which a variance based sensitivity analysis is possible [GMW17]. A total of 6 weather variables are stochastically generated to be representative of usual weather conditions in Geneva in winter, following the methodology described in [Ans+15; GMW17], as a time series constructed by a combination of statistical and deterministic features. The characteristics are extracted on the basis of representative weather data : the TMY weather file [Per+14]. The TMY file, standing for Typical Meteorological Years, is built by concatenation of typical months. Each month is chosen from 30 years actual data: each monthly dataset is weighted as a sum of 13 Finkelstein-Schafer statistics [FS71] from the temperature, wind and solar radiation data. In the end, the chosen monthly dataset is the one that shows statistics closest to mean, median of the 30 years data distribution, after having discarded years with exceptionally long periods of consecutive warm, cold or low radiation days. The stochastic generation [GMW17] contains then as much variability as in the TMY file : if the TMY has for one particular variable a lower variability than the rest of the 30 years actual weather data, it will reflect in the synthetic data.

From the TMY file, [GMW17] select 6 weather variables to stochastically generate 2000 weather files, the rest of the variables are left unchanged. The generated variables are exterior dry bulb temperature, relative humidity, direct normal solar irradiation, horizontal diffuse solar irradiation, wind speed and wind direction.

Finally, the weather data is generated as to calculate sensitivity indices through a Sobol variance method able to cope with groups of time-dependent inputs, such as here time dependency of each weather variable. Sensitivity indices by groups estimate the effect of the entire time series of the meteorological variable under study. The sensitivity indices are therefore scalars even when the variables are time series. The indices are calculated from two sets of 1000 samples, each sample of the first 1000 being defined by the characteristic features extracted from the TMY file of each

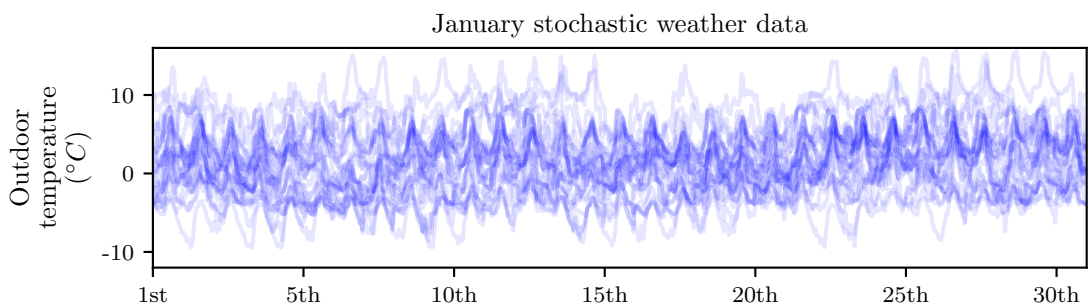


(a) Overall framework for the study of weather conditions influence



(b) Selection of data subsets from each synthetic simulated dataset

Figure 3.5: Framework for repeatability assessment

Figure 3.6: Stochastically generated weather data: example of the outdoor temperature profiles in January. The stochastic data varies between -10°C and $+13^{\circ}\text{C}$, as usual in January in Geneva

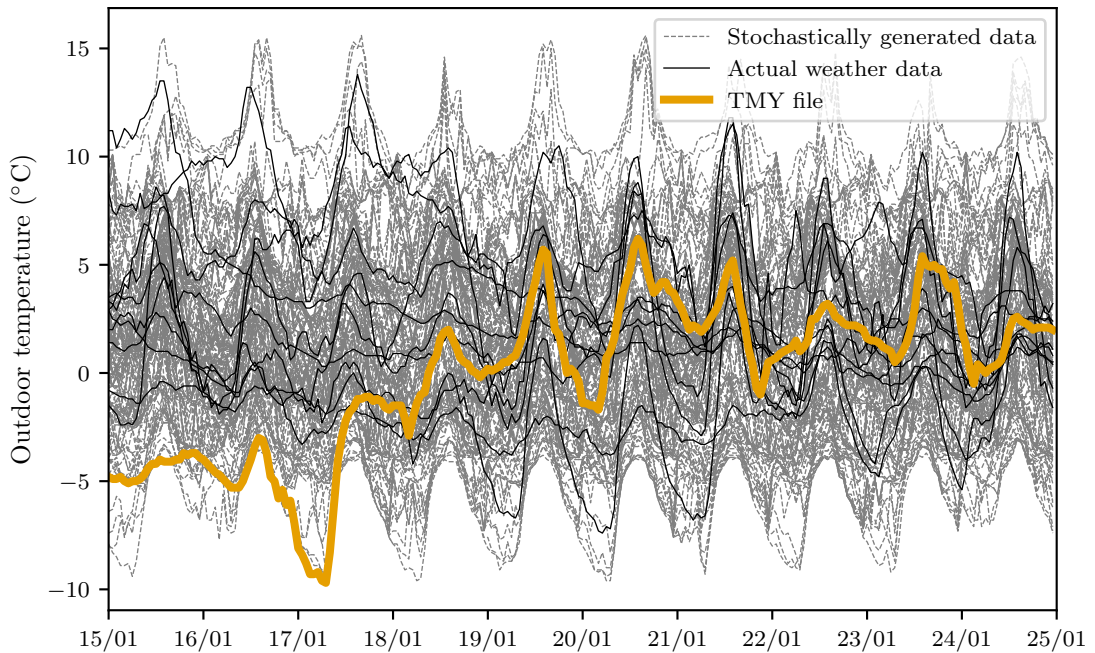


Figure 3.7: Comparison of the stochastic outdoor temperature profiles with actually measured temperatures: stochastic data seems rather realistic

weather variable, the second 1000 samples being a rearrangement of the first.

In this study, the output of interest for the sensitivity analysis is the R_{eq} estimation and in particular whether the weather conditions lead to increased or decreased estimates. The variability of the R_{eq} estimations with respect to weather variability is expected to become negligible as the data becomes more informative with longer datasets. To understand more in depth how each weather variable influences the output, partial variance and sensitivity indices are calculated.

In order to check the representativeness of the generated weather data, Figure 3.8 compares the synthetic data to the actual data from Geneva. The figure shows the empirical cumulative distributions of the 6 weather variables for the month of January of the actual weather data in black and in orange the data used to generate the synthetic data. The grey areas represent the 50 %, 75 % and 95 % quantiles of the synthetic weather data.

Synthetic outdoor dry bulb temperatures seem to be representative of the actual measured temperatures. Synthetic wind direction is in good agreement with actual measurements as well.

Synthetic relative humidity seems to be lower than some of the actual measurements. The synthetic diffuse radiation however seems slightly overestimated, as does the wind speed. This is due to the fact that the *TMY* weather dataset has indeed higher wind speed than other years: in Figure 3.8 the orange line representing the *TMY* file is indeed significantly lower than the black lines representing 10 years of actual weather data.

The generated direct normal radiation data does not cover a range as wide as the actual data: some of the real data may have much higher or lower direct radiation. This might have an impact on the following results.

Finally, considering that the generated weather data concerns January only, all subsets to be submitted to model training should begin as early in the month as possible. Datasets will thereby be less biased by accumulated thermal inertia as they would have undergone similar weather in December. At the same time, there is small discontinuity in the weather data between December 31st and January 1st. All data subsets start therefore on January 2nd.

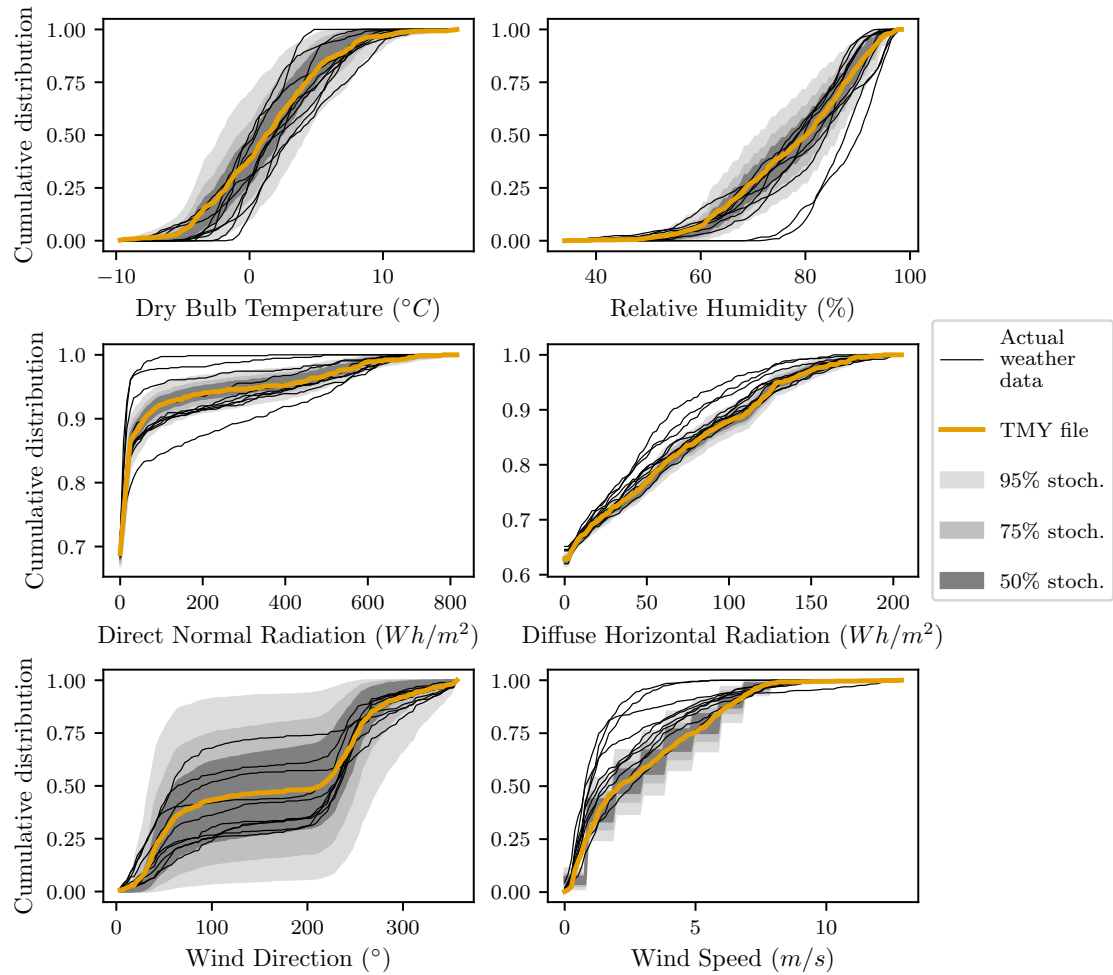


Figure 3.8: Cumulative distribution quantiles of the 6 stochastic weather variables against cumulative distributions of actual weather data. Representativeness of the stochastic generation can be assessed by the position of the actual data distributions in the quantiles.

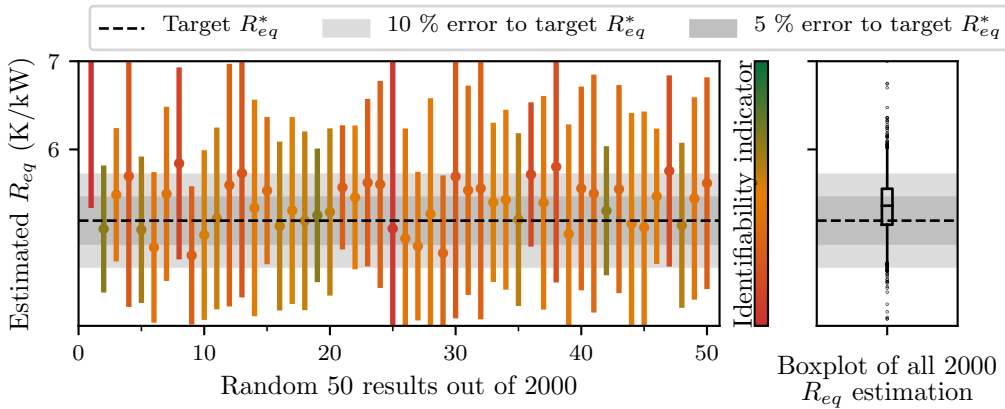


Figure 3.9: Variability of the R_{eq}^* estimation with 2-days training:

3.2.3 Decrease in variability of R_{eq} estimation with experiment duration

Variability with a 2-days model training

For each of the 2000 data sets and for each subset, the stochastic RC model $T_w T_i R_o R_i A_w$ is calibrated. In each case, R_{eq} is inferred as the sum of the resistive parameters estimations. Figure 3.9 shows on the left hand side 50 randomly picked R_{eq} maximum likelihood (ML) estimations with their confidence interval.

Looking at these individual results, there are three cases to distinguish:

- the R_{eq} estimation is close to the target R_{eq}^* value: the estimation is accurate and the credible interval includes the target R_{eq} . This case is the most desirable case;
- the R_{eq} estimation is far from the target R_{eq}^* value but the credible interval includes the target R_{eq}^* : the estimation is not accurate but the credible interval relates to this inaccuracy which keeps the result trustworthy;
- the R_{eq} estimation is far from the target R_{eq}^* value and the credible interval does not include the target R_{eq}^* : not only is the result inaccurate but also give a false sense of confidence on an inaccurate result.

The latter case is the most sensitive one. It is therefore paramount to understand under what conditions over- or under- estimation occur. In order to discriminate these unwanted estimations from the others, an interpretability indicator is calculated, under the frequentist gaussian hypothesis. This indicator, defined earlier in the previous chapter (see 3.1.2), represents the area under the bell curve that is $\pm 5\%$ of the target R_{eq}^* . The interpretability indicator takes values between 0 and 1. For example, the case (c) with strong error on the estimation has an interpretability indicator close to zero.

On the right hand side, Figure 3.9 displays the boxplot of all R_{eq} ML-estimations showing a wide variability: the median of the 2000 estimations falls at 5.36 K/kW with a standard deviation of 0.35 K/kW (5^{th} quantile 4.82 and 95^{th} quantile 5.98). The outlier estimations show absolute errors beyond 20% of target R_{eq}^* . This variability shows that the influence of weather conditions on the ML-estimation of R_{eq} is not negligible. A data subset longer than 2 days is certainly needed to decrease this variability.

Minimal measurement duration for model training

Figure 3.10 shows boxplots of all 2000 R_{eq} ML-estimations with the 7 data subsets: model training from 2, 3, 5, 8, 11, 15 and 25 days data. From the figure can be inferred that the longer the data subset, the lower the variability. There is distinctively a decrease in total variance, towards a median value slightly above the target value R_{eq}^* . Calibrations from 11 days data and more show

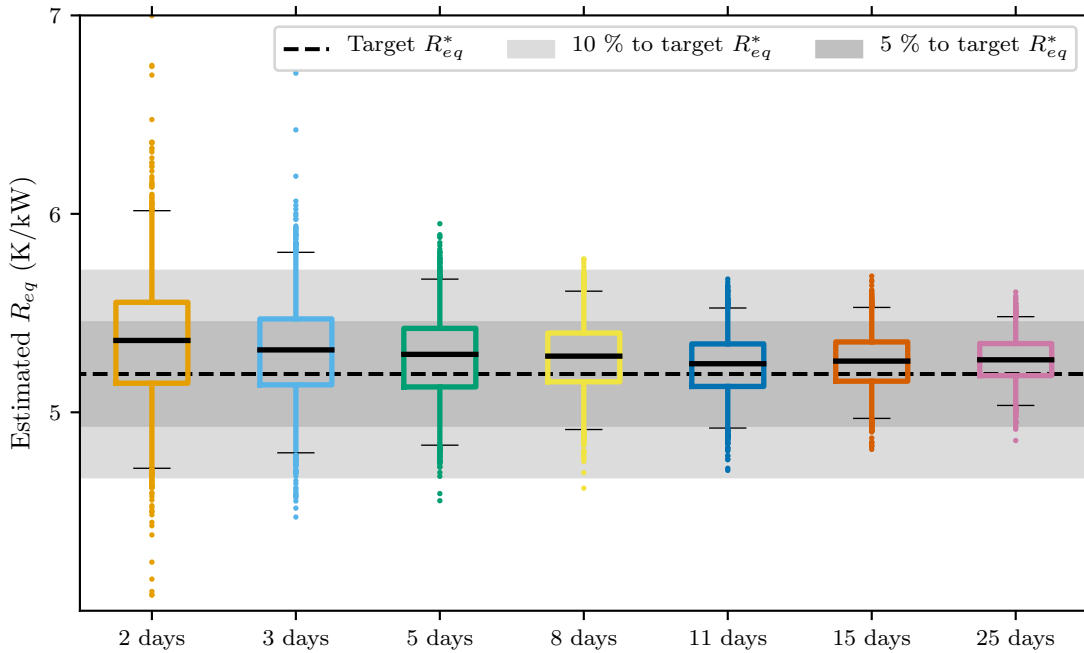


Figure 3.10: 2000 R_{eq} ML-estimations for growing duration datasets: datasets over 11 days are all within $\pm 10\%$ error to the target R_{eq}^* .

all estimated R_{eq} values within 10 % of their median value, hence ensures low variability in the R_{eq} estimation with respect to weather influence.

To validate the impression of decrease in variability from Figure 3.10, Figure 3.11 shows for each data subset the evolution of the total variance of ML-estimations.

From the 2 days and 3 days training, the R_{eq} ML-estimations have a total variance around $1.2 \times 10^{-7} \text{ K}^2/\text{W}^2$. With 8, 11 and 25 days training, the total variance decreases respectively by a factor 3, 4 and 6. Partial variance evolution will be further discussed in the next section.

As a partial conclusion, 11 days training suffices to reduces the error below the $\pm 10\%$. Longer training still significantly reduces the overall variance. However, from a practitioner's point of view, longer experiments might be unnecessary, as it would immobilize the experimental setup almost twice as long for an all in all relative decrease in uncertainty.

3.2.4 Influential weather variables on an R_{eq} estimation

The synthetic weather files allow a global sensitivity analysis on the output with respect to 6 weather variables. Figure 3.12(a) shows the sensitivity indices of the estimations of some parameters with respect to the weather variables: R_{eq} . The sensitivity indices are calculated for all 7 data subsets. The indices shown in Figure 3.12(a) are the first order indices, meaning that they only show the direct influence of each weather variable. If the sum of each first order indices is close to 1, it would imply that there were almost no second order effects, i.e. combined effects of the weather variables.

The values of the sensitivity indices are always simply estimated. The indices given in Figure 3.12(a) should mainly be interpreted as order of magnitudes. Indices below 0.1 may be considered insignificant, given the uncertainty of their estimation.

In Figure 3.12(a) can be seen that the variability of the R_{eq} ML-estimations are influenced by the outdoor temperature and the wind speed. With shorter datasets, the sum of the first order indices is significantly inferior to 1. This means that the variability is also explained by interactions of weather variables. Variability from with longer datasets is on the contrary almost only explained

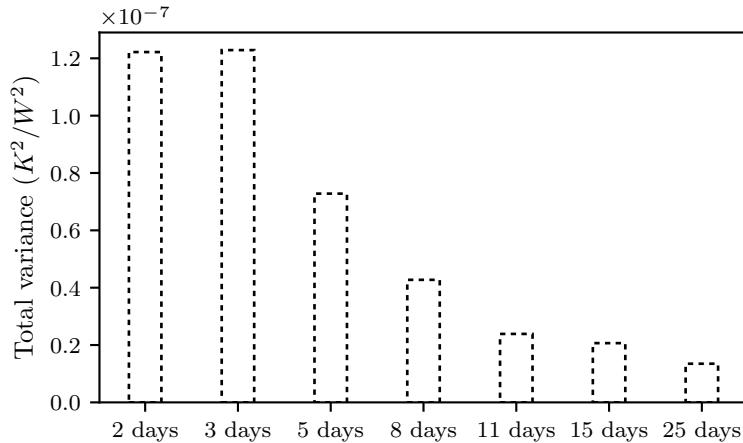
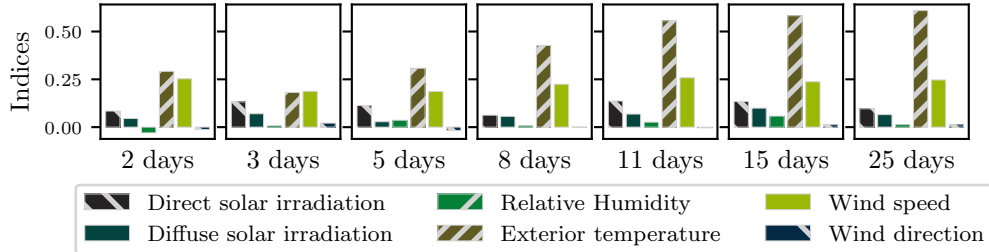
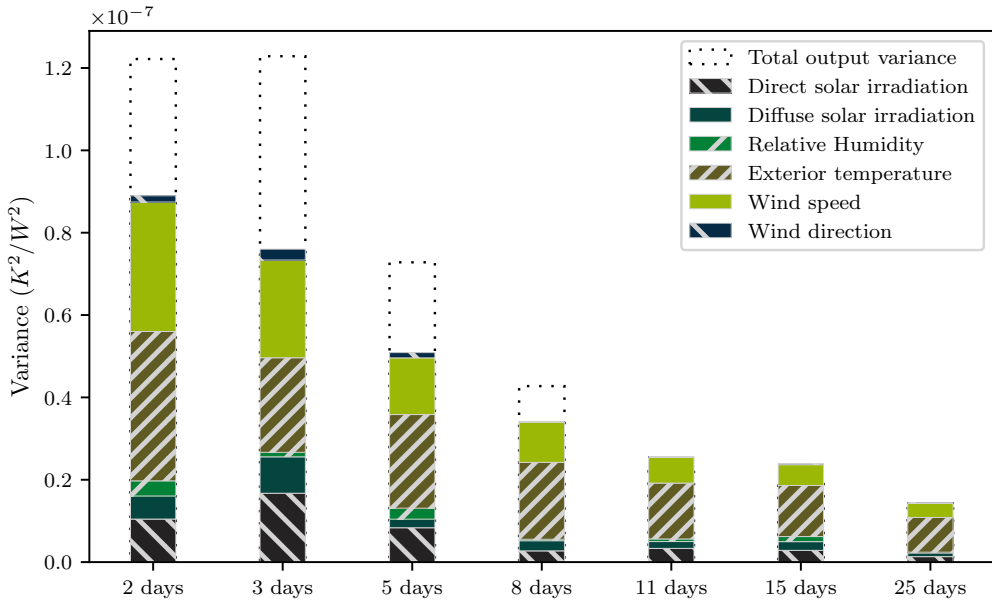


Figure 3.11: Decrease of the total variances with longer datasets



(a) First order sensitivity indices of the R_{eq} ML-estimations: outdoor temperature and wind speed are the main factors to variability



(b) Decrease of the total and partial variances with longer training datasets

Figure 3.12: Individual effect of weather inputs on the estimations of R_{eq}

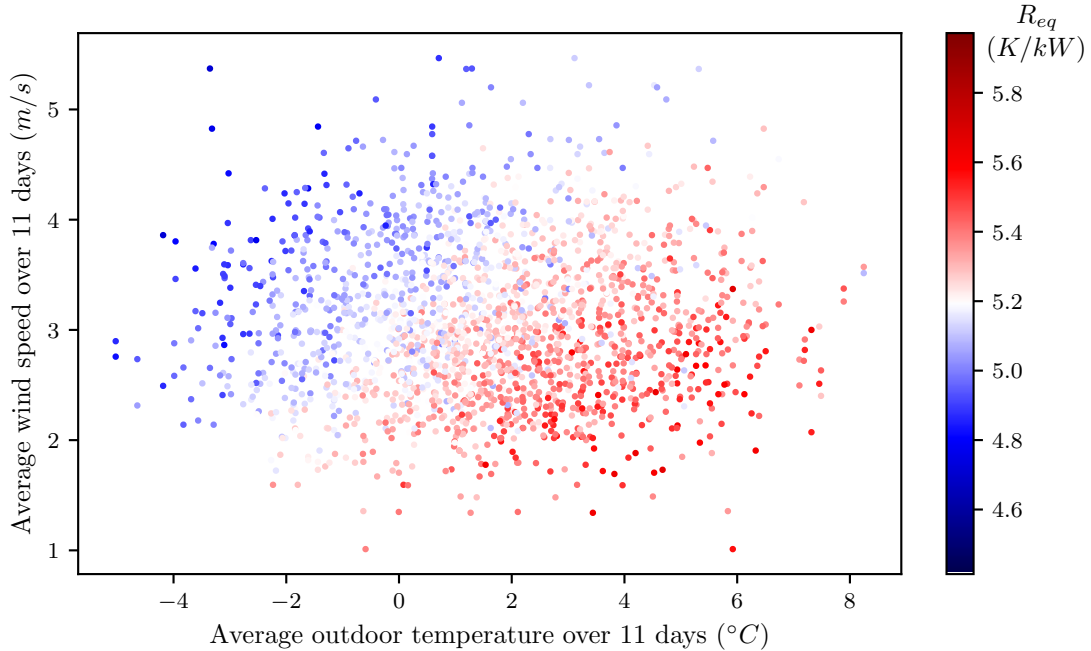


Figure 3.13: Variability of the R_{eq} ML-estimations from 11 days training with respect to outdoor temperature and wind speed. Colours refer to $\pm 15\%$ errors to target R_{eq}^* .

by the variability of outdoor temperature and wind speed, seeing that the indices add up to 1. Let us also note that wind direction was not expected to have an influence on the estimations as it is not used in the infiltration and ventilation model of EnergyPlus. Its sensitivity indices are indeed insignificant.

This outcome is also visible in the evolution of the partial variances of each weather variable shown in Figure 3.12(b). Let us remind that the total variance is the sum of all order partial variances. The figure shows the first order partial variances, i.e. the partial variances due to the effect of each weather variable individually. With these elements in mind, it is visible that the total variance of the 11, 15 and 25 days datasets is solely explained by first order effects of the weather variables, mainly outdoor temperature and wind speed.

Let us now examine how outdoor temperature and wind speed influence the R_{eq} ML-estimations. Figure 3.13 shows how the R_{eq} ML-estimations from 11 days training vary with the average outdoor temperature on the abscissa and the average wind speed on the ordinate. Warmer training periods tend to produce over-estimations and colder days under-estimations. At the same time, non windy days produce in overall over-estimations, windy days under-estimations.

At the same time, an interaction can also be seen in Figure 3.13: training from warm and unwindy days results in over-estimation, cool and windy days in under-estimations.

This outcome is in agreement with the hypothesis that the large air change rates in the reference model are a cause of inaccuracy in the estimation of the overall thermal resistance. As the ventilation related heat losses have been modelled in the EnergyPlus simulation environment, there is a direct relationship between temperature difference between indoors and outdoors and wind speed. Ventilation related heat losses are larger with cold outdoor temperatures and with high wind speed and on the contrary smaller with warmer or unwindy days.

Finally, Figure 3.14 shows more clearly how the influence of outdoor temperature and wind speed evolves from short to longer model training.

As seen earlier, this figure too shows the decrease in total variance of the R_{eq} ML-estimations

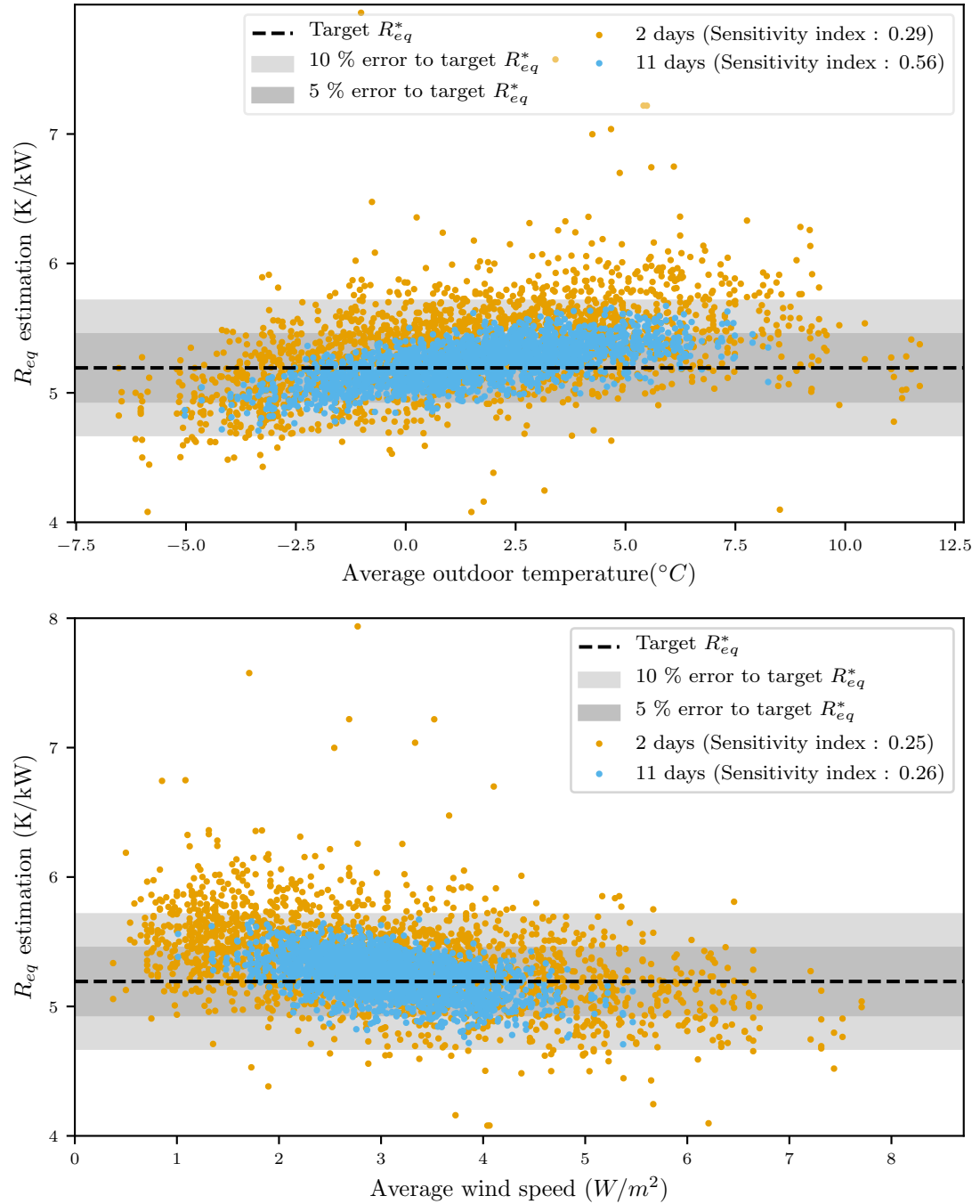


Figure 3.14: Variability of the R_{eq} ML-estimations with respect to averaged outdoor temperatures and wind speeds, for 2 days and 11 days training.

with longer training sets: the vertical spread of all estimations are narrower with the 11 days training. Interestingly, while the total variability does decrease, the angle representative of the correlation remains quite similar whatever the dataset length. Longer datasets produce averages that are less spread horizontally, but the relationship between temperature and R_{eq} estimation is almost unaltered.

A natural assumption would have been to consider that colder days lead to more accurate estimations than warmer days, as colder days increase the heat losses and thus the heating power needed to keep up with the indoor temperature set point. This assumption does not seem to hold here. If it were, the variance would be significantly narrower under cold days than under warm days. Here, there is no significant difference in vertical spread between cold and warm days, nor is there any between windy and unwindy days.

3.3 Decomposition of heat losses in a building

Diagnosis of the thermal performance of a building envelope from non intrusive data would benefit most from an accurate estimation of different sources of heat loss. Determining how much energy is lost on ventilation and infiltration or through specific parts of the envelope is more informative in the perspective of building retrofit than a simple overall thermal resistance. It is however unknown whether on-site measurements in non intrusive conditions are sufficiently informative to make this type of detailed estimations. The dynamical nature of data collected in these conditions could however be beneficial for training of RC models.

This chapter proposes to apply the model assessment framework defined in Chapter 3.1 to this purpose. The idea is to determine whether stochastic RC trained models deliver individually interpretable parameter estimates.

So far, the model assessment framework has been applied to assess repeatability of a RC model when weather conditions are variable. Convergence has been found to be achieved within 11 days for the estimation of an overall thermal resistance. Interpretability of each parameter separately has however not been established.

In particular, this chapter will examining if identifiability and interpretability of heat transfers by ventilation and heat transfer to an unheated crawl space can be achieved. The corresponding parameters will be identifiable if they can be estimated even from poorly informative data, as is simulated in the model assessment framework designed in 3.1. Interpretability is then assessed by comparing the estimations from the theoretical target values.

Section 3.3.1 describes in detail how the model assessment framework is applied to the aforementioned objective. Section 3.3.2 then presents the results of the application to the assessment framework on the interpretability of heat losses by ventilation.

3.3.1 Model assessment framework for heat transfer decomposition

Interpretability of parameter estimates taken individually means that they actually represent the physical property (or aggregated properties) they are supposed to represent. In other words, a given parameter estimate should take the value of the exact actual (aggregated) property(ies) it is supposed to represent, without lumping the dynamics or the influence of an unrelated other physical property. The interpretability assessment framework proposes to verify that a change in the actual property value translates as a change in the value of the ad hoc parameter.

The general idea is therefore to make a number of variations in the thermal properties of the reference model and to study the induced variability in the parameters' estimations. This section first establishes reasonable objectives for the estimation of decomposed heat transfer, secondly exposes how the numerical model assessment methodology is applied to answer the stated problem, then details what state space models are fit to the simulated data and finally establishes the convergence

of the sensitivity analysis performed in the model assessment framework, proving that the results exposed in the following sections can be trusted.

What decomposition can be reasonably expected?

In the expectation of diagnosing energy performance of a building and in particular thermal performance of the envelope, the more detailed the diagnosis, the more useful it will be for establishing pertinent retrofit strategies. However, in a non intrusive design of experiment, the data available reduces the possibilities, in particular as only temperatures of the heated space are measured. Not all physical characteristics or systems may be diagnosed from only temperature measurements.

This restrictions are similar to issues in calibrating whole detailed building models from experimental data. [Str93] addresses them by suggesting a global sensitivity analysis to determine the adequate spatial and temporal measurements. The idea behind this suggestion is that an input parameter in a whole building model may be estimated from data if it has an influence on the measured output. [Jos17] too, aiming at fault detection in the building envelope, found through a Morris sensitivity analysis that thermal bridges and local insulation defaults could not be estimated from temperature measurements as their influence is found insignificant on temperature differences.

Back to the model assessment framework, it can be understood that the only estimable thermal properties are the ones that have a detectable influence on the measured model output (indoor air temperature). This leads to determine the physical characteristic that have a significant influence on indoor temperature.

[Jos17] found that the influential parameters detectable in indoor temperature are the insulation thicknesses, in particular when considered equal in all walls. When a locally faulty insulation is considered, for example in the wall of a particular room, that default would not be detectable on a south oriented wall, but would be on the other orientations. An application of the method on a case study aiming at quantifying a linear thermal bridge was not successful, showing that a local default like a thermal bridge does not have a detectable influence on indoor temperatures. The method and results in [Jos17] are developed on a case study of a newly built highly energy efficient dwelling, which has specific heat transfer dynamics: solar gains contribute largely to the energy balance. For this reason, a similar analysis on a poorly insulated house would probably show different influential parameters. Also, for the sake of simplicity, [Jos17] did not vary the ventilation characteristics, although heat transfers through ventilation can be considered significant.

All in all, decomposition of heat transfers of different parts of the envelope seems to be an achievable objective. Heat losses to neighbouring unheated spaces, where the boundary temperature can be measured is a possible focus and presents an actual interest in thermal diagnosis. In the same order of magnitude, heat losses through ventilation seems to be a reasonable objective too.

Notations for the targeted values vary from one author to the other. But with the acknowledged notations of the Section 3 of ISO 13789 [ISO17], this chapter aims at the following heat transfer decomposition:

$$HTC = H_{ve} + H_{tr} = H_{ve} + H_d + H_u \quad (3.5)$$

with:

- HTC the Heat Transfer Coefficient (W/K): heat flow rate from indoors to outdoors divided by the temperature difference,
- H_{tr} the Transmission Heat Transfer coefficient (W/K): heat flow rate due to transmission through the fabric, divided by the temperature difference,
- H_{ve} the Ventilation Heat Transfer Coefficient (W/K): heat flow rate due to air entering the heated space, divided by the temperature difference,

- H_d the direct transmission heat transfer coefficient between the heated or cooled space and the exterior, for the whole building (W/K),
- and H_u (W/K): transmission heat transfer coefficient through unconditioned spaces.

To bridge these objectives with the state space models used for the estimation of said thermal properties, the rest of the chapter will rather focus on the estimation of thermal resistances, as the inverse of the heat transfer coefficients: $R_{eq} = \frac{1}{HTC}$, $R_{ve} = \frac{1}{H_{ve}}$, etc...

Application of the model assessment framework

The objectives of this application of the model assessment methodology are threefold:

- (A) examine the interpretability of the overall thermal resistance,
- (B) identify independently the air change rate,
- (C) decompose heat losses towards unheated neighbouring spaces from losses to the outdoors.

This subsection details in 3.3.1 what modifications are done to the reference model in the model assessment framework and in 3.3.1 what post-processing is done to the simulated data.

The case study model described in section 3.1.1 undergoes modifications as to cover a wide range of building thermal properties : from poorly to highly insulated, from low to high air change rates, from low to high thermal inertia. However, neither the reference model structure nor its design change.

The modifications for the simulations are done on wall, attic and ground floor insulations, as well as on ground floor slab and brick wall thermal capacity (serving objectives (A) and (C)) and on air change rates (serving objective (B)). The modifications of the thermal properties of the reference model, the *inputs*, follow a specific design of experiments allowing both a thorough exploration of the inputs space and a sensitivity analysis. A Latin Hypercube Sampling is therefore chosen, and sampled on uniform distributions on all 6 physical properties. Table 3.2 gives the boundaries between which the parameters vary, as well as complementary thermal properties of interest.

The 300 building configurations are simulated from January 1st to February 28th on the basis of an actual weather dataset.

The weather has been measured in Le Bourget du Lac (73, France) in 2019. The measurements have a 1 minute timestep and have been adapted to the EnergyPlus weather input file format, such as to contain: dry bulb temperature (°C), field dew point temperature (°C), relative humidity (%), atmospheric pressure (Pa), horizontal infrared radiation intensity (Wh/m²), global horizontal radiation (Wh/m²), direct normal radiation (Wh/m²), diffuse horizontal radiation (Wh/m²), wind direction (°), wind speed (m/s), total sky cover, opaque sky cover, field visibility (m) and ceiling height (m).

From the two months simulated data, a training period must be chosen. A small selection would, as found in Section 3.2, induce a non negligible effect of the weather conditions on the result. At the same time, a long dataset would just unnecessarily burden the computational cost without adding significant information to the calibration process. A length of 11 consecutive days will be selected in agreement with the outcomes of Section 3.2.

Also, to avoid the influence of the warm-up process of EnergyPlus, which repeats multiple times the first day of simulation to initiate usual temperature conditions, the dataset selection for calibration should not start in the first 2 weeks of the simulation.

Finally, the data used for calibration is resampled with a timestep of 8 minutes. Larger timesteps may imply aliasing. But again shorter timesteps will enhance computational burden without proving to be much more informative than a 8 minutes timestep.

With the aforementioned constraints in mind, the chosen selected dataset runs arbitrarily between January 31st and February 10th. As shown in Figure 3.15, the selected 11 days present rather mild outdoor temperatures, varied solar irradiation with sunny and cloudy days and varied wind speed conditions.

	Object Variable in EnergyPlus	Bounds	Units	Other info
Walls insulation thickness	(Material) Thickness	[0.05;0.25]	m	$\lambda = 0.032 \text{ W}/(\text{m} \cdot \text{K})$
Attic insulation thickness	(Material) Thickness	[0.05;0.25]	m	$\lambda = 0.04 \text{ W}/(\text{m} \cdot \text{K})$
Ground floor insulation thickness	(Material) Thickness	[0.05;0.25]	m	$\lambda = 0.022 \text{ W}/(\text{m} \cdot \text{K})$
Air Change Rate	(ZoneVentilation: DesignFlowRate) Air changes per Hour	[0.2;2.0]	h^{-1}	(-)
Thermal capacity brick wall	(Material) Specific Heat	[0.6;1.0]	J/kgK	$e = 13 \text{ cm}$
Thermal capacity floor concrete cast	(Material) Specific Heat	[1.0;2.0]	J/kgK	$e = 20 \text{ cm}$

Table 3.2: Physical thermal properties variations of the reference model for the decomposition study

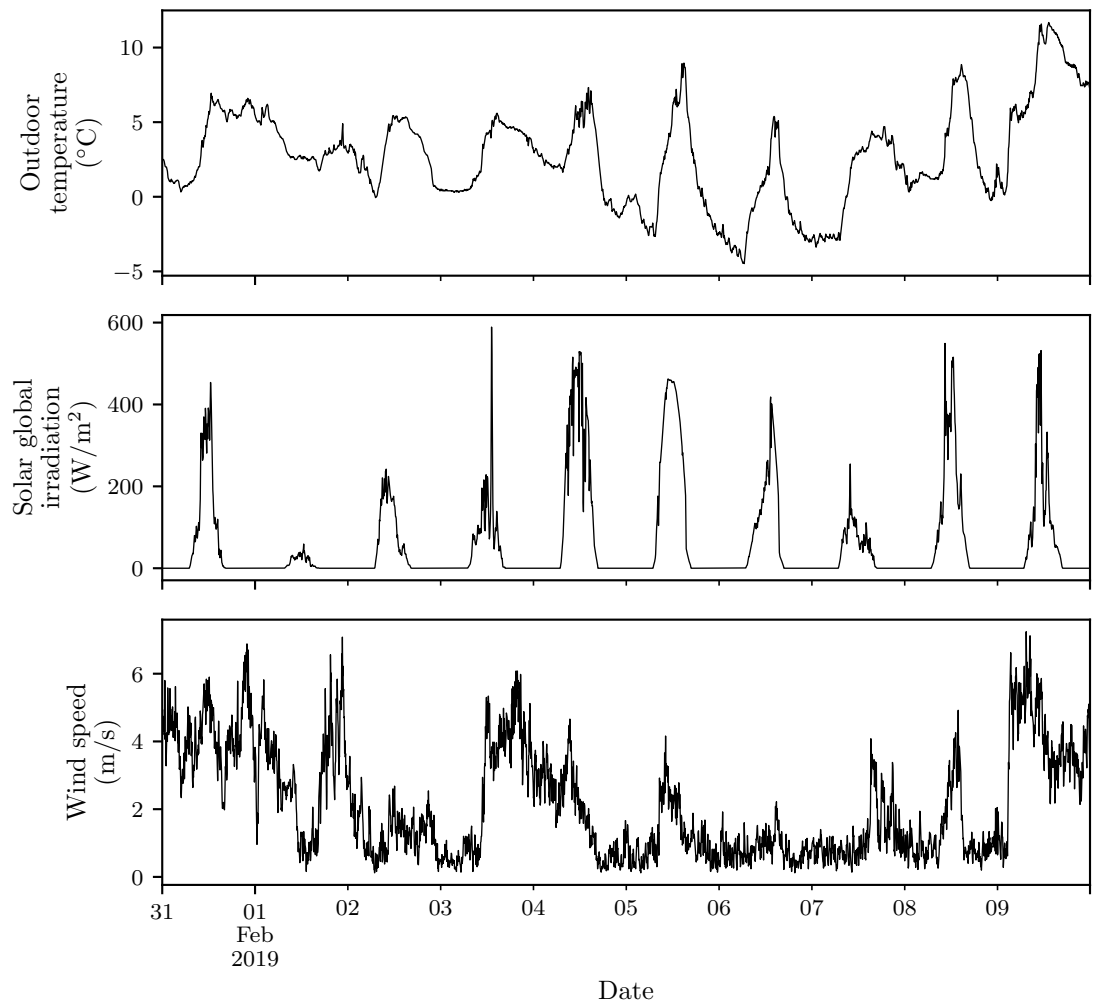


Figure 3.15: Selected weather dataset used in the 300 simulations: outdoor temperature, solar irradiation and wind speed

State space model selection and validation

300 datasets have been produced from 300 different configurations of the reference building. To exploit the datasets and estimate the thermal resistances set as objectives, adequate stochastic RC models need first to be selected. Then, after appropriate model calibration, the most appropriate models are selected through a likelihood ratio procedure. If the selected models also achieve model validation tests, physical interpretability may be assessed.

The first step is to select an appropriate model : the model best fitting the data and which residuals are significantly not autocorrelated and have white noise properties, in which case the significant heat dynamics are covered by the model. One node models are not proposed in the process as they show very poor fit to the data. In the end, a set of structurally identifiable is selected and tested:

- two nodes: $T_w T_i R_o R_i A_i$, $T_w T_i R_o R_i A_w$ and $T_w T_i R_o R_i A_w A_i$,
- two nodes with infiltration/ventilation term: $T_w T_i R_o R_i A c_v$,
- two nodes with measured temperature in a neighbouring unheated space: $T_w T_i R_o R_i A R_b$,
- two nodes & one node towards neighbouring space: $T_w T_i R_o R_i A T_b R_{ib} R_{bb}$.

From each of the 300 simulations, a subset of data from January 31st to February 11th is used as synthetic data for parameter estimation through model calibration.

As a first step, model selection is performed, but cannot however be done on a single dataset, as the best fitting model is likely to be related to the reference model configuration. Best fitting model for one dataset may then not be valid for other datasets. This implies that for all models tested in the selection process and for each of the 300 datasets, a calibration needs to be performed. The number of calibrations adds up to at least 1500.

A Bayesian calibration, although preferred as it draws from the actual posterior distribution, would here bring a considerable computational burden. On the other side, model selection based on likelihoods comparison has been proven reliable [BM11]. Therefore, the model selection process is performed on the basis of a frequentist calibration of a set of adequate state space models, through a BFGS optimisation.

Each of the 300 configurations undergoes the same model selection process, based on a likelihood ratio test [BM11]. Each data subset is used to calibrate models in a certain order, respecting the principle of nested models: $\mathcal{M}_{null} \subset \mathcal{M}_{alt}$ if upon setting one or more parameters of \mathcal{M}_{alt} to 0, it becomes identical to \mathcal{M}_{null} .

A likelihood ratio test then compares a proposed model \mathcal{M}_{alt} , also called alternative model, to a basic model \mathcal{M}_{null} , also called the null hypothesis model. These models need to verify $\mathcal{M}_{null} \subset \mathcal{M}_{alt}$. For a dataset, both models are fitted. The logarithmic ratio of their likelihoods is calculated. To test if there is a significant improvement in the likelihood, the significance of the test, the p-value, is estimated through the χ^2 value of the ratio. If the p-value is smaller than for example the usual 0.05, than the alternative model is significantly better than the null hypothesis model.

The model selection test would then normally start with one basis "null" model, the one node model for example. This model however was found to be an extremely poor fit to the data and has been discarded. It is proposed here to rather start with two nodes models and unusually start with choosing between $T_w T_i R_o R_i A_i$ and $T_w T_i R_o R_i A_w$. As the reference model originating the simulated data is subject to solar irradiation, a two nodes model without solar parameter makes no physical sense. Starting with choosing between $T_w T_i R_o R_i A_i$ and $T_w T_i R_o R_i A_w$ alleviates the computational cost of calibrating a model on another 300 datasets.

Models $T_w T_i R_o R_i A_i$ and $T_w T_i R_o R_i A_w$ are however not nested and the comparison is made with simple log-likelihoods calculations, asis shown in Figure 3.16: the higher the log-likelihood, the better the fit. The grey dotted diagonal line marks the place where models have an equally good fit to the data. Points **under** the diagonal line have a higher likelihood for the x-axis model whereas points **over** the diagonal line have a higher likelihood for the y-axis model.

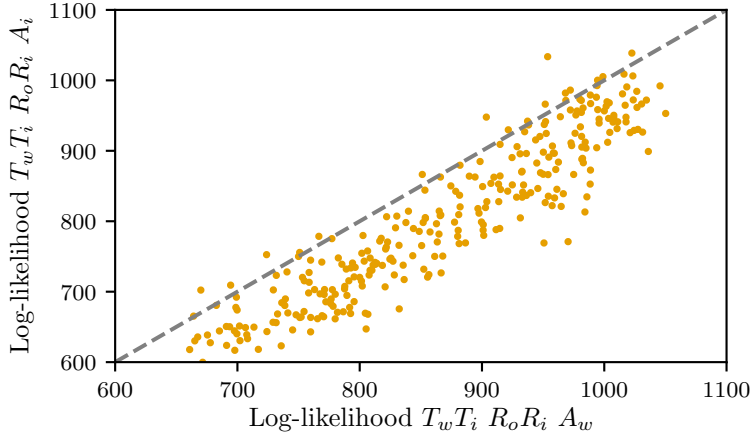


Figure 3.16: Log likelihoods of best fits for models $T_w T_i R_o R_i A_i$ and $T_w T_i R_o R_i A_w$ for each 300 samples: all points under the 45° line favour the x-axis model ($T_w T_i R_o R_i A_w$).

From Figure 3.16 can therefore be inferred that the model selection process should start with model $T_w T_i R_o R_i A_w$ as a vast majority of points are under the diagonal line, favouring therefore the x-axis model $T_w T_i R_o R_i A_w$.

The next round of test will consider the null hypothesis as being the model $T_w T_i R_o R_i A_w$, which has just been selected. The alternative models, verifying $\mathcal{M}_{null} \subset \mathcal{M}_{alt}$, are models $T_w T_i R_o R_i A_w c_v$, $T_w T_i R_o R_i A_w R_b$ and $T_w T_i R_o R_i A_w A_i$. The likelihood ratio test is applied to infer whether there is a significant difference between the null hypothesis and the alternative models, with results of the rest shown in Figures 3.17.

Figure 3.17(a) shows all 300 p-values of the likelihood ratio tests for all 3 alternative models against null hypothesis model $T_w T_i R_o R_i A_w$. All values except a few are below the 5% acceptance limit. In overall, it can then be considered that all 3 alternative models are significantly better than null hypothesis model.

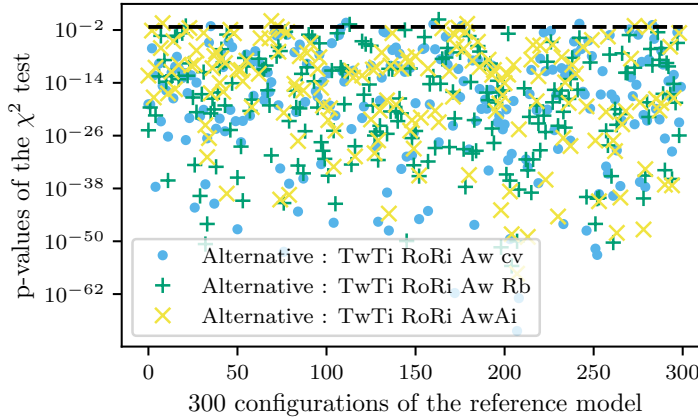
To distinguish between different alternative models, [BM11] select the one with the better score on likelihood. Figure 3.17(b) therefore shows for all 300 results the log-likelihoods for all 3 alternative models on the y-axis, while the x-axis shows the log-likelihood of the null hypothesis model.

Similarly to Figure 3.16, if the y-axis models perform better than the x-axis model, the points would be driven on the upper side of the grey dotted diagonal line. Figure 3.17(c) shows for one that alternative model $T_w T_i R_o R_i A_w A_i$ in yellow crosses is spread around the diagonal line and rather lower than the other alternative models. Model $T_w T_i R_o R_i A_w A_i$ may be discarded for now. Figure 3.17(c) also shows that the two other alternatives seem to perform similarly. Figure 3.17(c) therefore pictures the log-likelihoods of the two alternative models one against the other. The points are spread around the diagonal line, meaning that the choice between one or the other would be case dependent. A statistical study of their individual residuals could yield additional information on their performance to help for a choice.

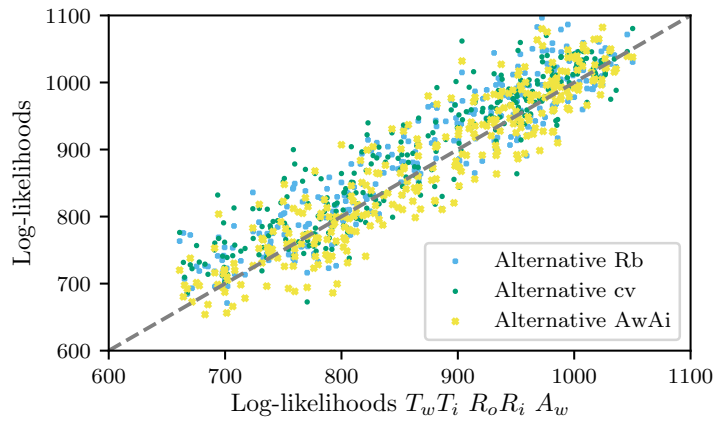
From the model selection based on prediction fitness of the previous section, models $T_w T_i R_o R_i A_w R_b$, $T_w T_i R_o R_i A_w c_v$ and basis model $T_w T_i R_o R_i A_w$ seemed rather appropriate.

As final validation step, as suggested by the workflow in 2.3, the white noise property test of the models' prediction residuals is performed. Figure 3.18(a) shows the autocorrelation of the residuals (with filter) for all 3 models and Figure 3.18(b) shows the quantile-quantile plot for normality verification of the residuals (on filtered predictions too).

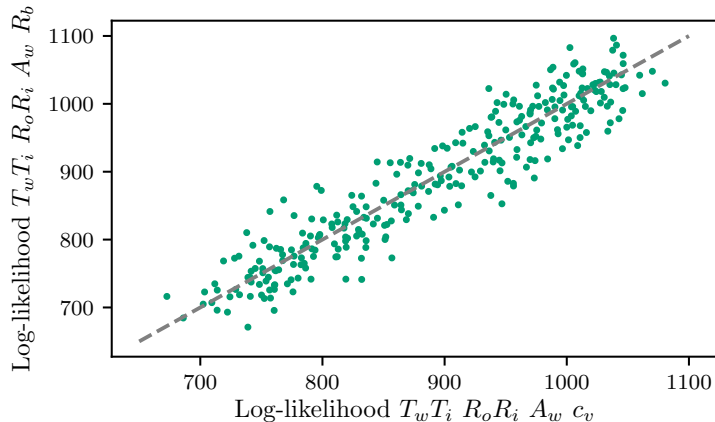
Figure 3.18(a) shows that the residuals of the two alternative models $T_w T_i R_o R_i A_w R_b$ and $T_w T_i$



(a) χ^2 test p-values : values are significant if lower than 0.05 (dotted black line).
All 3 tested models are better than $T_w T_i R_o R_i A_w$.

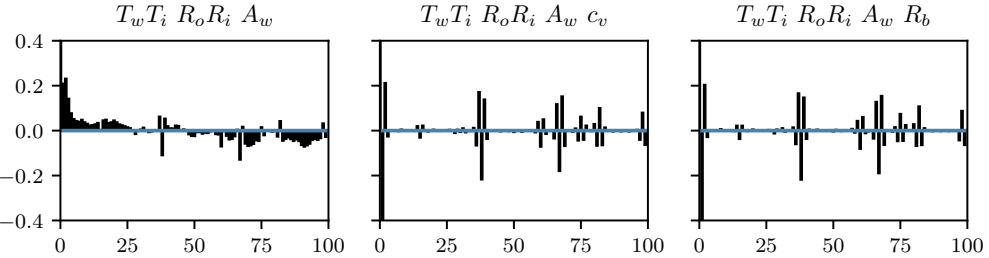


(b) Log-likelihoods of the three alternative models against x-axis null hypothesis model $T_w T_i R_o R_i A_w$: the yellow cross points are slightly lower than the blue and green points. Alternative model $T_w T_i R_o R_i A_w A_i$ seems not a good as the other two alternatives.

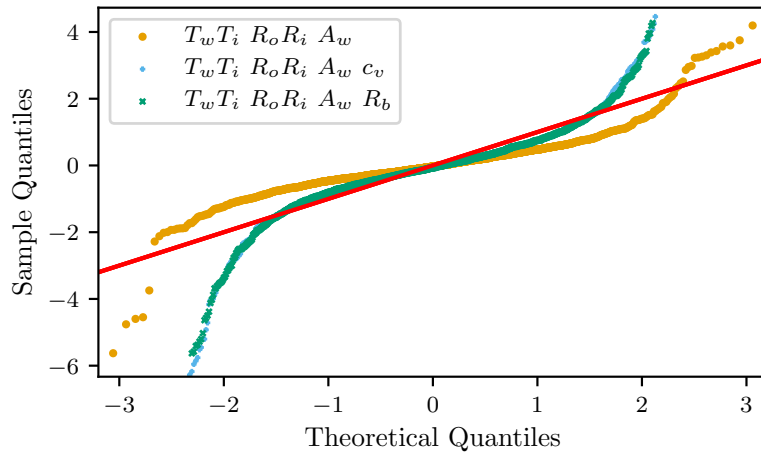


(c) Comparison of the log-likelihoods of the two best alternative models: $T_w T_i R_o R_i A_w R_b$ or $T_w T_i R_o R_i A_w c_v$

Figure 3.17: Model selection between $T_w T_i R_o R_i A_w R_b$, $T_w T_i R_o R_i A_w c_v$ and $T_w T_i R_o R_i A_w A_i$ against null hypothesis model $T_w T_i R_o R_i A_w$



(a) Autocorrelation of the residuals of all 3 models. Left plot shows significant autocorrelation while the two others are more satisfactory. Further analysis of their normality would be needed.



(b) Quantile-quantile plot of the filtered prediction residuals for normality verification. The red line gives a reference for what a normal distribution would score. Models $T_w T_i R_o R_i A_w$ and $T_w T_i R_o R_i A_w c_v$ have larger tails than a normal distribution. Model $T_w T_i R_o R_i A_w R_b$ has smaller tails than both the others, but scores not very satisfactorily in the middle quantiles, which suggest non normal residuals.

Figure 3.18: Validation tests of the 3 models under consideration. The autocorrelation and the qq-plot for normality of the residuals are ways to verify that the residuals have white noise property, i.e. are sufficient to explain the dynamics in the data.

Abbreviation	Thermal property	Sampling bounds	Units
Floor	Ground floor insulation thickness	[0.05; 0.25]	cm
Walls	Walls insulation thickness	[0.05; 0.25]	cm
Attics	Attic insulation thickness	[0.05; 0.25]	cm
CthFloor	Thermal capacity floor concrete cast	[1.0; 2.0]	J/kgK
CthWall	Thermal capacity brick wall	[0.6; 1.0]	J/kgK
ACH	Air Change Rate	[0.2; 2.0]	h ⁻¹

Table 3.3: Reminder meaning and sampling bounds of all 6 inputs to the sensitivity analysis

$R_o R_i A_w c_v$ are much less autocorrelated than null hypothesis model $T_w T_i R_o R_i A_w$. This indicates that both the alternatives should be a better fit for the data.

Figure 3.18(b) shows how the residuals perform compared to a reference normal distribution. Although tails are large and show no normally distributed behaviour, both alternative models' residuals are rather normally distributed. The tails might be larger than for normal distributions because of the temporal resolution of the data. If the building has low characteristic times and the heating power is fast compared to the measurement temporal granularity, the residuals will show a certain lag when the temperature setpoint changes. In other words, the indoor air temperature seems to respond fast to the heating power delivered, which is not well caught by the 8 minutes time step. This would call to future smaller time steps, if the case study or the actual building is thought to have low characteristic times.

As a conclusion, it seems that models $T_w T_i R_o R_i A_w R_b$ and $T_w T_i R_o R_i A_w c_v$ fit rather satisfactorily the available data, although not perfectly. On the basis of prediction, the good practice workflow would not prefer any of them. More comprehensive models were found in any case practically non identifiable. They are good candidates to a further interpretability, for both an overall R_{eq} estimation and for individual interpretability assessment.

3.3.2 Estimation of the heat losses through ventilation

As heat losses through air change have shorter time characteristics than heat losses through the building envelope, it might be expected that models taking this time characteristic in their formulation might enable to decompose losses through the envelope from losses by air change.

In this section, the model assessment methodology is applied to study the ability of model $T_w T_i R_o R_i c_v$ to achieve such a decomposition. Parameter c_v should physically represent heat losses through air change whereas parameters R_o and R_i rather account for losses through the envelope, with a longer time characteristic induced by the thermal capacity.

Let us remind here in Table 3.3 the meanings and bounds of the thermal properties used as inputs of the sensitivity analysis.

Variability of parameters C_w, C_i, R_o, R_i, A_w and c_v of model $T_w T_i R_o R_i c_v$

The inputs variability induce different configurations that may reflect on the estimated values of the parameters of model $T_w T_i R_o R_i c_v$.

Figure 3.19 shows the variability of parameters R_o, R_i, C_w, C_i, A_w and c_v of the state space model with respect to the variability of the 6 inputs.

Both thermal resistances R_o and R_i show a correlation with mainly the air change rate and secondly with the attic insulation. The insulation of the walls seems to have on the contrary no influence on the value taken by the resistances, compared to the variability induced by the air change rate and the attic insulation. Parameter c_v seems to be only correlated to the air change rate input. The rest of variability looks like random noise.

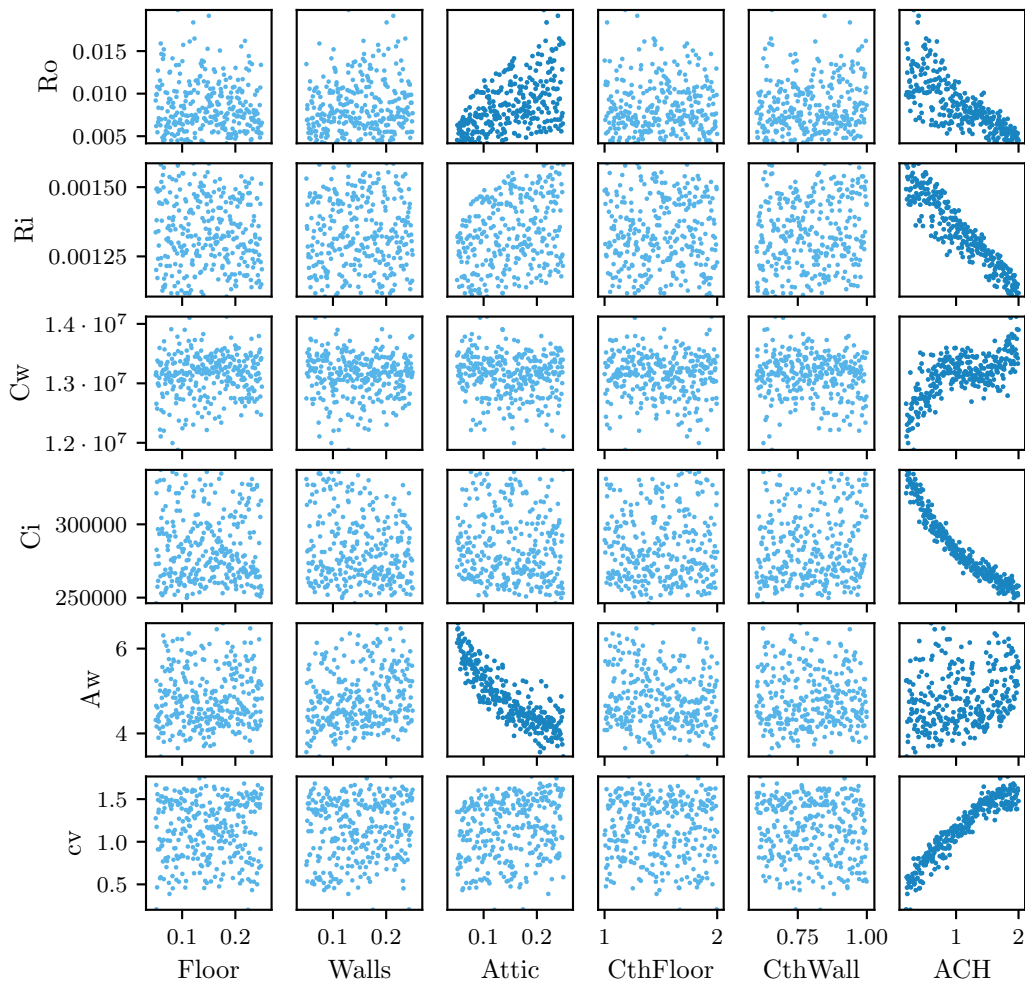


Figure 3.19: Variability of each parameter of model $T_w T_i R_o R_i c_v$ (y-axis) with respect to the variability of the 6 inputs (x-axis). The darker colours suggest influential inputs on the parameter.

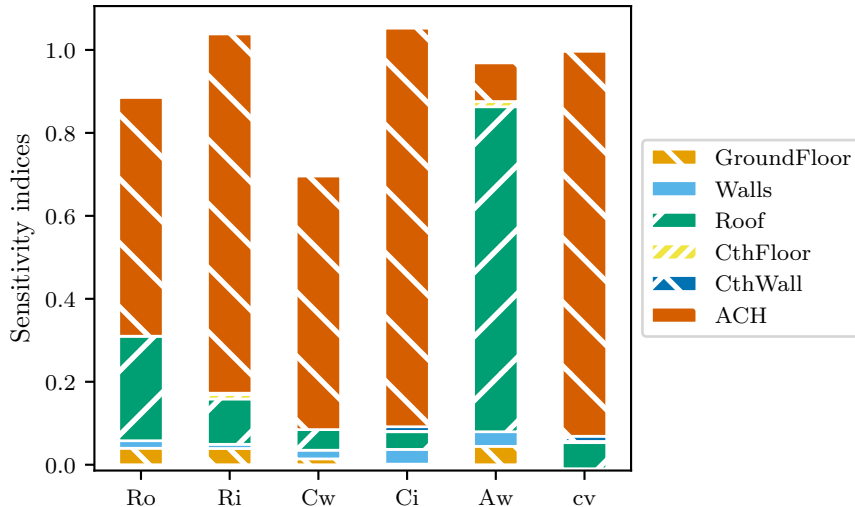


Figure 3.20: Sensitivity indices of all 6 physical parameters of model $T_w T_i R_o R_i c_v$

Both thermal capacities C_w and C_i also have a strong dependence to the air change rate, whereas it could have been expected that the two inputs of thermal capacities (that of the ground floor slab and that of the brick wall) had the major influence.

Parameter A_w shows a large correlation to the attic insulation input. It is likely due to solar irradiation on an almost flat roof causing significant temperature variations. These temperature variations induce heat transfers between the attic and the indoor space that are proportional to the thickness of the insulation between the attics and the indoor space, i.e. to the input variable 'Roof insulation'.

Sensitivity analysis of parameters C_w, C_i, R_o, R_i and c_v

Previous section established possible correlations between certain inputs and the studied outputs. A global sensitivity analysis through variance decomposition will in addition quantify the part of variability due to each input variable and assert significance of their influence.

Figure 3.20 shows the sensitivity indices calculated with the RBD-FAST method. Let us remind first that the convergence is achieved and that the indices may therefore be interpreted. Sensitivity indices have been calculated for quantities of interest R_o, R_i and c_v .

The global variability of R_o is mainly explained by the variability of input air change rate (index 0.58) and to a much lesser extent by input attic insulation (index 0.25). A small part of the variability is explained by effect of the interaction of several inputs, as the total sum of the indices of parameter R_o is not quite close to 1, even considered the uncertainty of the indices.

Similarly, the variability of R_i is explained by the variability of the air change rate (index 0.87) and to a lesser extent the attic insulation (index 0.11). Here, the sum is very close to 1, meaning no interaction effects. Variability of c_v is only explained by air change rate (index 0.93), the rest being insignificant.

Estimation and physical interpretability of ventilation and infiltration

That all R_o, R_i, C_w, C_i and c_v show correlation to the air change rate may also suggest that they all just have a strong covariance, from the parameter estimation, which would indeed translate as a fortuitous correlation. To support this hypothesis, Figure 3.21 shows the probability density functions of all 300 covariances between each couple of parameters.

The covariance between two parameters $\theta_1 \theta_2$ is large when around the optimal fit a small variation in θ_1 is correlated to an identical or opposite variation in θ_2 without affecting much the

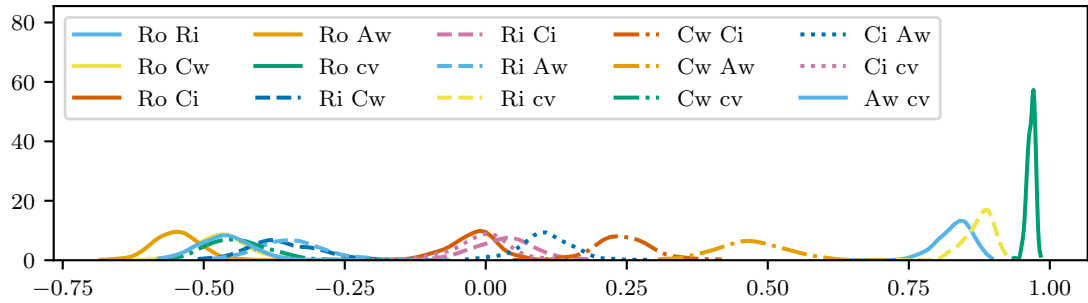


Figure 3.21: Covariance between parameters of model TwTi RoRi cv: parameter cv has a large correlation with parameters R_o and R_i , as are R_o and R_i together

likelihood. Then, it is very likely that both parameters are practically non identifiable. Although the combination of model parameters reaches the best fit, it is impossible to determine the best fitting values for each parameter individually when their covariance is high.

In this figure for example, the covariance of parameters R_o and R_i may be calculated after each calibration. As there are 300 calibrations, all 300 covariances between R_o and R_i may be rendered as a probability density function. Functions higher than 0.5 or lower than -0.5 mean that all 300 covariances are higher than 0.5 or lower than -0.5, meaning that the covariance is significant in all configurations. Figure 3.21 then suggests that $R_o R_i$, $R_o cv$ and $R_i cv$ have strong covariances. To a lesser extent, set $R_o A_w$ also shows significant negative covariances. Taken individually, parameters R_o , R_i and cv should probably not be physically interpreted.

Model $T_w T_i R_o R_i c_v$ introduces parameter c_v to take into account ventilation and infiltration dynamics as a heat flux on the indoor temperature node. The flux is defined as follows:

$$\Phi_v = c_v V \rho c_p (T_{ext} - T_{int}) \quad (3.6)$$

In 3.6, V the heated volume of the building, ρ the volumic mass of air and c_p the specific heat capacity of air are known, which leaves one unknown in the equation to estimate: c_v . With this definition, c_v is then an average air change rate over the duration of the experiment, with dimension h^{-1} . Let us shortly mention that in the simulation conditions, the air change rate actually varies in time with the temperature difference and with the wind speed.

As c_v could be interpreted as an averaged air change rate, let us take a closer look to the variability of parameter c_v in Figure 3.22 where the dotted 45° grey line would be the perfect estimation of the air change rate. Parameter c_v is positively correlated to the air change rate: the higher the air change rate the higher the parameter c_v . However, low air change rates induce a systematic overestimation and high air change rate a systematic large under-estimation.

Seeing the significant covariances between all resistance parameters and seeing that variability of the estimation of c_v and its error to the simulated value of air change rate, it is expected that ventilation and infiltration losses cannot be properly identified from the current design of experiment. Figure 3.23 shows the estimated sum $R_o + R_i$, $R_{ventilation}$ and R_{eq} against their target values for each of the 300 reference model configurations.

The sum $R_o + R_i$, supposedly representing the heat resistance between the indoor space and the exterior, shows no significant correlation with the target value. As for ventilative losses, the order of magnitude seems to be rather well estimated, but with a high variability: for an identical target value, the error spreads from -50% up to 90%. In overall however, the equivalent thermal resistance is well in agreement with the target value.

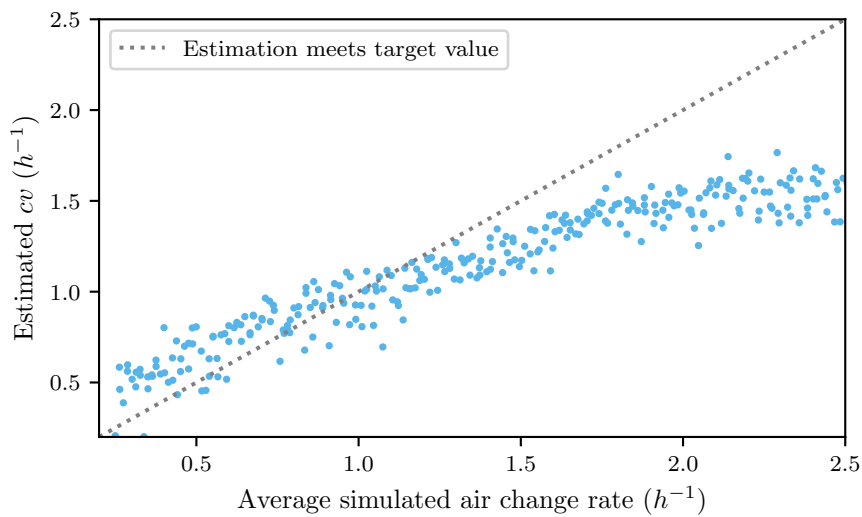


Figure 3.22: Estimation of parameter cv for varying values of air change rate

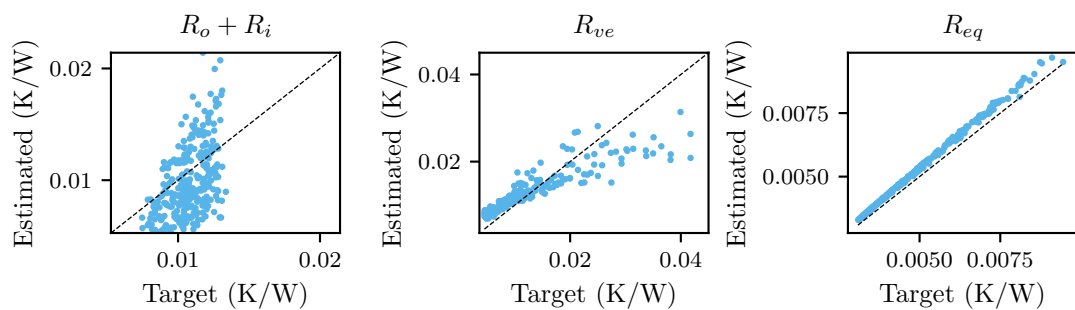


Figure 3.23: Interpretability of $R_o + R_i$, R_{ventil} and R_{eq} for model $T_w T_i R_o R_i c_v$

Conclusions on decomposing ventilative heat losses

Section 3.3.2 applied the numerical model assessment methodology to assess the ability of model $T_w T_i R_o R_i c_v$ to separately identify heat losses through ventilation from the rest of the heat losses, by means of the estimation of an averaged air change rate parameter. The results indicate that model $T_w T_i R_o R_i c_v$ estimates the air change rate parameter c_v with errors up to 90% in absolute regardless of the target rate, implying that the order of magnitude is rather well estimated, but that physical interpretation would be risky.

Highly correlated parameters, visible in significant covariances, are in this study a clear hint that the physical interpretation of the parameters separately is not possible. The performed sensitivity analysis was a confirmation that the high covariances translate in unlogical variability in the parameter estimations with respect to the changes in the reference model.

Model $T_w T_i R_o R_i c_v$ was however found in the model selection process as to fit satisfactorily the data. The results of this section confirm it by showing that the overall thermal resistance R_{eq} is in good agreement with the target value. This indicates that high covariances between parameters may still bear physical meaning when said parameters are combined, as in R_{eq} .

4. Practical applications

Chap. 3 presented a theoretical study of the limitations and potential of building energy performance assessment based on in-situ measurements. A methodology based on a numerical benchmark and sensitivity analysis was developed to assess the feasibility of model calibration and the physical interpretability of estimated model parameters.

The present chapter is the practical part of the contribution of the BAYREB project to the field of building energy performance assessment. It is a collection of practical case studies, using real measurement data from either experimental test cells or occupied buildings. During the project, the methods presented in Chap. 2 for modelling and inference were applied to various monitored buildings, each with its own characteristics: size, occupancy, type and year of construction, HVAC systems, measurement setup and available sensors, monitoring time. In order to sort these applications into useful information for the reader, **the layout of this chapter is centered on the methods and the questions they were used to answer**. These questions are summarised in Tab. 4.1 and match the structure of the following sections.

The following sections can be read independently from each other. They are written in the form of practical exercises, including Python code that the reader may copy and use. In most cases, we tried to make the data accessible so that the code is directly applicable. These examples may also be available in two forms:

- Jupyter notebooks published on the tutorial website <http://buildingenergygeeks.org>, where some of the data may also be downloaded.
- Publications in journals.

4.1 Energy signature: performance assessment with little information



This section is available as a Jupyter notebook on <http://buildingenergygeeks.org>. This is why some parts of the description of the energy signature method, which was already given in Sec. 1.2.2, are repeated here.

The energy signature of a building is a very simple model of its energy consumption profile (all energies combined) as a function of the outdoor temperature. Provided a long enough monitoring

Method	Question	Case study	Occupancy
Energy signature	Performance assessment with little information	Office buildings	Yes
Linear regression	Identifying the influences of the energy balance	House	Yes
State-space models	Robust parameter estimation	Experimental house	No
Latent force models	Robust performance prediction	Experimental house	Virtual
Sequential Monte-Carlo	Real-time HLC estimation	Experimental cell	No
Linear regression, SSM, IMM	Decomposing HLC into HTC and infiltration	House	Yes

Table 4.1: Layout of the practical applications and the questions they wish to answer

period of a building, the method is able to provide a crude estimation of its heat loss coefficient (HLC), and to separate its energy consumption into two (or three) main parts: heating and/or cooling, and other uses. Using a trained energy signature model to predict the energy use is possible, but comes with a large uncertainty.

The appeal of this method is that the data we need to train the model is very easy to obtain:

- Outdoor air temperature
- Energy consumption

We don't even need a short time step between each meter reading, as the data will be resampled (averaged) over samples of one or several days.

4.1.1 The model

The model is written here in terms of the average power Φ (W) between energy readings (kWh).

The total electrical power used in a building is decomposed into three parts: the baseline consumption Φ_b (lighting, appliances, DHW...), heating power Φ_h and cooling power Φ_c

$$\Phi = \Phi_b + \Phi_h + \Phi_c \quad (4.1)$$

The energy signature method relates the heating and cooling energy use to easily measured environmental parameters, typically the outdoor temperature. The model relies on the following, very convenient hypotheses:

- Steady-state: each data point is the average of readings over a sufficiently long period (several days), so that dynamic effects can be overlooked.
- The baseline consumption Φ_b is constant over this broad sampling frequency.
- The indoor temperature is assumed to be quasi-constant, so that heating only is needed when the outdoor temperature T_e is lower than a base temperature T_{b1} . The heating power is then only proportional to the HLC.
- The influence of all other environmental factors is neglected.

The heating power is then approached by the following equations:

$$\Phi_h = \text{HLC}_1 (T_{b1} - T_e) \quad \text{if } T_e \leq T_{b1} \quad (4.2)$$

$$\Phi_h = 0 \quad \text{if } T_e > T_{b1} \quad (4.3)$$

If the building has air conditioning, the same relation can be assumed for cooling, if the outdoor temperature exceeds a threshold T_{b2} :

$$\Phi_c = 0 \quad \text{if } T_e < T_{b2} \quad (4.4)$$

$$\Phi_c = \text{HLC}_2 (T_e - T_{b2}) \quad \text{if } T_e \geq T_{b2} \quad (4.5)$$

The model therefore has either three or five unknown parameters: the baseline power Φ_b ; the heat loss coefficient HLC, which may have a different value in heating than in cooling conditions; one or two threshold temperatures T_b

4.1.2 The data: commercial buildings

The data used in this example to illustrate the energy signature method is the hourly energy consumption and outdoor air temperature data for 11 commercial buildings (office/retail), publicly available here¹.

The code written below supposes that the data files have been downloaded and saved to a /data folder. We are only going to use three of the available data files, which are three consecutive years from a single office building: `building60preoffice.csv`, `building61duringoffice.csv` and `building62postoffice.csv`.

It starts by some imports.

```
import pandas as pd
import numpy as np
import matplotlib.pyplot as plt
```

A data analysis exercise usually starts by taking a look at the formatting of the data files.

```
df = pd.read_csv('data/building60preoffice.csv')
df.head()
```

	Date	OAT	Building 6 kW
0	1/2/2009 0:00	41.6	23.3
1	1/2/2009 1:00	40.9	23.1
2	1/2/2009 2:00	39.5	23.7
3	1/2/2009 3:00	36.3	29.1
4	1/2/2009 4:00	32.8	35.6

The datafile is already "clean" with no missing value. The only data processing we will do before defining and training the model is:

- Translating the Date column into a datetime object which Python understands as temporal data
- Converting the outdoor air temperature OAT from (F) to (C) because the data originates from the USA
- Averaging the data over periods of one day
- Noting the day of the week, because this factor usually has an impact on the consumption of retail and office buildings

¹<https://openei.org/datasets/dataset/consumption-outdoor-air-temperature-11-commercial-buildings>

```

df.set_index(pd.to_datetime(df['Date']), inplace=True)
df['Te'] = (df['OAT']-32) * 5/9

# New dataframe for the daily averaged data
df_day = df.resample('D').mean()

# Week days
df_day['week_day'] = [df_day.index[_].weekday() for _ in range(len(df_day))]
weekend = (df_day['week_day']==5) | (df_day['week_day']==6)

df_day.head()

```

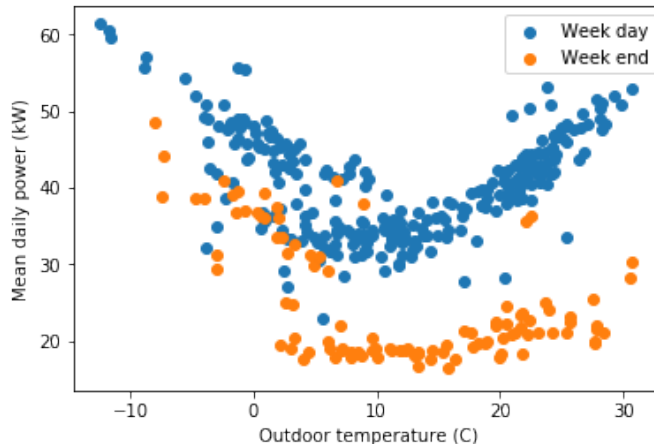
Date	OAT	Building 6 kW	Te	week_day
2009-01-02	33.375000	36.787500	0.763889	4
2009-01-03	18.908333	44.187500	-7.273148	5
2009-01-04	17.700000	48.645833	-7.944444	6
2009-01-05	23.445833	51.983333	-4.752315	0
2009-01-06	45.941667	41.891667	7.745370	1

We can now take a look at the relationship between air temperature and power, in order to see if there is a trend.

```

plt.figure()
plt.scatter(df_day['Te'][~weekend], df_day['Building 6 kW'][~weekend])
plt.scatter(df_day['Te'][weekend], df_day['Building 6 kW'][weekend])
plt.xlabel('Outdoor temperature (C)')
plt.ylabel('Mean daily power (kW)')
plt.legend()
plt.show()

```



Each dot is one day. This plot clearly shows two things:

- Week days and week ends are separated: in the following, we should only keep week days for the energy signature model.

- The power is clearly influenced by low and high temperatures. The trend seems close to linear on each side, confirming the choice of the energy signature model (this particular building was not chosen randomly...)

4.1.3 Model definition and training

The energy signature model is an expression of the total electric consumption of a building as a function of the outdoor temperature and up to five fixed parameters. The notations of the code below match the equations given earlier.

```
def signature(T, Phi_b, T_b1, T_b2, HLC_1, HLC_2):
    """
    input : temperature T, and five parameters
    output: power P
    """

    P = Phi_b * np.ones(len(T))

    mask1 = T < T_b1
    P[mask1] += HLC_1 * (T_b1-T[mask1])

    mask2 = T > T_b2
    P[mask2] += HLC_2 * (T[mask2]-T_b2)

    return P
```

Now that this evaluation function is defined, we can use it in a curve fitting algorithm which will find the optimal parameters to match a given dataset: the `curve_fit` method of the `scipy.optimize` library. The week end days are filtered out. The method requires a starting point `p0` for the parameters, which we can estimate from the graph above.

```
from scipy.optimize import curve_fit

T = df_day['Te'][~weekend]
P = df_day['Building 6 kW'][~weekend]

popt, pcov = curve_fit(signature,
                       xdata = T,
                       ydata = P,
                       p0 = [20, 10, 15, 1.5, 1.5])

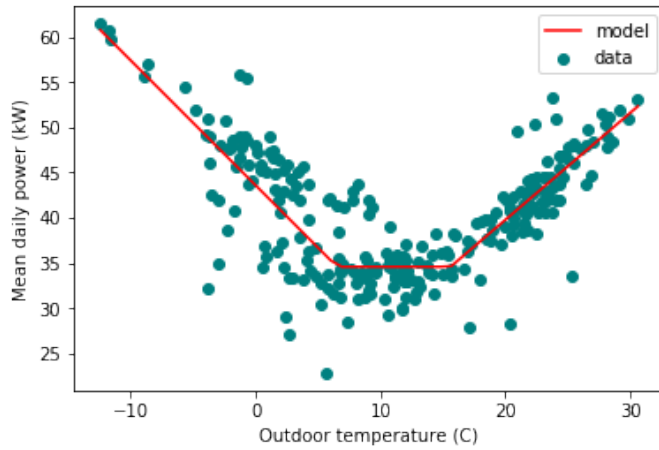
print('Baseline power: %.2f kW' % popt[0])
print('Lower threshold temperature: %.2f C' % popt[1])
print('Upper threshold temperature: %.2f C' % popt[2])
print('HLC (winter): %.2f kW/K' % popt[3])
print('HLC (summer): %.2f kW/K' % popt[4])

Baseline power: 34.57 kW
Lower threshold temperature: 6.53 C
Upper threshold temperature: 15.62 C
HLC (winter): 1.38 kW/K
HLC (summer): 1.18 kW/K

# Plot the results: comparing the fitted model with its data
xx = np.linspace(T.min(), T.max())
```

```
yy = signature(xx, popt[0], popt[1], popt[2], popt[3], popt[4])

plt.figure()
plt.scatter(T, P, label='data', color='teal')
plt.plot(xx, yy, label='model', color='red')
plt.xlabel('Outdoor temperature (C)')
plt.ylabel('Mean daily power (kW)')
plt.legend()
plt.show()
```



The model seems well fitted with the trend in the data. As this is a simple exercise, we are not analysing the indicators of statistical significance of the parameters: this will be done in other methods such as ordinary linear regression.

4.1.4 Further questions

Comparing the HLC estimation across several years

Since we have three data files for the same building, and each file is one year of measurements, we can check if the estimation of HLC is consistent across these years. In order to do this quickly, let us automate the steps described above into a single function that will return the optimal parameters as a function of only the datafile (this function requires that the labels of all files match).

```
def prepare_data(datafile):

    # Read data
    df = pd.read_csv(datafile)
    # Process the data
    df.set_index(pd.to_datetime(df['Date']), inplace=True)
    df['Te'] = (df['OAT']-32) * 5/9
    # New dataframe for the daily averaged data
    df_day = df.resample('D').mean()
    # Week days
    df_day['week_day'] = [df_day.index[_].weekday() for _ in range(len(df_day))]
    df_day['weekend'] = (df_day['week_day']==5) | (df_day['week_day']==6)

    return df_day

def estimate_hlc(datafile):
```

```

df_day = prepare_data(datafile)

popt, pcov = curve_fit(signature,
                        xdata = df_day['Te'][~df_day['weekend']],
                        ydata = df_day['Building 6 kW'][~df_day['weekend']],
                        p0 = [20, 10, 15, 1.5, 1.5])

return popt

popt_0 = estimate_hlc('data/building60preoffice.csv')
popt_1 = estimate_hlc('data/building61duringoffice.csv')
popt_2 = estimate_hlc('data/building62postoffice.csv')

print('HLC (heating): %.2f kW/K, %.2f kW/K, %.2f kW/K'
      % (popt_0[3], popt_1[3], popt_2[3]))
print('HLC (cooling): %.2f kW/K, %.2f kW/K, %.2f kW/K'
      % (popt_0[4], popt_1[4], popt_2[4]))

HLC (heating): 1.38 kW/K, 1.25 kW/K, 2.03 kW/K
HLC (cooling): 1.18 kW/K, 0.98 kW/K, 0.89 kW/K

```

The values are somehow consistent, but the last year of observation shows a much higher heating consumption relatively to the outdoor temperature. This method can for instance be used to estimate the impact of energy conservation measures.

Predicting the energy use

Another purpose of the energy signature model is to predict the energy use of a building, supposing that forecasts of the outdoor temperature are available. In the example below, we will see if the parameters learned in the first year of measurements, using `building60preoffice.csv`, can forecast the consumption observed on the next two years.

```

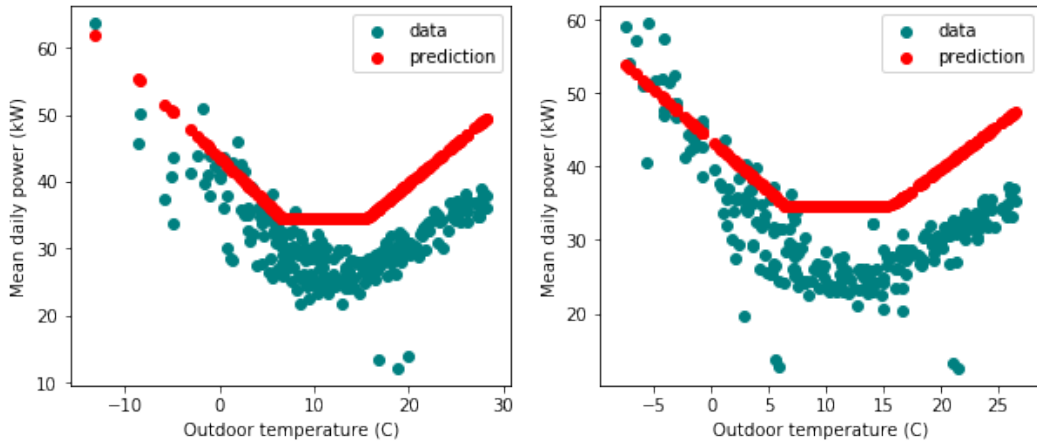
# Loading and processing the data files for the second and third years
df_day_1 = prepare_data('data/building61duringoffice.csv')
df_day_2 = prepare_data('data/building62postoffice.csv')

# Measured consumptions and temperatures
T_1 = df_day_1['Te'][~df_day_1['weekend']]
T_2 = df_day_2['Te'][~df_day_2['weekend']]
P_real_1 = df_day_1['Building 6 kW'][~df_day_1['weekend']]
P_real_2 = df_day_2['Building 6 kW'][~df_day_2['weekend']]
# Consumptions predicted by the model trained with the first dataset
P_pred_1 = signature(T_1, popt_0[0], popt_0[1], popt_0[2], popt_0[3], popt_0[4])
P_pred_2 = signature(T_2, popt_0[0], popt_0[1], popt_0[2], popt_0[3], popt_0[4])

plt.figure(figsize=(10,4))
plt.subplot(121)
plt.scatter(T_1, P_real_1, label='data', color='teal')
plt.scatter(T_1, P_pred_1, label='prediction', color='red')
plt.xlabel('Outdoor temperature (C)')
plt.ylabel('Mean daily power (kW)')
plt.legend()
plt.subplot(122)
plt.scatter(T_2, P_real_2, label='data', color='teal')

```

```
plt.scatter(T_2, P_pred_2, label='prediction', color='red')
plt.xlabel('Outdoor temperature (C)')
plt.ylabel('Mean daily power (kW)')
plt.legend()
plt.show()
```



We can clearly see that the model trained on the first year of data overestimates the actual consumption of the next two years. The main difference seems to be the baseline consumption which has significantly decreased, although it does not seem that the HLC has. This might be the consequence of energy conservation measures concerning other energy uses than heating and cooling.

4.2 Linear regression: identifying what influences the energy balance



This section is available as a Jupyter notebook on <http://buildingenergygeeks.org>. This is why some parts of the description of the energy signature method, which was already given in Sec. 1.2.2, are repeated here.

Linear regression models are one of the most simple forms of relationship that can be proposed between measured data. They often serve as an introduction to statistical learning [HTF01] because they offer a simple framework to demonstrate the important steps that a data analyst should follow: model selection, hypothesis testing, validation...

Under some strong hypotheses, the energy balance of a building can be approximated by linear functions. They however have several limitations: they cannot represent non-linear phenomena, such as radiative heat exchange between walls; they don't allow identifying the parameters driving dynamical phenomena; they impose a fixed structure to the energy balance equation.

Despite these limitations, linear regression models can however be very useful as a first insight into the heat balance of a building: they allow a quick assessment of which types of measurements have an impact on the global balance and guide the choice of more detailed models. Moreover, if a large enough amount of data is available, the estimates of some coefficients such as the HLC often turn out to be quite reliable.

In this section, we show a practical application of linear regression to the identification of the important phenomena that influence the energy use in a house.

4.2.1 The data: ORNL test house

The data used in this example was published² by the Oak Ridge National Laboratory, Building Technologies Research and Integration Center (USA). It contains end use breakdowns of energy use and various indoor environmental conditions collected at the Campbell Creek Research House #3, at a 15 minute time stamp. The data availability ranges from 10/1/2013 to 9/30/2014.

This dataset was chosen in this example for the diversity and duration of the available measurements.

Before taking a look at the data, let us start with some imports.

```
# The holy trinity
import pandas as pd
import numpy as np
import matplotlib.pyplot as plt

# What we will use for regression
import statsmodels.api as sm

# bokeh is very good for a first exploration of a dataset
from bokeh.plotting import figure, show
from bokeh.layouts import column
from bokeh.palettes import Category10
from bokeh.io import output_notebook
output_notebook()

# Opening the data file and showing the timestamps to pandas
df = pd.read_excel('data/ornlbtricdatafromcc3fy2014.xlsx', header=1).iloc[2:]
df.set_index(pd.to_datetime(df['TIMESTAMP']), inplace=True, drop=True)

# Dealing with missing values
df.replace('NAN', np.nan, inplace=True)
df.fillna(method='pad', inplace=True)
```

This dataframe has quite a lot of features, as shown by the output of the `.head()` method. The meaning of each column is specified in a separate table. This is where I recommend using the bokeh library for its convenient plotting tools, shown as an example below.

The house is heated and cooled by a heat pump, and most energy uses (plugs, appliances, hot water production...) are broken down and measured separately. Temperatures, relative humidities are also available in several locations. We are going to use the **energy use of the heat pump** as the output variable of linear regression models, and try to explain it with the other available variables.

In the following block, a new dataframe is created to only keep variables that we believe may influence the heating and cooling energy consumption of the house. Note that this is already an important decision in the data analysis process, as we might be filtering out information that could have been useful.

- Energy readings: heat pump, domestic hot water production, ventilation fan power and other uses.
- Temperatures: average indoor temperature, garage (adjacent unheated space), ventilation supply temperature and outdoor temperature.
- Weather variables: solar irradiance and wind speed are usually known to impact the energy balance.

Finally, only the months of November to March are kept in this exercise.

²<https://openei.org/datasets/dataset/ornl-research-house-3>

```

df2 = pd.DataFrame(index=df.index)

# Energy readings: heat pump, hot water, fan and other uses
df2['e_hp'] = df[['HP_in_Tot', 'HP_out_Tot']].sum(axis=1)
df2['e_dhw'] = df['HW_Tot']
df2['e_fan'] = df['Fantech_Tot']
df2['e_other'] = df['main_Tot'] - df2['e_hp'] - df2['e_dhw'] - df2['e_fan']

# Temperatures: indoor, garage, ventilation supply, and outdoor
df2['ti'] = (df[['Din_tmp_Avg', 'Grt_tmp_Avg', 'Brkf_tmp_Avg', 'Kit_tmp_Avg',
                  'BedM_tmp_Avg', 'Bed3_tmp_Avg', 'Bed2_tmp_Avg', 'BedB_tmp_Avg',
                  'Mbatch_tmp_Avg']]).mean(axis=1) - 32 ) * 5/9
df2['tg'] = (df['garage_tmp_Avg'] - 32) * 5/9
df2['ts'] = (df['FanTsup_RH_Avg'] - 32) * 5/9
df2['te'] = (df['Outside_Tmp_Avg'] - 32) * 5/9

# Other weather variables: solar irradiance and wind speed
df2['i_sol'] = df['SlrW1_Avg']
df2['wind_speed'] = df['wind_speed_mean']

# Let's only keep winter for now
df2.drop(df2.index[(df2.index < pd.to_datetime('2013-11-01')) | 
                    (df2.index >= pd.to_datetime('2014-04-01'))], inplace=True)

```

The following block creates a bokeh plot of the variables we just selected. This library offers convenient features such as the ability to zoom in or pan on a graph, and to hide legend entries by clicking them.

```

palette = Category10[5]

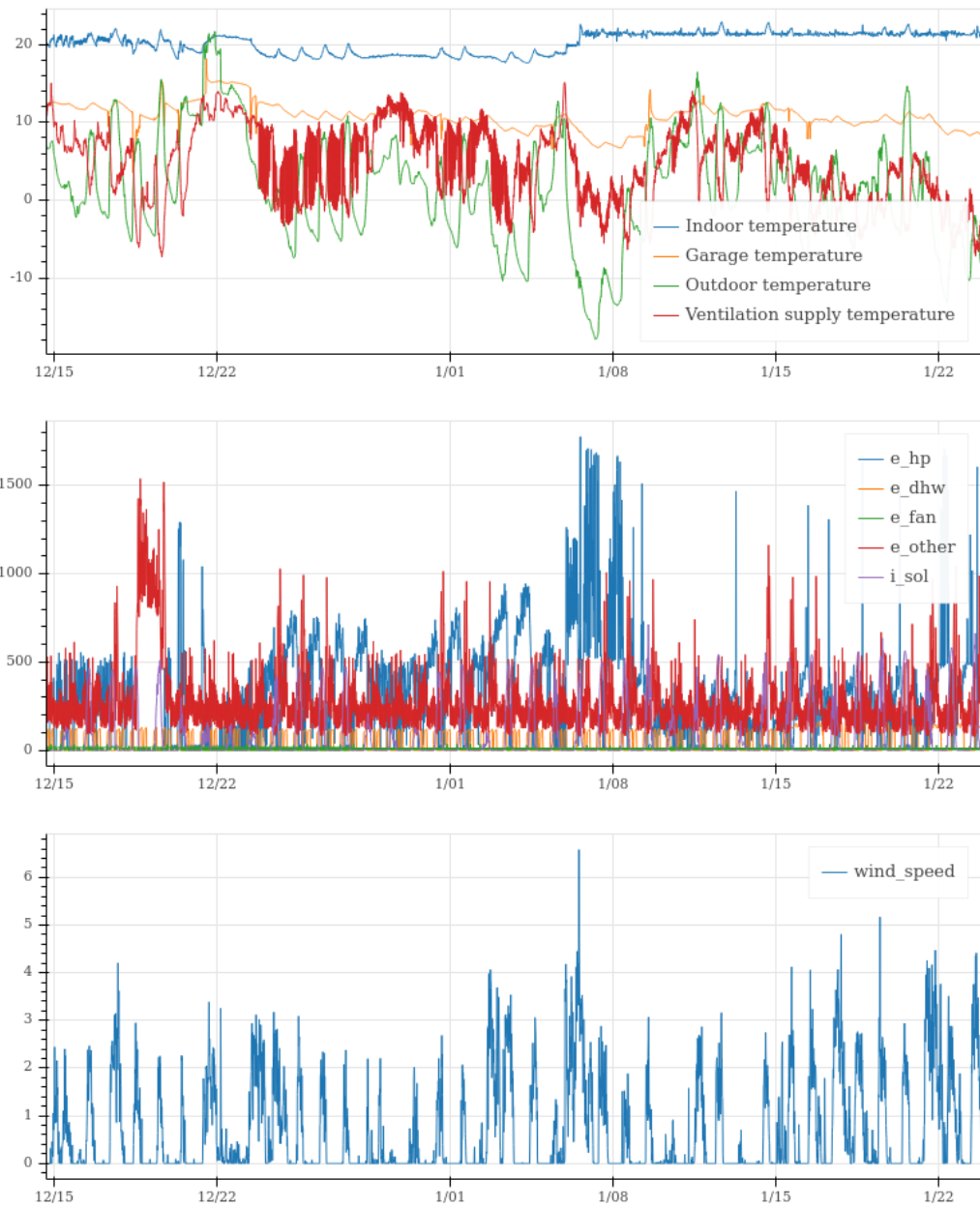
p1 = figure(x_axis_type="datetime", y_range=(-20, 40),
            plot_width=800, plot_height=300)
p1.line(df2.index, df2['ti'], color=palette[0], legend='Indoor temperature')
p1.line(df2.index, df2['tg'], color=palette[1], legend='Garage temperature')
p1.line(df2.index, df2['te'], color=palette[2], legend='Outdoor temperature')
p1.line(df2.index, df2['ts'], color=palette[3], legend='Vent. supply temperature')
p1.legend.location = "bottom_right"
p1.legend.click_policy="hide"

p2 = figure(x_axis_type="datetime", x_range=p1.x_range,
            plot_width=800, plot_height=300)
p2.line(df2.index, df2['e_hp'], color=palette[0], legend='e_hp')
p2.line(df2.index, df2['e_dhw'], color=palette[1], legend='e_dhw')
p2.line(df2.index, df2['e_fan'], color=palette[2], legend='e_fan')
p2.line(df2.index, df2['e_other'], color=palette[3], legend='e_other')
p2.line(df2.index, df2['i_sol'], color=palette[4], legend='i_sol')
p2.legend.location = "top_right"
p2.legend.click_policy="hide"

p3 = figure(x_axis_type="datetime", x_range=p1.x_range,
            plot_width=800, plot_height=300)
p3.line(df2.index, df2['wind_speed'], color=palette[0], legend='wind_speed')
p3.legend.location = "top_right"

show(column(p1, p2, p3))

```



4.2.2 The model

Since we have time series data, the most informative way to use it would be a time series model, typically of the family of autoregressive models with exogenous variables, or an RC state-space model. This would allow us to identify the influences on the dynamics of the output variable.

The present notebook however proposes a more simple, stationary balance equation. This is the full model equation that we are going to consider, supposing that the heat pump is operating in winter conditions:

$$\Phi_{hp} + \Phi_s + \Phi_v + \Phi_{inf} = H(T_i - T_e) + H_g(T_i - T_g) \quad (4.6)$$

On the left side are the heat sources Φ (W), some of which may be negative

- $\Phi_{hp} \propto e_{hp}$ is the heating power provided by the heat pump to the indoor space. It is proportional to the energy reading e_{hp} (Wh), which we will use as output variable, and to the time step size and the COP of the heat pump, supposed constant.
- $\Phi_s = A_s I_{sol}$, are the solar gains, supposed proportional to the measured outdoor solar irradiance I_{sol} (W/m^2) and an unknown constant solar aperture coefficient A_s (m^2).
- $\Phi_v = \dot{m} c_p (T_s - T_i)$ is the ventilation heat input, with a ventilation supply rate \dot{m} and supply temperature T_s , which is measured (the house has a mechanical ventilation system with heat recovery)
- $\Phi_{inf} \sim V_{ws}(T_e - T_i)$ is the heat input from air infiltration. We suppose it is proportional to the wind speed V_{ws} and the outdoor-indoor temperature difference.

On the right side are two terms of heat loss through the envelope:

- $H(T_i - T_e)$ is the direct heat loss from the heated space at temperature T_i and the outdoor at T_e
- $H_g(T_i - T_g)$ is the heat loss through the partition wall between the heated space and an unheated garage at T_g .

Linear regression should allow us to identify the coefficients of each term, supposing that they have enough variability and influence on the output Φ_{hp} . The outcome of the regression method will let us judge if this hypothesis is appropriate.

In the next step, we create new features in the df2 dataset to match the hypothesis of this model. Next, data are resampled over daily steps, in order to allow the hypothesis of stationary conditions.

```
df2['tits'] = df2['ti'] - df2['ts']
df2['vtite'] = df2['wind_speed'] * (df2['ti'] - df2['te'])
df2['tite'] = df2['ti'] - df2['te']
df2['titg'] = df2['ti'] - df2['tg']

df_day = df2.resample('1D').mean()
```

4.2.3 Training

First simple model

Before fitting the full model shown above, let us try one with a single explanatory variable, which we assume has the most influence on the energy use of the heat pump: the heat transmission through the envelope.

$$e_{hp} = a_1(T_i - T_e) \quad (4.7)$$

where the a_1 parameter includes the heat loss coefficient H , the COP of the heat pump and the time step size. Since the COP is unknown, we won't be able to estimate H . This is fine, as the point of the exercise is mostly to identify influential features.

```

# Choosing output and inputs
y = df_day['e_hp']
x = df_day[['tite']]

# Model fitting
res = sm.OLS(endog=y, exog=x).fit()

# Summary of the results in a table
print(res.summary())

# Scatter plot of the fitted model
fig, ax = plt.subplots()
fig = sm.graphics.plot_fit(res, 0, ax=ax)
ax.set_ylabel('Heat pump energy (Wh)')
ax.set_xlabel('$T_i - T_e$ (C)')
plt.show()

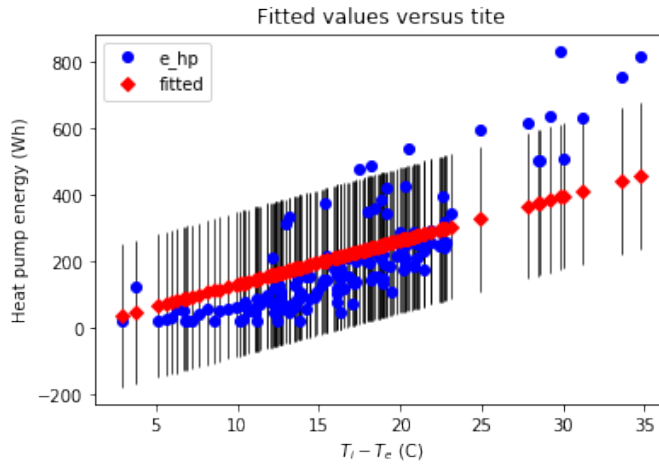
OLS Regression Results
=====
Dep. Variable:          e_hp    R-squared:       0.817
Model:                 OLS     Adj. R-squared:   0.816
Method:                Least Squares  F-statistic:      670.2
Date:      Wed, 01 Apr 2020  Prob (F-statistic): 3.30e-57
Time:          13:52:50    Log-Likelihood:   -923.13
No. Observations:      151     AIC:             1848.
Df Residuals:          150     BIC:             1851.
Df Model:                  1
Covariance Type:        nonrobust
=====
            coef      std err      t      P>|t|      [0.025      0.975]
-----
tite      13.2377      0.511    25.888      0.000     12.227     14.248
=====
Omnibus:           64.945  Durbin-Watson:      0.389
Prob(Omnibus):      0.000  Jarque-Bera (JB): 160.288
Skew:              1.857  Prob(JB):      1.56e-35
Kurtosis:           6.417  Cond. No.:      1.00
=====

Warnings:
[1] Standard Errors assume that the covariance matrix of the errors is
    correctly specified.

```

The table displays the results of the linear regression fitting by ordinary least squares. Some indicators are useful to judge if the model sufficiently explains the output data, or if some input features are redundant.

- The t-statistic and p-value indicate whether an input has a significant influence on the input: $P>|t|$ should be close to zero, meaning that the null hypothesis should be rejected. In this case, the only input is relevant.
- R-squared measures the goodness of fit of the regression. 0.817 is a rather low value, which hints that the output should be explained by additional features in the model.
- AIC and BIC will be used to compare several models. A lower value is preferred.
- A low Durbin-Watson statistic suggests a high autocorrelation of residuals, which means that the model structure is inappropriate.



The plot confirms that the data is not solely explained by a linear function of $(T_i - T_e)$, and the model should be improved.

Complete model

Now we can try a more complete linear regression model, which matches the full model described by Eq. 4.6

$$e_{hp} = a_1(T_i - T_e) + a_2(T_i - T_g) + a_3 I_{sol} + a_4(T_i - T_s) + a_5 V_{ws}(T_i - T_e) \quad (4.8)$$

This model has five inputs, which we defined as functions of the columns of the original dataset.

```
# Model definition and fitting
y = df_day['e_hp']
x = df_day[['tite', 'titg', 'i_sol', 'tits', 'vtite']]
res = sm.OLS(endog=y, exog=x).fit()
print(res.summary())

OLS Regression Results
=====
Dep. Variable:          e_hp    R-squared:       0.866
Model:                 OLS     Adj. R-squared:   0.861
Method:                Least Squares  F-statistic:      188.1
Date:      Wed, 01 Apr 2020  Prob (F-statistic): 8.93e-62
Time:      13:52:50        Log-Likelihood:   -899.85
No. Observations:      151        AIC:             1810.
Df Residuals:          146        BIC:             1825.
Df Model:                  5
Covariance Type:    nonrobust
=====
            coef    std err        t     P>|t|      [0.025]     [0.975]
-----
tite      22.3649    2.203    10.151      0.000     18.010     26.719
titg      1.2207    5.845     0.209      0.835    -10.332     12.773
i_sol     -0.3868    0.202    -1.917      0.057     -0.785     0.012
tits     -8.2306    3.605    -2.283      0.024    -15.354     -1.107
vtite     -0.1931    0.710    -0.272      0.786     -1.596      1.209
=====
Omnibus:           28.379  Durbin-Watson:      0.585
```

```

Prob(Omnibus):          0.000   Jarque-Bera (JB):        38.606
Skew:                  1.066   Prob(JB):            4.14e-09
Kurtosis:              4.263   Cond. No.             97.1
=====

```

Warnings:

[1] Standard Errors assume that the covariance matrix of the errors is correctly specified.

The R-squared has improved, and the AIC and BIC criteria have decreased: this model seems to be a better choice than the first one.

Two input variables however have a very high *p*-value: $(T_i - T_g)$ and $V_{ws}(T_i - T_e)$. This suggests that the heat transfer between the heated space and the garage, and the wind, have little impact on the energy consumption of the heat pump. We can simplify the model by removing these two features:

```

y = df_day['e_hp']
x = df_day[['tite', 'i_sol', 'tits']]
res = sm.OLS(endog=y, exog=x).fit()
print(res.summary())

```

OLS Regression Results

```

=====
Dep. Variable:           e_hp      R-squared:                 0.866
Model:                 OLS       Adj. R-squared:            0.863
Method:                Least Squares   F-statistic:            317.5
Date:      Wed, 01 Apr 2020   Prob (F-statistic):        3.04e-64
Time:          13:52:50       Log-Likelihood:          -899.93
No. Observations:      151        AIC:                   1806.
Df Residuals:          148        BIC:                   1815.
Df Model:                      3
Covariance Type:    nonrobust
=====
      coef    std err          t      P>|t|      [0.025      0.975]
-----
tite     22.4237    1.783     12.573      0.000     18.899     25.948
i_sol    -0.3878    0.189     -2.050      0.042     -0.762     -0.014
tits     -7.7897    2.601     -2.995      0.003    -12.930     -2.650
=====
Omnibus:             27.272   Durbin-Watson:            0.591
Prob(Omnibus):        0.000   Jarque-Bera (JB):        36.240
Skew:                  1.048   Prob(JB):            1.35e-08
Kurtosis:              4.170   Cond. No.             46.0
=====
```

Warnings:

[1] Standard Errors assume that the covariance matrix of the errors is correctly specified.

With fewer dimensions, the AIC and BIC criteria have decreased. Furthermore, the R-squared was not impacted by the removal of two features, suggesting that they were indeed not influential.

This model seems to be a decent compromise, although some influences still appear to be missing.

Adding features

Eq. 4.6 includes the influences that we assumed the most relevant to the energy consumption of the heat pump. The data may contain some additional explanatory variables, which may help predict e_{hp} outside of this formalisation. For instance, the energy for DHW production e_{dhw} and other uses e_{other} indicate occupancy, which could be correlated to e_{hp} .

```
y = df_day['e_hp']
x = df_day[['tite', 'titg', 'titst', 'e_dhw', 'e_other']]
res = sm.OLS(endog=y, exog=x).fit()
print(res.summary())

# Scatter plot of the fitted model
fig, ax = plt.subplots()
fig = sm.graphics.plot_fit(res, 0, ax=ax)
ax.set_ylabel('Heat pump energy (Wh)')
ax.set_xlabel('$T_i - T_e$ (C)')
plt.show()
```

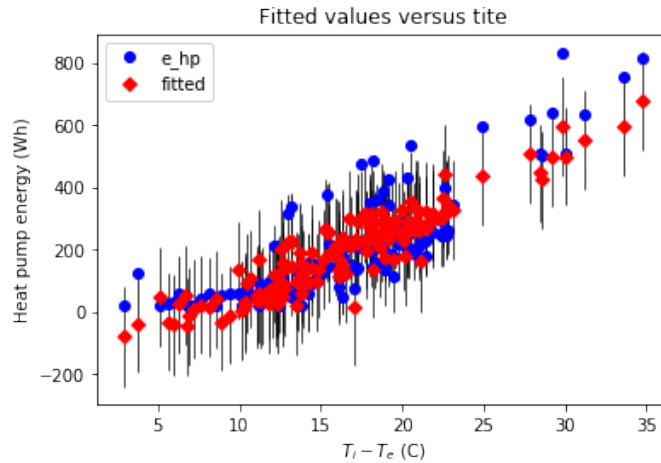
OLS Regression Results						
=====						
Dep. Variable:	e_hp	R-squared:	0.909			
Model:	OLS	Adj. R-squared:	0.906			
Method:	Least Squares	F-statistic:	292.1			
Date:	Wed, 01 Apr 2020	Prob (F-statistic):	3.87e-74			
Time:	13:52:50	Log-Likelihood:	-870.33			
No. Observations:	151	AIC:	1751.			
Df Residuals:	146	BIC:	1766.			
Df Model:	5					
Covariance Type:	nonrobust					
=====						
	coef	std err	t	P> t	[0.025	0.975]
=====						
tite	23.4624	1.657	14.157	0.000	20.187	26.738
titg	19.3457	4.825	4.010	0.000	9.810	28.881
titst	-10.3815	2.062	-5.035	0.000	-14.457	-6.306
e_dhw	-2.0580	0.429	-4.796	0.000	-2.906	-1.210
e_other	-0.3216	0.083	-3.890	0.000	-0.485	-0.158
=====						
Omnibus:	10.411	Durbin-Watson:	0.832			
Prob(Omnibus):	0.005	Jarque-Bera (JB):	10.964			
Skew:	0.659	Prob(JB):	0.00416			
Kurtosis:	3.085	Cond. No.	203.			
=====						

Warnings:

[1] Standard Errors assume that the covariance matrix of the errors is correctly specified.

Using the same indicators as before, it seems that the model has been improved again. The graph seems to confirm this result.

As a further improvement, we could suggest using qualitative features such as the day of the week. The energy signature (see Sec. 4.1) shows that in some buildings, this information is very relevant on the energy use. This building is however a house, with probably less difference between week days and week ends than in office buildings.



4.3 Stochastic state-space models: dynamic parameter estimation



This section is a summary of the article published in [RRO18].

Most of the time, the inverse problem of parameter characterisation is formulated supposing an unbiased model [MJP11b]. According to this hypothesis, there exists a set of parameter values that will allow the model to accurately simulate reality, and the only deviation between its output and experimental observations is measurement noise. This hypothesis is exceedingly optimistic, especially when models used for the characterisation of building thermal behaviour are simplified resistor-capacitor (RC) structures [Jan16a]. Accounting for modelling approximations is essential for the legitimacy of calibrated models and the interpretability of their parameters. One possible way to do so is using stochastic differential equations, solved with a Kalman filter for the estimation of states [SS16a]. Another option for the quantification of model uncertainty is to calibrate a discrepancy function in an iterative model updating procedure [AAC12; KO01].

The literature offers many applications of parameter estimation and forecasting with stochastic models [AMH00; BM11; KMJ04; MH95], but no direct comparison with their deterministic counterpart. According to [KMJ04]: *stochastic models give more reproducible results and less bias, because random effects due to process and measurement noise are not absorbed into the parameter estimates but specifically accounted for by the noise terms.* Separately, [BO14] stated and demonstrated that *an analysis that does not account for model discrepancy may lead to biased and over-confident parameter estimates and predictions.* The target of this section is to show this effect.

The theory of stochastic state space models and Kalman filtering was presented in Sec. 2.3.2. The following describes the questioning, case study and results that were published in [RRO18]

4.3.1 Questioning and case study

The question

The calibration of building energy models, such as simplified RC structures, can be done either in the aim of physical parameter estimation or the identification of a system for predictive purposes. In both cases, the user starts by formulating the model in continuous time (see Eq. 2.9 and 2.10 for an example), which after discretisation resembles Eq. 2.14. This formulation can then be used for states estimation, parameter estimation and forecasting.

The process noise w_t is often not included in the system equation, although RC models are very simplified. This means that a potentially important source of error is neglected in an inverse problem, where each error may have important consequences on results.

The question this paper aims to answer is: **what are the effects of accounting for modelling uncertainty on the results of parameter estimation and indoor temperature forecasting?** In order to answer it, model calibration was carried with seven separate training datasets from the same building, operating in similar conditions (described below) from May to August 2017. The same RC model structure was thus calibrated seven times, resulting in seven estimates (posterior PDF's) for each parameter of the model (resistances, capacitances, effective solar aperture). Results will be presented in two parts:

- **Parameter estimation:** estimated parameter values and their uncertainty intervals are compared across all datasets, in order to show whether using a stochastic rather than deterministic model result in more robust (consistent) parameter estimates;
- **Forecasting:** each dataset is used alternatively as a training set or a test set, in a form of 7-fold cross-validation, in order to assess the predictive bias and variance of deterministic and stochastic alternatives.

In the stochastic modelling situation, the procedure for parameter estimation and forecasting follows the steps presented in Sec. 2.3.2. In the deterministic case, the system noise w_t is removed from Eq. 2.14: states $\mathbf{x}_{1:N}$ are single point values and no Kalman filtering is applied. The objective function of the parameter estimation problem is simply the sum of squared errors, as described above.

Case study: Armadillo Box

The experimental test cell used in this study is called the Armadillo Box. It is a demonstration building of 42 m^2 floor area, designed for the 2010 European Solar Decathlon by the ENSAG-GAIA-INES team. The envelope is a light wood framed construction with integrated insulation. Heating and cooling is performed by a “3 in 1” heat pump, and photovoltaic solar panels provide recharge for electric vehicles. A large glazing area on the southern facade ensures solar heat gain in winter, while shadings have been sized to reduce summer overheating. The building considered in this study, shown on Fig. 4.1, is a copy of the original Armadillo Box, built on the INES test facilities to investigate its performance on the long term. A technical room on the northern side hosts monitoring equipment.

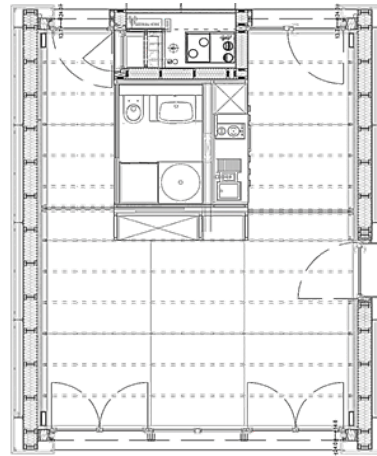


Figure 4.1: View of the southern facade and floor plan of the Armadillo Box

The building is monitored by a variety of sensors, but the present study only uses records of indoor temperature and prescribed heating power, in addition to weather data. The indoor temperature profiles used here have been averaged over several sensors distributed in the living space. Seven separate experimental sequences of four days each were used in this study. One of

these test sequences is shown on Fig. 4.2: Fig. 4.2(a) shows indoor temperature T_{in} , adjacent room and outdoor temperature T_{out} ; Fig. 4.2(b) shows the indoor heat input P_h and global solar irradiance on a southern surface I_{sol} .

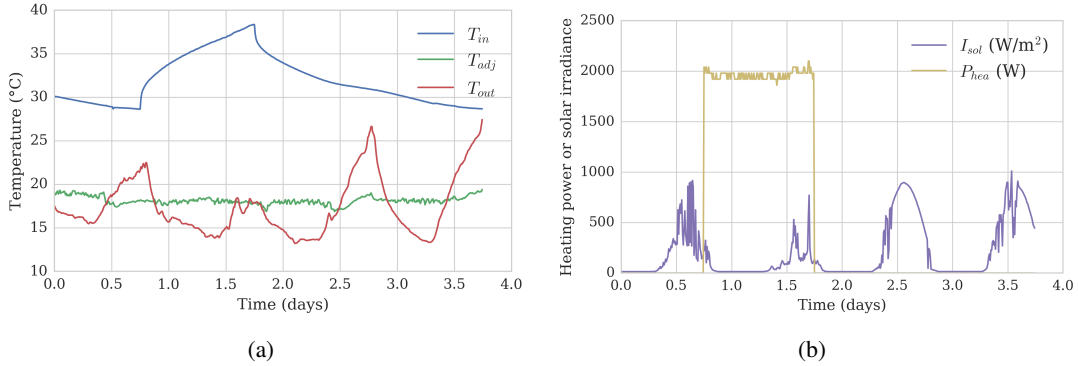


Figure 4.2: One measurement sequence in the Armadillo box

Sequence	Duration (h)	Heating (2 kW)		Weather	
		Start (h)	Duration (h)	\bar{T}_{ext} (C)	\bar{I}_{sol} (W)
D4	72	0	24	23.5	320.6
D5	90	18	24	21.5	256.5
D6	90	18	24	20.0	286.9
H1	100	3	48	16.3	225.4
H2	116	20	48	18.6	278.4
K1	90	18	24	17.4	207.3
K2	90	18	24	21.1	272.8

Table 4.2: Description of the test sequences

The test sequences resemble solicitations imposed in similar studies [MPR12]. Each sequence has a duration of 3 to 5 days, and includes a period of imposed indoor heating of 2 kW, for either 24 or 48 hours. Heating may start right after the beginning of the test, or after a period of free-floating temperature. Tab. 4.2 shows the conditions of each sequence, as well as its average outdoor temperature and solar irradiance. It is important to notice that all sequences are very similar: a single model, if calibrated correctly, *should* be able to reproduce all of them accurately. The point of the paper is to check if deterministic and/or stochastic models indeed show such a robustness.

Modelling

The questioning stated above supposes that a given RC model structure is trained twice from each data set: once in a deterministic formulation, once in a stochastic formulation. The robustness of each formulation is assessed by comparing parameter estimates arising from all datasets. An additional dimension is however added to the problem by applying the methodology to three types of RC models.

It seems reasonable to think that the lack of system uncertainty would be more problematic for simple models than for complex models: in an overly simplified model, such as one with a single thermal resistance R and capacitance C , modelling errors should be larger than in a model with close to no bias. As a result, we expect that if the system error w_t is neglected (deterministic setting), parameter estimates should be highly inconsistent across different training datasets. We expect this effect to be reduced with models of higher complexity and lower bias.

An additional dimension is added to the problem by investigating the above questioning with several levels of model complexity: 1R1C, 2R2C, 3R3C. The procedure begins by writing Eq. 2.12 and 2.13 for a given model structure (1R1C, 2R2C or 3R3C) and modelling type (deterministic or stochastic). Some variables are common to all situations:

$$\mathbf{u}(t) = \begin{bmatrix} T_{out} & I_{sol} & P_h \end{bmatrix}^T \quad (4.9)$$

$$\mathbf{y}(t) = \begin{bmatrix} T_{in} \end{bmatrix} \quad (4.10)$$

$$\mathbf{v}(t) \sim \mathcal{N}(0, r^2) \quad (4.11)$$

Other variables depend on the model structure and are listed on Tab. 4.3.

Model	1R1C	2R2C	3R3C
$\mathbf{T}(t)$	$\begin{bmatrix} T_1 \end{bmatrix}$	$\begin{bmatrix} T_1 & T_2 \end{bmatrix}^T$	$\begin{bmatrix} T_1 & T_2 & T_3 \end{bmatrix}^T$
\mathbf{A}_θ	$\begin{bmatrix} -\frac{1}{R_1 C_1} \end{bmatrix}$	$\begin{bmatrix} -\frac{1}{R_1 C_1} & \frac{1}{R_1 C_1} \\ \frac{1}{R_1 C_2} & -\frac{1}{R_1 C_2} - \frac{1}{R_2 C_2} \end{bmatrix}$	$\begin{bmatrix} -\frac{1}{R_1 C_1} & \frac{1}{R_1 C_1} & 0 \\ \frac{1}{R_1 C_2} & -\frac{1}{R_1 C_2} - \frac{1}{R_2 C_2} & \frac{1}{R_2 C_2} \\ 0 & \frac{1}{R_2 C_3} & -\frac{1}{R_2 C_3} - \frac{1}{R_3 C_3} \end{bmatrix}$
\mathbf{B}_θ	$\begin{bmatrix} \frac{1}{R_1 C_1} & \frac{k_1}{C_1} & \frac{1}{C_1} \end{bmatrix}$	$\begin{bmatrix} 0 & \frac{k_1}{C_1} & \frac{1}{C_1} \\ \frac{1}{R_2 C_2} & \frac{k_2}{C_2} & 0 \end{bmatrix}$	$\begin{bmatrix} 0 & \frac{k_1}{C_1} & \frac{1}{C_1} \\ 0 & \frac{k_2}{C_2} & 0 \\ \frac{1}{R_3 C_3} & \frac{k_3}{C_3} & 0 \end{bmatrix}$
\mathbf{C}_θ	$\begin{bmatrix} 1 \end{bmatrix}$	$\begin{bmatrix} 1 & 0 \end{bmatrix}$	$\begin{bmatrix} 1 & 0 & 0 \end{bmatrix}$
\mathbf{Q}_c	$\begin{bmatrix} q_1^2 \end{bmatrix}$	$\begin{bmatrix} q_1^2 & 0 \\ 0 & q_2^2 \end{bmatrix}$	$\begin{bmatrix} q_1^2 & 0 & 0 \\ 0 & q_2^2 & 0 \\ 0 & 0 & q_3^2 \end{bmatrix}$

Table 4.3: Matrices of the RC state-space models in continuous form

- Each model has a number of temperature nodes; the \mathbf{C}_θ matrix indicates the position of the observed (indoor) temperature. In each model, the temperature T_1 is observed.
- The 2R2C and 3R3C models respectively have one and two unobserved temperature states. Their initial states $\{T_{2,0}, T_{3,0}\}$ are unknown parameters of the problem.
- C_i is the heat capacitance (J.K^{-1}) of state T_i , k_i is its equivalent solar aperture (m^2) and q_i is the standard deviation of the system error associated to it.
- The models are written with the assumption that the system error covariance matrix \mathbf{Q}_c is diagonal. The standard deviations of system errors q_i and measurement error r are considered unknown, and will be inferred along with the other parameters of the models.

As an example, the lists of all unknown parameters of the 2R2C model structure, in the deterministic and stochastic cases respectively, are:

$$\boldsymbol{\theta}_{2\text{R2C}}^{det} = \begin{bmatrix} R_1 & R_2 & C_1 & C_2 & k_1 & k_2 & T_{2,0} & r \end{bmatrix} \quad (4.12)$$

$$\boldsymbol{\theta}_{2\text{R2C}}^{sto} = \begin{bmatrix} R_1 & R_2 & C_1 & C_2 & k_1 & k_2 & T_{2,0} & r & q_1 & q_2 \end{bmatrix} \quad (4.13)$$

Once written in continuous form, each system undergoes discretisation (see Sec. 2.3.2). Each resulting discrete system is trained in a combination of the following settings:

- Deterministic or stochastic modelling;
- 1R1C, 2R2C or 3R3C model structure;
- One of 7 training data sets.

This results in 42 sets of posterior PDFs $p(\theta|y_{1:N})$ that were calculated by the MCMC algorithm. The questioning of the paper is answered in two sections: Sec. 4.3.2 compares these PDFs to show the ability of stochastic and deterministic models for robust parameter estimation; Sec. 4.3.2 uses these estimated parameters to assess each model's ability to predict the indoor temperature in test datasets that are different from their training datasets.

4.3.2 Results and discussion

Model fit

Before showing the results of the robustness tests, let us first ensure that the selected model structures may capture the dynamics of the variable they aims at predicting (indoor air temperature).

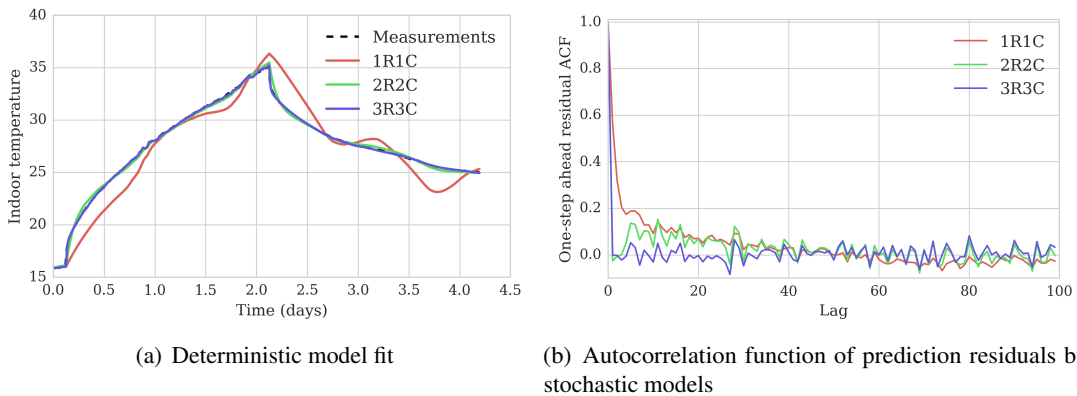


Figure 4.3: Proof of sufficient model complexity

As an example, Fig. 4.3(a) displays the indoor temperature measurements of a dataset, and prediction by the three model structures, calibrated using this dataset for training, in a deterministic setting (the system uncertainty is neglected). It is clear that the 1R1C model is unable to reproduce the dynamics of the indoor air temperature, while the other two models have a sufficient number of degrees of freedom. The 3R3C is especially indistinguishable from measurements.

Showing the fit of stochastic models is less informative since the Kalman updating step always ensures that model predictions will fit measurements. Assessing whether a model may describe the dynamics of a system is done by examining prediction residuals or their auto-correlation function (ACF). Fig. 4.3(b) shows the ACF of residuals between observations and each of the predictions from the 3 models structures, in a stochastic setting. A low ACF is a necessary condition for parameter estimates to be reliable [BM11]: the 2R2C model has very few occurrences of an ACF value above the 0.1 threshold, while the 3R3C model has none.

This analysis is not a careful model selection procedure: it merely shows that there is no need to add degrees of freedom to the models under investigation in this study. Examples of RC model selection procedures include for instance [BM11].

Parameter estimation

Heat loss coefficient

The first relevant indicator, that can be compared across all model structures, is the global heat loss coefficient (HLC) of the building. In each model structure, its PDF is obtained by reciprocating the sum of the PDFs of all resistances. The HLC is therefore comparable across all model structures: its estimate is expected to be consistent.

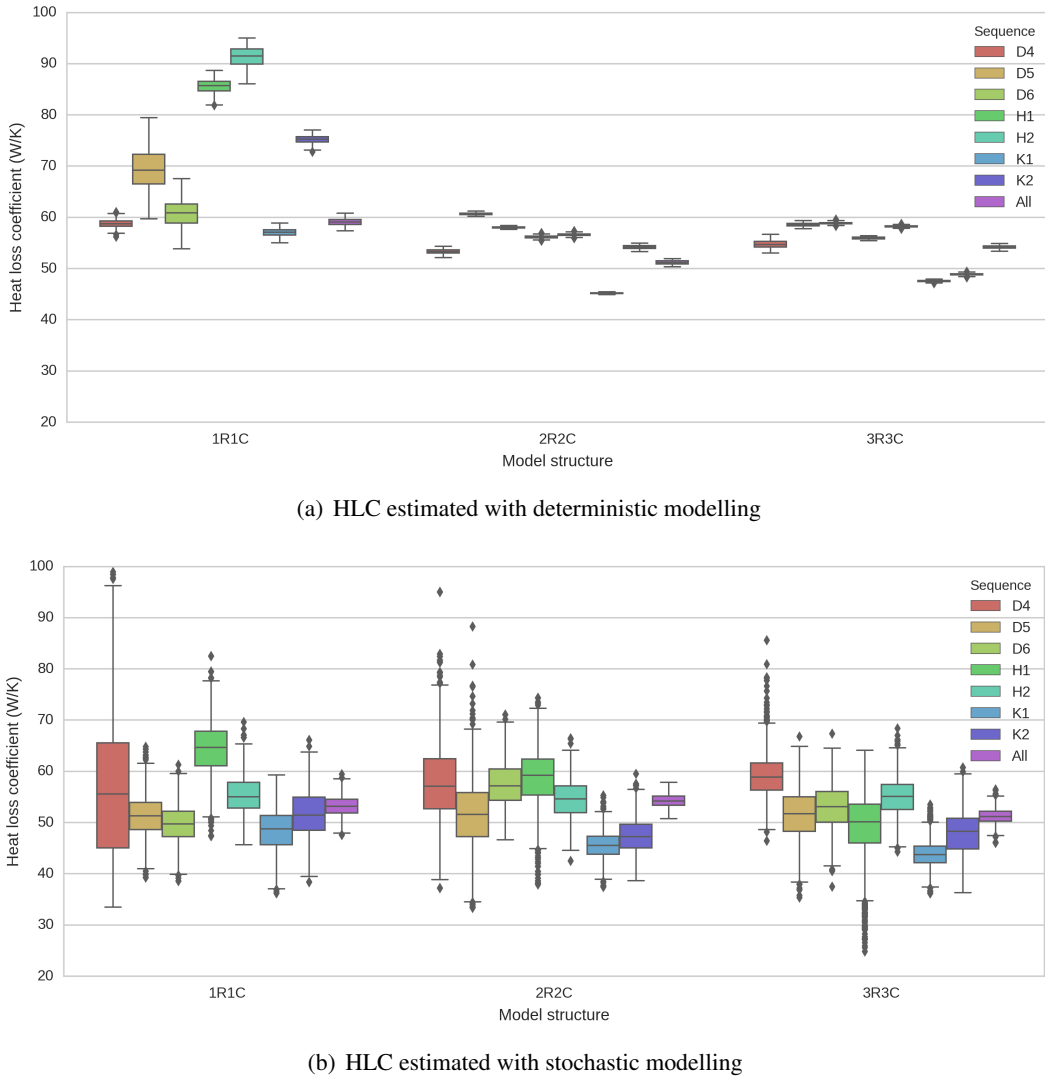


Figure 4.4: Estimation of the heat loss coefficient

Fig. 4.4(a) compares the HLC estimated using deterministic models. Each box is the posterior PDF of the HLC from one model structure, trained with one data set. The left part shows the PDFs obtained using a 1R1C model, trained by each of the 7 training data sets. The last box of this series shows the HLC estimated by using all data sets altogether: this value is supposedly the most realistic of the series, since it uses seven times more information than each of the other estimates. The center of Fig. 4.4(a) compares HLC estimates from the deterministic 2R2C model, and the right part compares estimates from the 3R3C model.

Several observations can be drawn from Fig. 4.4(a) only, before comparing these results to the stochastic alternative. The first observation is a high inconsistency of the HLC parameter estimated with the same model but from different data. This is especially true in the case of the 1R1C structure: this model is overly simplified, and its inadequacy is not included in its formulation. The median value of posterior PDFs may span from 57 to 92 W/K. This means that using a single data set of a few days of observation offers no guarantee of accurate results for parameter estimation. This problem is mitigated, although still observable, in the case of the 2R2C and 3R3C models, which are able to mimic the behaviour of the building more appropriately. There is still a dispersion in the HLC estimation results.

The second observation is the narrowness of confidence intervals. By using a supposedly unbiased model for inference, the only admitted discrepancy between model output and observations is measurement noise. This leads to an overconfident parameter estimation, especially with a higher model complexity. More importantly, the confidence intervals of HLC do not overlap from one training data set to another. This means that these confidence intervals cannot be trusted, since the point of confidence intervals is to include all likely solutions. The issue is that they have been calculated by neglecting part of the uncertainty of the problem.

Fig. 4.4(b) shows the same display of results, if the model used for inference is stochastic and employs a Kalman filter for the estimation of states. Each box is the posterior PDF of the HLC from one model structure, trained with one data set. The main difference with the deterministic setting is that confidence intervals are considerably larger. A likely explanation for this phenomenon lies in the principle of Bayesian filtering: at each time step, states are updated as a compromise between predictions and observations. The profile of one-step ahead predictions is more likely to match observations, resulting in a high likelihood for a larger range of parameter values. *Since the model is known to be wrong, the inference algorithm admits more parameter values as likely to be true.* As a result, confidence intervals are very conservative, especially for such simplified models (it should be noted that Fig. 4.4(b) shows no clear influence of the model complexity).

This should not be seen as an unsatisfactory result. The estimated HLC is now more reliable, and more importantly, its estimation is robust: indeed, there is an overlap between PDFs obtained from separate datasets. This means that the “true” value of the HLC may be included in the results of all trainings. Additionally, in each model structure, the PDF of the HLC estimated using all datasets overlaps each PDF from individual datasets. This is not the case when a deterministic model is used.

Heat capacitance

The global heat capacitance of the building is now investigated. It is the sum of the estimated values for all capacities of each model (they respectively have one, two or three). This variable is known to be model-dependent: we should not expect it to hold the same value across different model structures.

Fig. 4.5(a) and 4.5(b) show all PDFs of the global capacitance, estimated by using deterministic or stochastic models, respectively. The comparison allows the same discussion as the above investigation on the HLC:

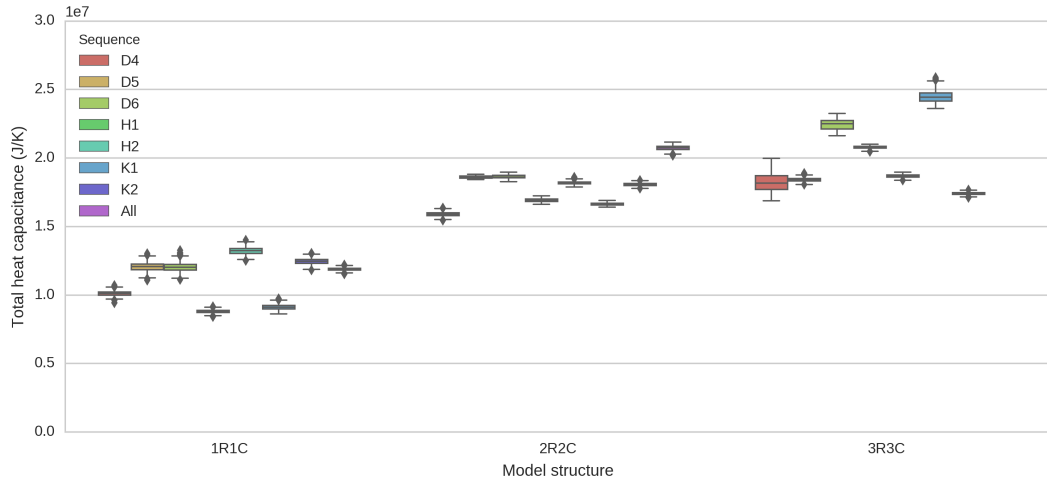
- When neglecting system error in the model formulation (Fig. 4.5(a)), parameter estimation results are not consistent across training datasets. Important uncertainties are overlooked, preventing a robust model calibration. With a given model structure, the confidence intervals from separate trainings do not overlap: a single training offers no guarantee of proposing the correct value of the thermal capacity.
- When accounting for system error (Fig. 4.5(b)), the estimation of the thermal capacity by each model structure is more reproducible and reliable.

The latter observation is contradicted by two trainings of the stochastic 3R3C model, which resulted in capacity PDFs that hardly overlap other trainings. A possible explanation is a low identifiability of series of thermal capacities in RC models.

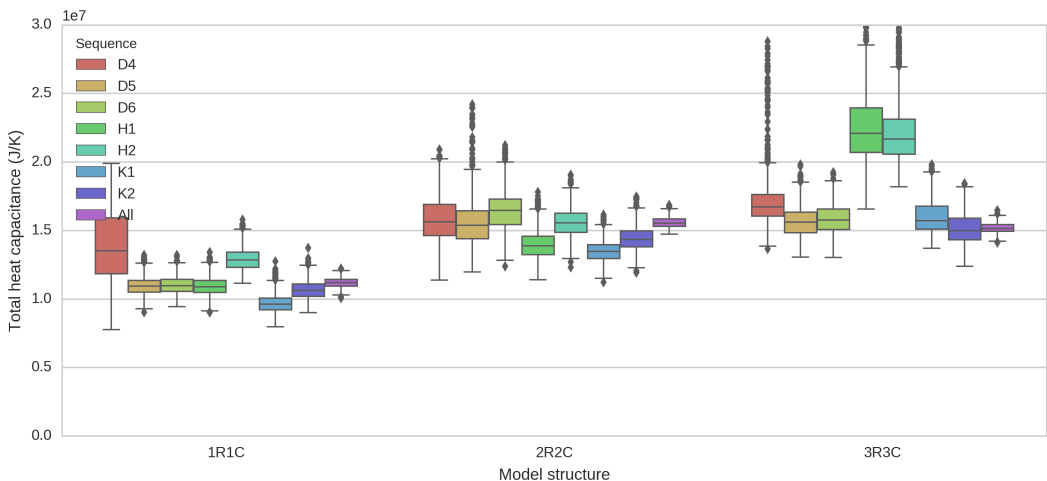
Measurement noise

The third indicator, used here to observe the relative robustness of deterministic and stochastic modelling in parameter estimation problems, is the standard deviation of observation noise r . Recall that observation noise appears in the measurement equation, regardless of whether system noise is considered or not. Its standard deviation r is an unknown parameter of our models.

The advertised inaccuracy of temperature sensors used in the experimental study is 0.15°C : the estimates of r should be lower than this value.



(a) Thermal capacitance estimated with deterministic modelling



(b) Thermal capacitance estimated with stochastic modelling

Figure 4.5: Estimation of the total thermal capacitance

Fig. 4.6(a) shows the estimation of r by deterministic models. The deterministic 1R1C model estimates its value between 1 K and 2 K, which is much higher than expected. This observation may be given the following explanation: when system error is neglected, the only possible deviation between observations and model predictions is the measurement noise. In reality, this deviation is caused by modelling errors, ignored by our model: the inference algorithm attributes the entirety of the deviation to measurement errors and increases the estimated value of r . Deterministic 2R2C and 3R3C models overestimate r as well, although by a lower amount. Again, confidence intervals of this parameter do not overlap across separate trainings.

Fig. 4.6(b) shows the estimation of r by stochastic models. This estimation is more satisfactory in terms of the absolute value of r , and in terms of robustness: all trainings overlap within a realistic range.

Forecasting

The decision of including system error in the formulation of a model considerably increases the confidence intervals of parameters estimated by inverse methods. The precision of parameter estimation is not increased, but its robustness is much higher. We now wish to observe if this

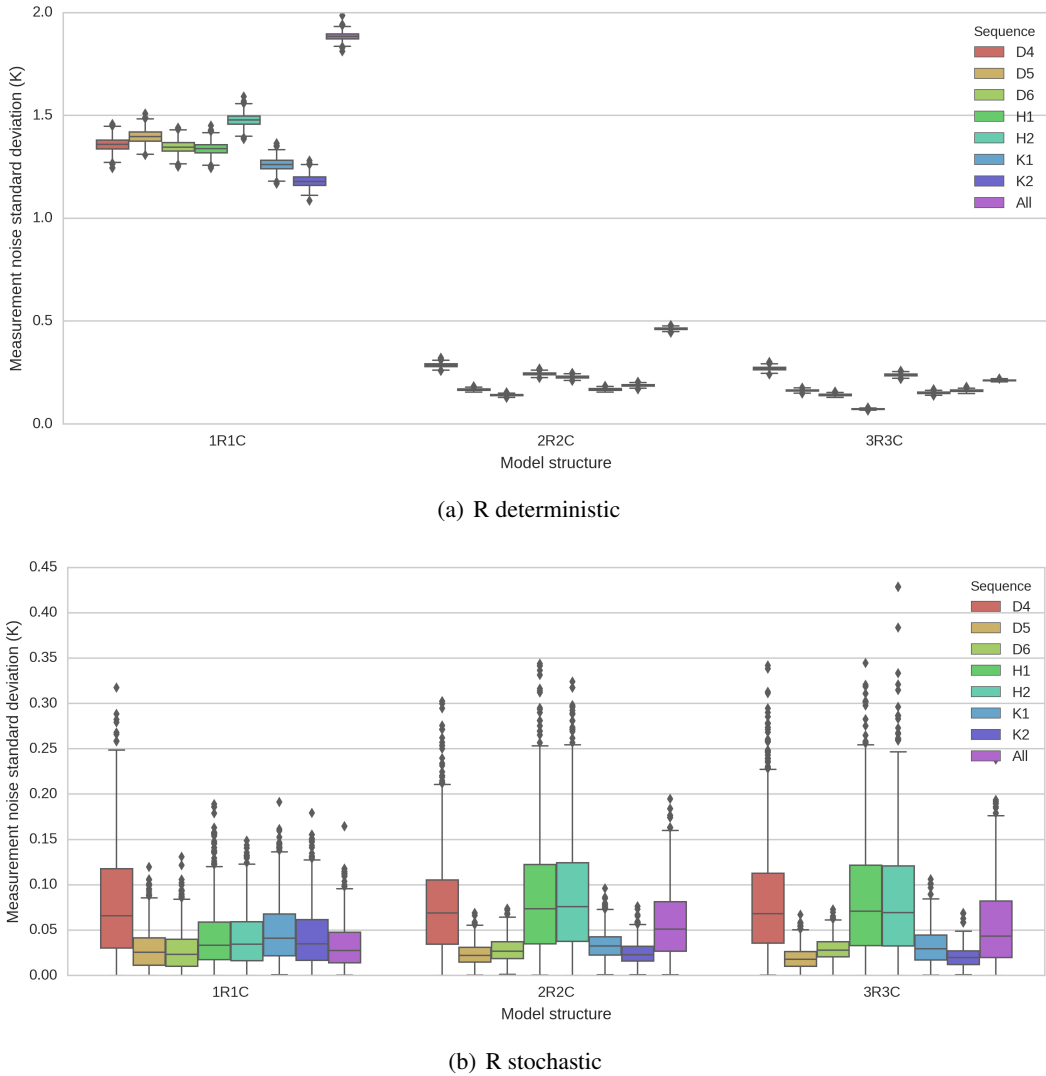


Figure 4.6: Estimation of the measurement noise standard deviation

decision has a similar impact on the forecasting capability of models.

Once a model has been calibrated with a training dataset, its forecasting accuracy and robustness may be assessed using another observation period as test set. Fig. 4.7 shows this test on two examples of training-test combinations: a successful prediction (Fig. 4.7(a)) and a less successful one (Fig. 4.7(b)). The predictions of indoor temperature by stochastic and deterministic 3R3C models, trained with a dataset, are compared to measurements of another set. Since parameter estimates are posterior PDFs, each prediction simulation is run $n = 100$ times by sampling the posterior: this results in confidence intervals on forecast profiles. Predictions by the stochastic model include the additional uncertainty on the states.

Fig. 4.7 shows that the stochastic model, where states are uncertain, predicts the indoor temperature with a much higher uncertainty than the deterministic model. In the latter, the only source of uncertainty is the variability of the parameter posterior. The former accounts for model inaccuracy in the forecast.

Next, a quantitative assessment of prediction accuracy and robustness is proposed, with a method inspired from k -fold cross validation.

- **Prediction accuracy** is measured by the cross-validation (CV) index, which is computed

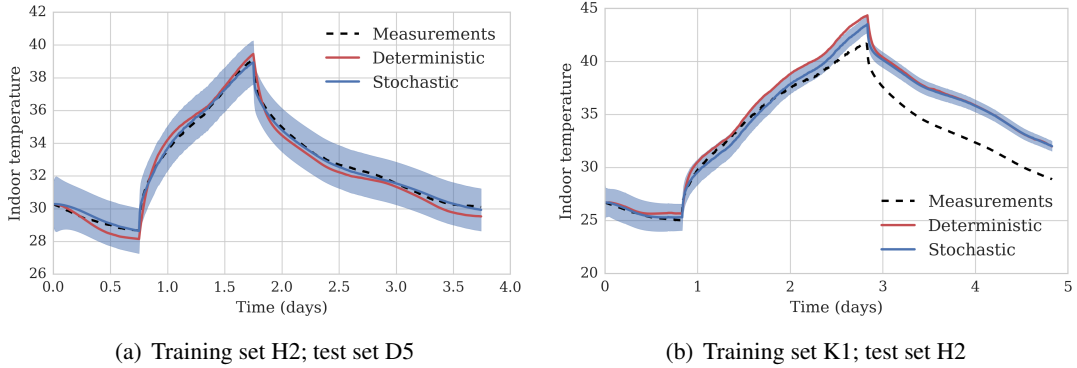


Figure 4.7: Examples of forecast by the 3R3C model, either deterministic or stochastic

by averaging test errors [Gar+13]. Using a model trained with the learning dataset i , we denote MSE_i the averaged test error of this model over all test sets. The CV index is then the average of all MSE_i values over all $D = 7$ datasets.

$$\text{MSE}_i = \frac{1}{D-1} \sum_{j \neq i} \left[\frac{1}{N} \sum_{t=1}^N (\mathbf{y}_t - \mathbf{C}\mathbf{x}_t) \right]_{(\text{train}=i; \text{test}=j)} \quad (4.14)$$

$$\text{CV} = \frac{1}{D} \sum_{i=1}^D \text{MSE}_i \quad (4.15)$$

- **Prediction robustness** is measured by an index denoted PR. Let us denote $\text{PR}_{i,j}$ the percentage of measurement points in the test dataset j , that fall inside the 95% confidence intervals of the predictions calculated by a model trained with dataset i . The global prediction robustness of one model is the averaged value of this indicator over all possible dataset combinations:

$$\text{PR} = \frac{1}{D} \sum_{i=1}^D \left(\frac{1}{D-1} \sum_{j \neq i} \text{PR}_{i,j} \right) \quad (4.16)$$

Prediction accuracy: CV index (K^2)		
	Deterministic	Stochastic
1R1C	6.54	5.00
2R2C	0.82	1.99
3R3C	0.86	1.10
Prediction robustness: PR index		
	Deterministic	Stochastic
1R1C	6%	56%
2R2C	8%	63%
3R3C	8%	72%

Table 4.4: Assessment of prediction accuracy and robustness by each model structure; a lower CV score is better, a higher PR score is better

Results show that including the system error in the model formulation does not increase the prediction accuracy, but considerably increases its robustness: when forecasting with a stochastic model, the confidence that the real process is within confidence bounds of the prediction can be higher.

There is no apparent incidence of the test conditions on the accuracy of predictions. The duration of the training sets, duration of heating input, and weather conditions, do not seem to predetermine which training sequence will yield the most robust model. These sequences are indeed very similar: the causes for prediction inaccuracy should be sought among phenomena that have not been observed, and not been considered by the simplified models.

4.3.3 Summary

Here is a summary of the results of both the parameter estimation and the forecasting investigations:

- Using a stochastic model in an inverse problem significantly increases the uncertainty of estimated parameters. The estimates are less confident, but more reliable as a consequence, since their confidence intervals overlap when using several training datasets separately.
- The uncertainty bounds of a parameter identified through a stochastic model give an insight of its identifiability. This allows pointing out which experimental training datasets are most informative, i.e. bring the most information into the parameter estimates.
- Using a deterministic model supposes that the model is unbiased. This hypothesis is especially inappropriate in the case of simpler models such as 1R1C. As a consequence, there is a larger variability of parameter estimates from separate training datasets. This problem is attenuated when the model complexity is increased.
- Predictions by stochastic models are not more precise, but more cautious: their confidence bounds are larger than from deterministic models. As a result, they are coherent with most of the validation data, whereas deterministic models are not.

4.4 Latent force models: performance prediction of occupied buildings



This section is a summary of a future article, not yet published as of the writing of this report (April 2020).

The process noise included in the linear stochastic differential equations (Eq. 2.12) only covers some types of modelling approximations. It cannot describe significant systematic errors or missing influences, and does not compensate for an overly simplified model structure [Gho+15]. As a consequence, the model complexity must be increased to an unpractical point in order to meet validation criteria (uncorrelated prediction residuals) and provide accurate predictions. Gaussian Processes (GP) [Ras04] were proposed to account for more uncertain, non-linear or unobserved phenomena that an RC model does not explicitly include. Two alternatives were proposed to include GP's in energy assessment models. The first approach was named Bayesian calibration by [KO01] and refers to using a GP as a surrogate model to reproduce a reference model, then training a second GP as the discrepancy function between this model and observations, then evaluating the posterior distribution of calibration parameters. Following this approach, [AAC12] investigated the question of the identifiability of calibration parameters. The first application of this method to building energy performance assessment was [HCA12] who calibrated the parameters of a building simulation model on monthly gas consumption data. [CM18] give a summary of publications using Bayesian calibration in building energy. The second approach is to use GPs to simulate dynamic systems through a state-space representation [Sol16] and include them as a non-observed input into a state-space model. This is the principle of Latent Force models [SAL18], which were first used for thermal modelling of buildings by [Gho+15], and also proposed in the present section.

The principle of Latent Force Models is described in Sec. 2.3.3. The present section displays preliminary results concerning a case study, where they were used to predict the energy performance of a house despite its occupancy.

4.4.1 Case study: twin houses

The dataset used in this case study was generated within the IEA EBC annex 71 and made freely available by the Fraunhofer Institute for Building Physics IBP. Originally intended to validate the performance of Building Energy Simulation (BES) tools in a two-stage, blind and open process [Ker+20]. Since this dataset is accompanied by a detailed description of the data and the experiment, including measurement uncertainty and baseline measurements as part of the quality control, this data set can be used for numerous other purposes.

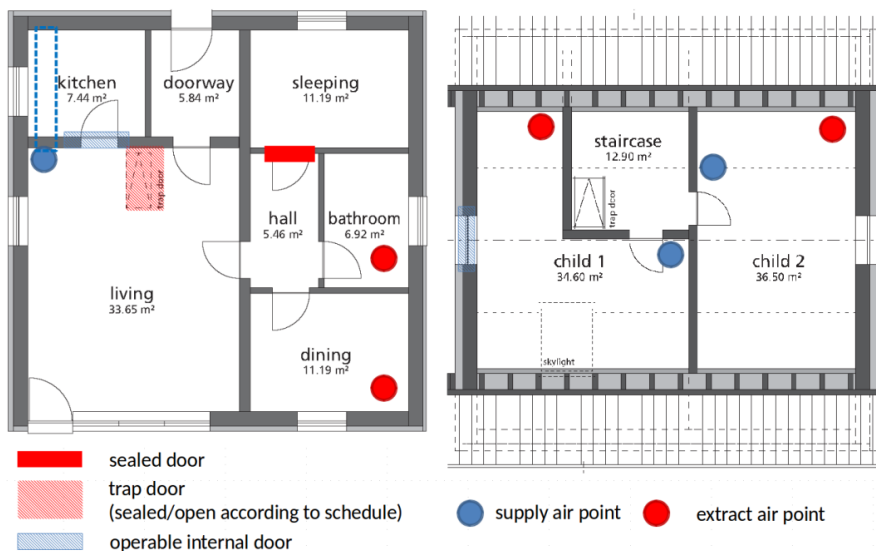


Figure 4.8: Ground and attic floor plan of the Twin Houses

As can be seen in Fig. 4.8 the experimental setup of both houses includes the ground floor and the attic while the cellars are heated to a constant temperature as a boundary. In all rooms the air temperatures in four heights, the globe temperatures and the heat inputs are recorded together with many other parameters related to the exterior climate, the heating and the ventilation system. This experiment is the successor of the IEA EBC annex 58 BES model validation experiment [Ker+20] that is also freely available [Jan16a]. It is extended from the annex 58 experiments by including the attic space, using underfloor heating and an air source heat pump in one building and adding synthetic, probabilistically acting users [FK16; FK17]. These synthetic users influence the heatings' set points, adding internal heat and moisture gains and operating external windows and internal doors. Baseline measurements, including a coheating test, served as a quality check to ensure both Twin Houses indeed have an identical behavior.

The entire Annex 71 experiment consists of seven different phases including free floating period, a period with random (PRBS) heat pulses, a coheating experiment suitable for analyzing the HTC and three "user" periods where the houses are occupied by synthetic users providing different degrees of detailed interactions. In the presented paper the dataset of the user 1 phase is used. In this phase of the experiment both Twin Houses were heated to the same constant set temperature with a night setback. The synthetic users' interaction with the building during user 1 is limited internal heat gains with a probabilistic element.

The user 1 phase dataset has been split in two parts. The period from the 26th December 2018 at midnight to the 25th January 2019 at 10:30 am is used for the identification and after this period, seven days (until the 1st February 2019) are used for the model prediction. The data are collected at one minute interval but provided as ten minutes averages.

4.4.2 Performance assessment despite unmeasured influences

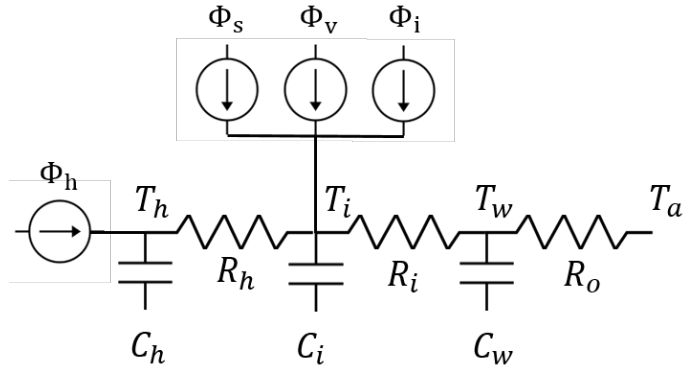


Figure 4.9: Third order thermal network

A third-order model shown by Fig. 4.9 is used. Φ_h is the total thermal power delivered by the underfloor heating system, estimated from water temperature measurements; T_a is the outdoor temperature; Φ_s is the global solar radiation measured on a horizontal surface. The indoor space has two additional heat sources: internal heat gains Φ_i (W) and heat supplied by the mechanical ventilation Φ_v (W).

Although the value of internal heat gains (from occupants and various appliances) Φ_i is known in the controlled Twin houses experiment, it is hardly measurable in practice. The purpose of this section is to demonstrate the use of LFM for estimating the thermal properties of the occupied building. Two versions of the model were trained with the training data subset:

- A regular RC model, shown by Fig. 4.9 but missing the influence Φ_i .
- A LFM, where a pseudo-periodic latent force is set to influence the indoor air temperature, in an attempt to compensate and estimate this missing influence: see Sec. 2.3.3 for the implementation.

Once trained, both models are compared in terms of: accuracy of the indoor temperature prediction relatively to the validation dataset (see Fig. 4.10); estimation of HLC compared to the reference value (see Tab. 4.5). Then, the estimated latent force is compared to the influence it was supposed to compensate, since it was measured by the experiment: this is shown by Fig. 4.11

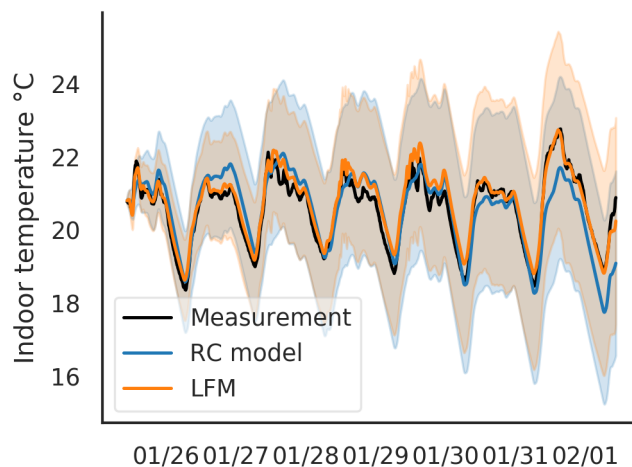


Figure 4.10: Indoor temperature prediction with regular RC model and LFM

Fig. 4.10 shows that the trained RC model, where the influence Φ_i is missing, already has a very satisfactory prediction ability. The addition of a latent force into the formulation still improves the accuracy, with a RMSE index going from 0.524 K to 0.289 K (see Tab. 4.5). The precision however remains similar. The ACF of the RC model is satisfactory as well, and is made even higher by the LFM.

	HTC (W/K)			Validation	
	mean	std	RMSE	ACF	CCF(Φ_i)
Reference	109				
RC	64.48	2.21	0.524	0.956	0.719
LFM	69.27	5.71	0.289	0.984	0.979

Table 4.5: Comparison of RC and LFM results with a missing influence

The value of the HTC estimated by both models, and compared with a reference value calculated according to DIN V 18559, are shown on Tab. 4.5. The accuracy of the estimation is not satisfactory, as HTC falls far from its reference value. By missing an indoor heat input, the RC model underestimates the global heat input inside the building, and therefore also underestimates HTC. The LFM, where the missing influence is estimated, only slightly improves the accuracy of HTC.

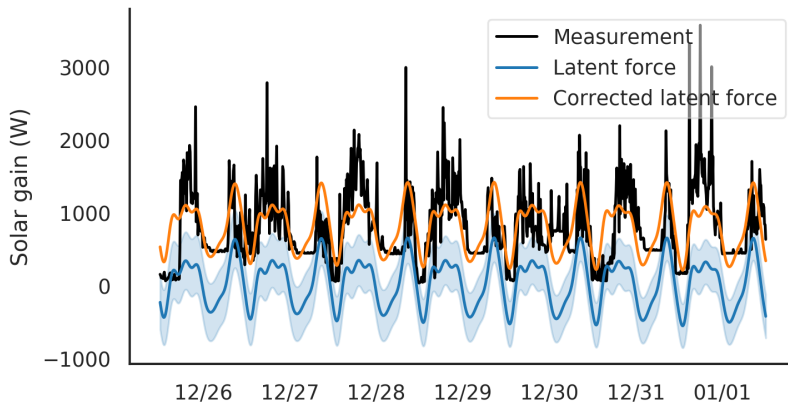


Figure 4.11: Estimation of the missing indoor heat gains by the LFM

The reason for such a small compensation of HTC by the LFM can be seen on Fig. 4.11, showing the measured profile of Φ_i that was hidden from the models. The LFM correctly estimates its dynamics, but with a constant offset: its mean value is close to zero, which explains why the HTC is underevaluated. The latent force should be corrected in order to only allow positive values.

This study shows some preliminary results concerning the capabilities of LFM for the performance assessment of buildings: they seem fit for the estimation of missing influence that have a high impact on the model output, especially when these influences display some periodic behaviour. However, the estimation of physical quantities such as the HTC is not necessarily improved by them: further investigation is required.

4.5 Real time parameter estimation with Sequential Monte Carlo



This section is a summary of the article published in [RJC19].

Parameter estimation is typically performed *off-line*: measurements of indoor and outdoor conditions are first carried in a test building, and data is processed after the experiment in a single batch. An interesting challenge is to carry parameter estimation *on-line*, during the observation period: starting from an initial guess for parameter values, these estimates are updated sequentially, every time a new observation becomes available.

There are several motivations for this: first, it would allow using the measurement period for computations, thus reducing the total time of the procedure [RG17]. It would also be a way to make use of the emerging wireless energy monitoring technology: smart meters, wireless sensor networks, etc. With frequent data collection and remote transfer, either off-line and on-line analysis can be performed non-intrusively during the monitoring period. The off-line alternative however requires restarting calculations from the beginning of the measurement period, which can become problematic if a frequent update on parameter estimates is expected. A second, more important advantage of on-line estimation lies in the amount of information gained from the experiment. Parameter estimates are to be updated after every new observation: this will allow directly observing which phenomena “bring information” to the parameters, by correlating the reduction in their estimation uncertainty with observed events. Such a thorough diagnosis can be useful for fault detection as well, particularly when the necessary length of the measurement period is not known a priori.

Bayesian inference offers the possibility of on-line estimation with Sequential Monte-Carlo (SMC) methods [DGA00]. Originally developed for the sequential estimation of states [Han70], SMC was later adapted to state and parameter estimation [Kan+15; LC98]. Building physics applications are scarce and very recent [RG17], but may become more common due to the motivations listed above.

The present paper applies SMC for the on-line estimation of the heat loss coefficient (HLC) of a test cell. Starting from a highly uncertain prior knowledge of HLC, the target is to dynamically observe what leads its estimation to narrow down to a more precise value. The identifiability of HLC regarding available data is then discussed. Sec. 4.5.1 presents the test cell the RC model chosen to simulate it. Sec. 4.5.2 shortly describes the SMC algorithm for on-line Bayesian parameter estimation. Results are then showed and discussed on Sec. 4.5.3.

4.5.1 Case study: Round Robin Test Box

Experimental setup

The present study uses measurements that were carried in the Round Robin Test Box (RRTB), within the framework of the IEA EBC Annex 58 [Jim16]. This experimental test cell, shown by Fig. 4.12 has a cubic form, with exterior dimensions of 120x120x120 cm³. The floor, roof and wall components of the box are all identical and have a thickness of 12 cm, resulting in an inner volume of 96x96x96cm³. One wall contains an operable wooden window with overall dimensions of 71x71 cm² and a glazed part of 52x52 cm². The double glazing has a U-value of 1.1 W/m²K and g-value of 0.63. Numerical simulation [Jim16] has estimated the overall HLC of the box to a target value of 4.08 W/K, assuming constant standard surface heat transfer coefficients. This value presents an uncertainty in the range 3.49-4.14 W/K due to variations produced by the presence of a thin air or glue layer between the different material layers, or approximations in the estimation of surface heat transfer coefficients depending on wind and surface temperature. This range will serve as reference to check the validity of the results below. The total solar aperture of the box was estimated at 0.162 m².

The test box was installed outdoors, in the LECE laboratory at Plataforma Solar de Almeria, in the South East of Spain. Experiments were carried during a 43-days period in the winter of 2013-2014. Measurements used in this study are: indoor temperature (which is the average of two type T thermocouples placed inside the box), outdoor air temperature, heating power, and global



Figure 4.12: Round Robin Test Box

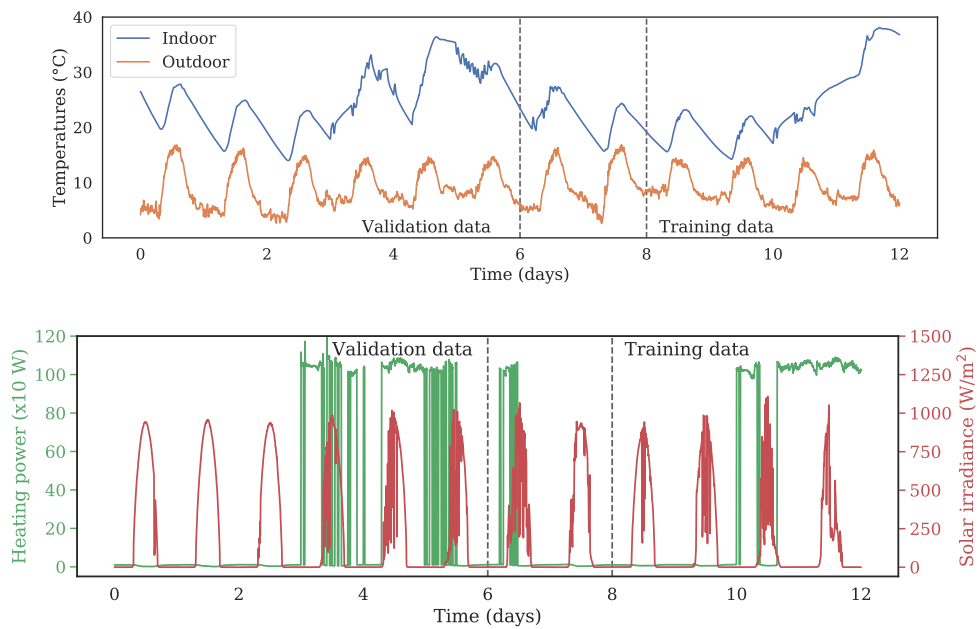


Figure 4.13: Measurements of indoor and outdoor temperature, heating power and solar irradiance

horizontal solar irradiance. The box is also equipped with sensors that were not used here: internal and external surface temperatures of each side, heat flow meters, diffuse horizontal solar irradiance, wind speed and direction, relative humidity, and horizontal and vertical long wave radiation from the sky. All sensor types are listed in [Jim16]. All measurements were received with a sampling time of 1 min, but were then resampled to a time step of 5 min in order to reduce calculation time without compromising precision.

A period of 12 days was chosen for the present investigation, starting from the 6th of December 2013 at 00:00. Measurements are shown in Fig. 4.13. The first 6 days will be used as validation data for the trained model, and the last 4 days as training data. The measured indoor temperature during the validation period will be compared to the output of the models calibrated with the training data. This particular partition of the original 12-days dataset is motivated by the following reasons:

- Both the training and the validation dataset comprise a period of free-floating indoor temperature, and a period of controlled indoor heat input. In terms of model calibration, these boundary conditions are not very informative at first, then become more informative: we expect to witness their effects on the evolution of the estimation of the heat loss coefficient.

- The training and validation sets are separated by a short "buffer period" in order to make them relatively independent from each other. By this precaution, we want to avoid a correlation between both datasets, that would not guarantee that the trained model is generalizable.

The 3R2C model

In order to estimate its heat loss coefficient (HLC) and other properties, the test box is represented by a lumped Resistor-Capacitance model. It is a 3R2C model described by:

$$\begin{bmatrix} \dot{T}_i(t) \\ \dot{T}_e(t) \end{bmatrix} = \underbrace{\begin{bmatrix} -\frac{1}{R_1 C_1} - \frac{1}{R_3 C_1} & \frac{1}{R_1 C_1} \\ \frac{1}{R_1 C_2} & -\frac{1}{R_1 C_2} - \frac{1}{R_2 C_2} \end{bmatrix}}_{\mathbf{A}} \begin{bmatrix} T_i(t) \\ T_e(t) \end{bmatrix} + \underbrace{\begin{bmatrix} \frac{1}{R_3 C_1} & \frac{1}{C_1} & \frac{k_1}{C_1} \\ \frac{1}{R_2 C_2} & 0 & \frac{k_2}{C_2} \end{bmatrix}}_{\mathbf{B}} \begin{bmatrix} T_a(t) \\ q(t) \\ I_{sol}(t) \end{bmatrix} + \mathbf{w}(t) \quad (4.17)$$

$$\mathbf{y}(t) = \underbrace{\begin{bmatrix} 1 & 0 \end{bmatrix}}_{\mathbf{C}} \begin{bmatrix} T_i(t) \\ T_e(t) \end{bmatrix} + \mathbf{v}(t) \quad (4.18)$$

where T_i , T_a and T_e are the indoor, ambient (outdoor) and envelope temperatures. The envelope temperature is associated with the thermal mass of the opaque surfaces, and does not represent a specific coordinate within the envelope. The model has two states T_e (unobserved) and T_i (observed, shown in Fig. 4.13(a)); q (W) is the indoor heating power; I_{sol} (W/m^2) is the solar irradiance on a southern vertical plane. A schematic view of the 3R2C model is shown in Fig. 4.14. The choice of this model structure is motivated by simplicity: in a previous study [RRO18], a 2R2C model was judged sufficient to describe the dynamics of a very simple mono-zone building. The 3R2C model is an extension of this model, applied to the RRTB where the influence of the window may be significant.

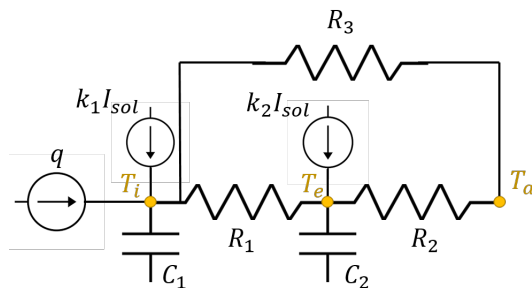


Figure 4.14: 3R2C model

In the continuous state equation (Eq. 4.17), $\mathbf{w}(t)$ denotes a Wiener process that represents modelling errors with an incremental covariance \mathbf{Q}_c [MH95], and $\mathbf{v}(t)$ is the measurement error of the indoor temperature, normally distributed white noise with zero mean and variance \mathbf{R}_c . The coefficients of the \mathbf{Q}_c matrix and \mathbf{R}_c are considered unknown and will be estimated along with the other parameters of the model.

The 3R2C model has 8 parameters that enable a physical interpretation of the RRTB: R_1 and R_2 (K/W) are two thermal resistances representing heat transfer through the opaque walls; R_3 is a resistance directly linking the outdoor and indoor temperatures, representing heat transfer through the window; C_1 and C_2 (J/K) are thermal capacities and k_1 and k_2 (m^2) are two solar aperture coefficients, one for each state of the model. The last parameter is the initial envelope temperature $T_e(0)$: since T_e is an unobserved state, its initial value is unknown. In the following, we denote as θ the vector of these parameters.

4.5.2 The SMC algorithm

The goal of the on-line parameter estimation exercise is to assess the value of all static parameters of the model, at each time coordinate of the measurement period: the expected output is a sequence of posterior distributions $\{p(\theta|y_{1:t}), t \in 1\dots T\}$, where T is the number of data points in the measurement period. This sequential estimation is performed by the SMC algorithm.

The SMC algorithm for parameter estimation is an adaptation of particle filtering for state variables. The foundation of this method is the Importance Sampling paradigm as described by [CGM07]: simulating samples under an instrumental distribution and then approximating the target distributions by weighting these samples using appropriately defined importance weights. The reader is referred to [CGM07] and [Kan+15] for a deeper explanation of SMC and its application to parameter estimation. The method used here is inspired from the Iterated Batch Importance Sampling algorithm [Cho02]. It is described in Fig. 4.15 and Algorithm 3.

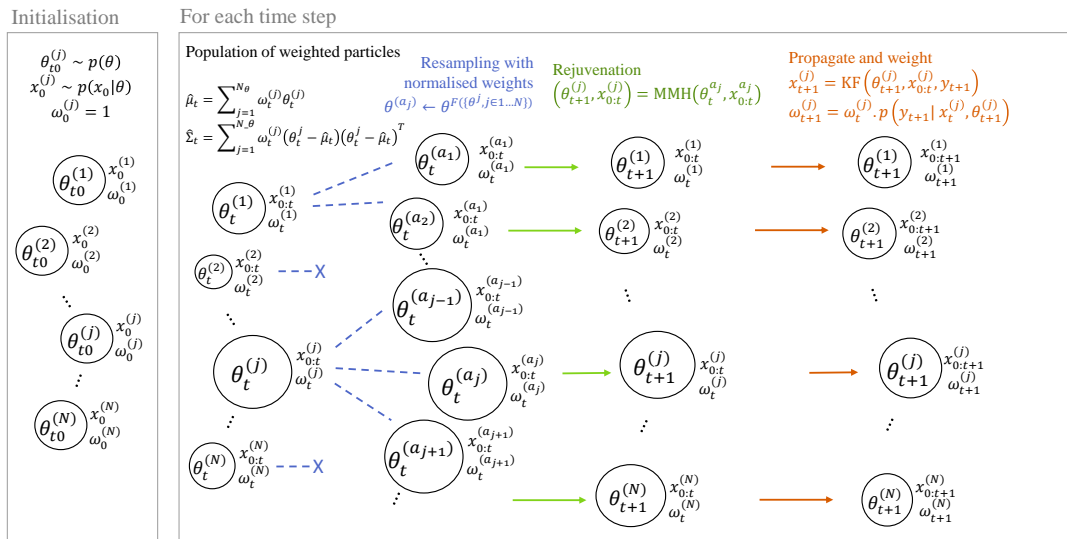


Figure 4.15: Principle of the SMC algorithm

The algorithm starts with the generation of a population of N_θ particles drawn from a prior distribution $p(\theta)$. Each parameter is assigned an initial state \mathbf{x}_0 and weight. At each time step t , a Kalman filter computes the states $\mathbf{x}_t^{(j)}$ and likelihood $L_t^{(j)}$ associated to each particle $\theta_t^{(j)}$. If the state-space model (Eq. 2.14) is non-linear, this filter can be replaced by a particle filter: this approach is known as the SMC² algorithm [CJP13]. By this operation, the population of particles is updated so that at each time t they are a properly weighted sample from $p(\theta|y_{1:t})$ [CJP13]. After several time steps, there is a risk that only a few of the initial N_θ particles are significantly more likely than the others and concentrate the majority of the total weight: a resampling step is then performed in order to generate a new population of particles from the most influential ones, and a MCMC rejuvenation step then restore the diversity of particles [Mur13].

Resampling does not occur every time a new observation becomes available, but only when required: this is measured by the effective number of particles that significantly contribute to the total weight of all particles [Mur13]. This operation decreases the number of unique particles, hence the subsequent rejuvenation step that restores diversity. The choice of $\mathcal{N}(\hat{\mu}_t, \hat{\Sigma}_t)$ as the proposal distribution for the MCMC rejuvenation step was proposed by [Cho02] and ensures a

Algorithm 3 Sequential Monte Carlo algorithm

1: **Initialisation:** generate a population of N_θ particles, their states and weights
 2: **for all** $j \in \{1 \dots N_\theta\}$ **do**
 3: $\theta_0^{(j)} \sim p(\theta)$
 4: $\mathbf{x}_0^{(j)} \sim p(X_0)$
 5: $\omega_0^{(j)} = 1$
 6: **end for**
 7: **for** $t = 1 \dots T$ **do**
 8: **for all** $j \in \{1 \dots N_\theta\}$ **do**
 9: **Resampling**
 10: $\{a_j, j \in 1 \dots N_\theta\} \leftarrow \text{MULTINOMIAL}(\omega_{t-1}^{(j)}, j \in 1 \dots N_\theta)$
 11: **Rejuvenation** by a single MMH step with proposal distribution $\mathcal{N}(\hat{\mu}_{t-1}, \hat{\Sigma}_{t-1})$
 12: $(\theta_t^{(j)}, \mathbf{x}_{0:t-1}^{(j)}, L_{t-1}^{(j)}) \leftarrow \text{MMH}(\theta_{t-1}^{(a_j)}, \mathbf{x}_{0:t-1}^{(a_j)}, \mathbf{y}_{0:t-1})$
 13: **Propagate and weight**
 14: $(\mathbf{x}_t^{(j)}, L_t^{(j)}) \leftarrow \text{KALMANFILTER}(\mathbf{x}_{t-1}^{(j)}, \theta_t^{(j)}, \mathbf{y}_t)$
 15: where $L_t^{(j)} = p(\mathbf{y}_t | \mathbf{x}_{t-1}^{(j)}, \theta_t^{(j)})$ is the incremental likelihood.
 16: $\omega_t^{(j)} = \omega_{t-1}^{(j)} \cdot L_t^{(j)}$
 17: **end for**
 18: Normalise weights
 19: $\omega_t^{(j)n} = \omega_t^{(j)} / \sum_{j=1}^{N_\theta} \omega_t^{(j)}$
 20: Calculate weighted mean and covariance of parameters
 21: $\hat{\mu}_t = \sum_{j=1}^{N_\theta} \omega_t^{(j)n} \theta_t^{(j)}$
 22: $\hat{\Sigma}_t = \sum_{j=1}^{N_\theta} \omega_t^{(j)n} (\theta_t^{(j)} - \hat{\mu}_t) (\theta_t^{(j)} - \hat{\mu}_t)^T$
 23: **end for**

reasonable acceptance ratio while leaving $p(\theta|y_{1:t})$ invariant. The rejuvenation step makes the algorithm quite computationally expensive, since the total likelihood of all particles $p(y_{1:t}|\theta)$ must be recalculated every time resampling occurs. This problem is mitigated by the fact that particles can be resampled independently, making this effort parallelisable.

4.5.3 Results

The RRTB was monitored for 12 days, 4 of which were used to train a 3R2C model. The model was trained separately by off-line and on-line Bayesian inference, using the MMH and SMC algorithms. In order to compare both methods at different points in time, the MMH algorithm was run several times by using 1 day, 2 days, 3 days or 4 days of training data, respectively.

Both methods used the same parameter prior $p(\theta)$, which will be displayed along with the results. It is a Gaussian prior with a wide support for each of the individual parameters. Indeed, we found that using a uniform prior could compromise the convergence ability of each algorithm in the case of parameters with low identifiability.



The on-line and off-line estimation results of the heat loss coefficient and solar aperture of the box are shown below. Theoretical values of these characteristics [Jim16] are available for comparison. We discuss the events that bring information to the estimates. More results on the same work is shown in [RJC19].

One of our targets is to determine which specific part of the data drives the parameter estimation towards more confident values. Therefore, Fig. 4.16(b) and 4.16(c) show the estimation results of HLC and the total solar aperture k by comparing them with measurement data in Fig. 4.16(a). The blue line and blue area show the average and 95% confidence interval of the posterior distributions obtained by SMC at each time coordinate. The box-and-whisker plots show the prior distribution at $t = 0$ in grey, and the four posterior distributions obtained by MMH using either 1, 2, 3 and 4 days of measurements, in red.

The 95% confidence interval of a parameter estimated by either SMC or MMH narrows down progressively, as data is sequentially added to the problem. A quick, stepwise decrease is an indicator of an event that “brings information” to the parameter. Both the HLC and the k properties have a similar behaviour in this matter: their confidence intervals are first narrowed down during the first day of measurements, as the solar irradiance rises. Then, a high information gain occurs as indoor heating is turned on, on the third day. It is general knowledge that the parameters of a building energy model are hardly identifiable without a heat source. This study however quantifies the effect of this input signal on the parameter uncertainty.

A fair match can be seen between results from both MMH and SMC algorithms: the distributions mostly overlap.

The SMC algorithm has two advantages compared to MMH in this situation: first, it was only run once to produce all sequential posterior distributions, whereas each off-line parameter estimation had to be started from the beginning of the sequence. The second advantage is the higher resolution in the temporal evolution of parameter estimates.

4.6 Separating transmission and air infiltration heat losses



This section is a summary of a future article, not yet published as of the writing of this report (April 2020).

The main motivation of the BAYREB project is to help justify retrofitting solutions, by identifying which measures would yield the best ratio of energy savings to investment. The permeability of

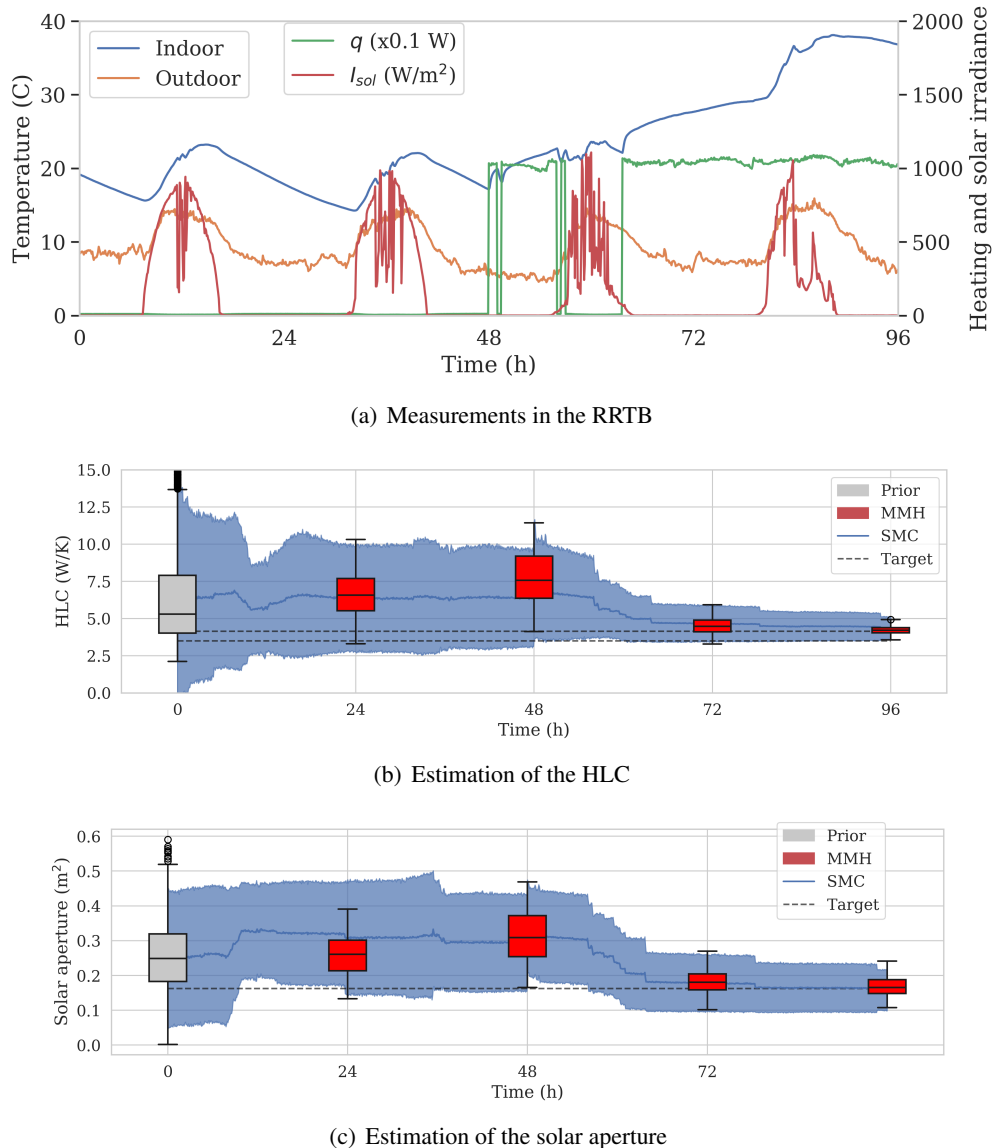


Figure 4.16: (a) Measured indoor and outdoor temperature, heating power and solar irradiance on the RRTB; (b) Estimation of HLC by the SMC and MMH algorithms compared to the reference value; (c) Estimation of the total solar aperture

the envelope is an important factor in this decision, since it determines air infiltration rates and its related heat loss. Pointing out that a building has significant leakage may motivate the decision to prioritize the retrofitting of windows. Although a blower door test measures the global permeability of the envelope, we wish in the project to assess whether non-disruptive measurements, which do not interrupt the normal operation of a building, may suffice for this estimation as well.

Using RC models for heat transfer, it is possible to respectively represent heat loss through the envelope construction and from air infiltration with two separate "branches": one including the heat capacity of the envelope, the other without heat capacity. The theoretical study based on a numerical benchmark however showed in Sec. 3.3 that such a representation involves identifiability issues when calibrating such a model structure from data. In other words, using only temperature measurements in relatively short periods of time does not allow disaggregating both effects.

We therefore consider two alternatives for the non-disruptive decomposition of the global heat loss into transmission and ventilation.

- Sec. 4.6.3: using longer datasets, in order to attempt to find correlations between environmental variables (wind speed and direction) and heat loss.
- Sec. 4.6.4: using more varied datasets, with CO₂ concentration measurements for the estimation of occupancy and air change rate.

But first, Sec. 4.6.1 will describe the variables we are looking for, and introduce some models for mechanical and natural ventilation.

4.6.1 Some theory on ventilation and heat loss

Ventilation and heat loss coefficients

We include the ventilation heat exchange into the overall heat balance of a thermal zone j :

$$C_j \frac{\partial T_j}{\partial t} = \Phi_h + \Phi_{int} + \Phi_{sol} + \underbrace{\Phi_{tr} + \Phi_{inf}}_{\propto HLC} + \Phi_{vent} \quad (4.19)$$

A distinction is made here between the heat gain (or loss) caused by an intended air change by mechanical ventilation Φ_{vent} , and by the uncontrolled infiltration heat exchange Φ_{inf} , which includes all natural ventilation if windows are closed).

- The intended ventilation heat exchange Φ_{vent} may come from outdoor at temperature T_e (with heat recovery efficiency η_{HR}), an adjacent unheated room at temperature T_u and another neighboring zone at temperature T_n , its expression will be:

$$\begin{aligned} \Phi_{vent} &= c_a Q_e (1 - \eta_{HR}) (\theta_e - \theta_i) + c_a Q_u (\theta_u - \theta_i) + c_a Q_n (\theta_n - \theta_i) \\ &= c_a \sum_j Q_{vent}^{(j)} (\theta^{(j)} - \theta_i) \end{aligned} \quad (4.20)$$

where c_a is the air specific heat and Q are mass flow rates (kg/s).

- Infiltration gains/losses arise along air leakage paths, and may come from separate flows (j) as well:

$$\Phi_{inf} = c_a \sum_j Q_{inf}^{(j)} (\theta^{(j)} - \theta_i) \quad (4.21)$$

Although it is often considered that infiltration is only a direct exchange with the outdoor air:

$$\Phi_{inf} = c_a Q_{inf} (\theta_e - \theta_i) \quad (4.22)$$

We then define the heat loss coefficient HLC and heat transfer coefficient HTC separately as:

$$\Phi_{tr} = \text{HTC} (\theta_e - \theta_i) \quad (4.23)$$

$$\Phi_{tr} + \Phi_{inf} = \text{HLC} (\theta_e - \theta_i) \quad (4.24)$$

By incorporating the infiltration losses through the building fabric, the definition of the HTC can be extended to the definition of the heat loss coefficient HLC:

$$\text{HLC} = \text{HTC} + \frac{\Phi_{inf}}{\theta_e - \theta_i} = \text{HTC} + H_{inf} \quad (4.25)$$

This equation displays the main target of the present section: not only estimating HLC, but also decomposing it into HTC and H_{inf}

Ventilation models

When infiltration and mechanical ventilation air flow rates are combined, the solution is simple additivity assuming the ventilation system has balanced flow. Because a balanced ventilation system does not impact internal pressure or the air flows through the envelope. In case of unbalanced systems, most commonly buildings with exhaust ventilation fans, they change the internal pressures and therefore need special consideration. Different approaches have recently been reviewed by [HSW16].

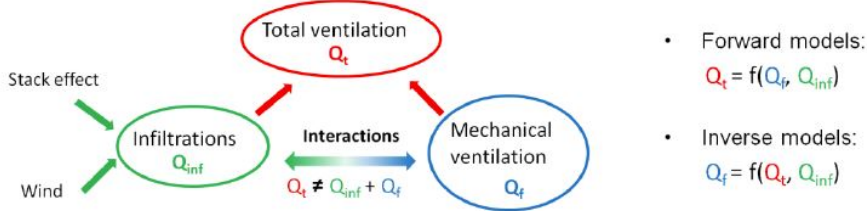


Figure 4.17: Total ventilation as a function of mechanical ventilation and infiltrations

With **balanced** mechanical systems, the solution is simple additivity, because such mechanical systems do not impact the internal pressure. Ventilation heat loss can be calculated from measurements of supply temperature, indoor temperature and ventilation flowrate.

$$\Phi_{vent} = c_a Q_{vent} \underbrace{(1 - \eta_{HR})(T_e - T_i)}_{(T_{sup} - T_i)} \quad (4.26)$$

If the supply temperature T_{sup} is not known, it should be estimated using the efficiency of the heat recovery η_{HR} . If there is no HR then $\eta_{HR} = 0$ and $T_{sup} = T_e$

- The small temperature rise over fans can be considered included in the temperature efficiency of the HR (one can consider 90 % of the fan power to be converted into heat which typically lead to a 0.5-1 °C temperature rise over the supply fan, but lost on the exhaust side, assuming the exhaust fan is located after the HR-unit).
- Duct losses and short-circuiting of supply and extract (for example surrounding the outlet and inlet on the building facade) may also impact ventilation efficiency, supply temperature and ventilation heat exchange. This may explain higher heat recovery efficiency than expected when efficiency is estimated based on supply temperature, indoor and outdoor temperatures.

- Some ventilation units have a heating coils on the supply side in addition to heat recovery (and/or a pre- heating coil operated for frost-protection). On residential units the heating coil is rarely hydronic (as is more common in large buildings), more commonly it is direct electric heating. Ventilation heating should be considered in the energy balance to adhere to the building physical framework, and in this case the supply temperature or at least the supply heating set-point (and operation strategy) will be needed.
- It may also relevant to know whether the ventilation unit and ductwork is located inside or outside of the heated building area (i.e. on an unheated attic, or basement).

With **unbalanced** systems (typically buildings with exhaust ventilation fans), the pressure changes can impact natural infiltration non-linearly and make it sub-additive. Quoting [Hur16]: *In the example of an exhaust fan, it corresponds to a situation where the neutral pressure level rises above the ceiling level. There is no exfiltration through the building envelope, and the infiltration is therefore only compensating for the exhaust fan flow. But the stronger the wind, the less likely this is to happen.*

Hurel et al. [HSW16] reviewed different approaches and proposed new sub-additive methods that are more robust across the full spectrum of air-tight to leaky buildings. In ESP-r's implementation of the AIM-2 model, the calculated natural infiltration air flow is adjusted subsequently by the Kiel-Wilson approach [KW87].

$$Q_t = \left((Q_{inf})^{1/n} + (0.5Q_f)^{1/n} \right)^n + 0.5Q_f \quad (4.27)$$

Where the net air flow rate from outdoors Q_t is caused by the combined influence of natural infiltration Q_{inf} and the unbalanced portion of the mechanical ventilation Q_f (matching notations of the Fig. 4.17).

Many infiltration of models for residential buildings have been developed based on statistical fits of infiltration data. Most empirical models rely on pressurization results (commonly obtained from blower door tests) and use flow theory and statistical techniques to fit data to common housing characteristics, but not all models are dependent on weather conditions. A review of applicable models for air infiltration calculations is given by [Orm99].

By considering weather is the dominant driving force, infiltration flow can be assumed to be linearly dependent on the outside-inside temperature difference and/or wind-speed. According to [SG80], previous work at that time had been found to be quite accurate for the site where the data was taken.

The Alberta Air Infiltration Model (AIM-2) can be expressed on the convenient form below where the calculated potential specific infiltration flow rate Q_{inf}^* (Pa^n) multiples with the infiltration coefficient C_{inf} . This flow coefficient can be estimated or obtained by using data from blower door pressurizations tests. AIM-2 uses a superposition technique where the infiltration flow rates due to wind Q_w^* and stack effects Q_s^* are added, and in addition an interaction term is introduced.

$$Q_{inf} = C_{inf} \left((Q_s^*)^{1/n} + (Q_w^*)^{1/n} - 0.33(Q_w^*Q_s^*)^{1/2n} \right)^n \quad (4.28)$$

The power law models the relationship between the indoor-outdoor pressure difference and the airflow rate through the leaks in the building envelope. Infiltration rates due to stack and wind effects are calculated as

$$Q_s^* = C_s(\Delta P_s)^n = C_s \left(\frac{9.8H p_a |T_e - T_i|}{T_i + 273.15} \right)^n \quad (4.29)$$

$$Q_w^* = C_w(\Delta P_w)^n = C_w (0.5U^2 \lambda_w^2 \rho_a)^n \quad (4.30)$$

where C_s and C_w are empirical parameters dependent on the building geometry, and U is the wind speed. Infiltration models are sensitive to parameters used for converting wind data measured at a weather station to the building site and for local wind shelter effects from typography and nearby buildings. This uncertainty can be reduced by wind measurements on site.

Estimating air flow rates from data

Without using a blower door test to estimate the permeability of the envelope, other ways of estimating infiltration rates must be found. Air flow is a difficult variable to measure in a building, especially when many leakage paths are involved. We will therefore attempt to assess the magnitude of infiltrations from other measured variables, which infiltration influence, or which are influenced by infiltrations. All these mutual influences are summarised by Fig. 4.18

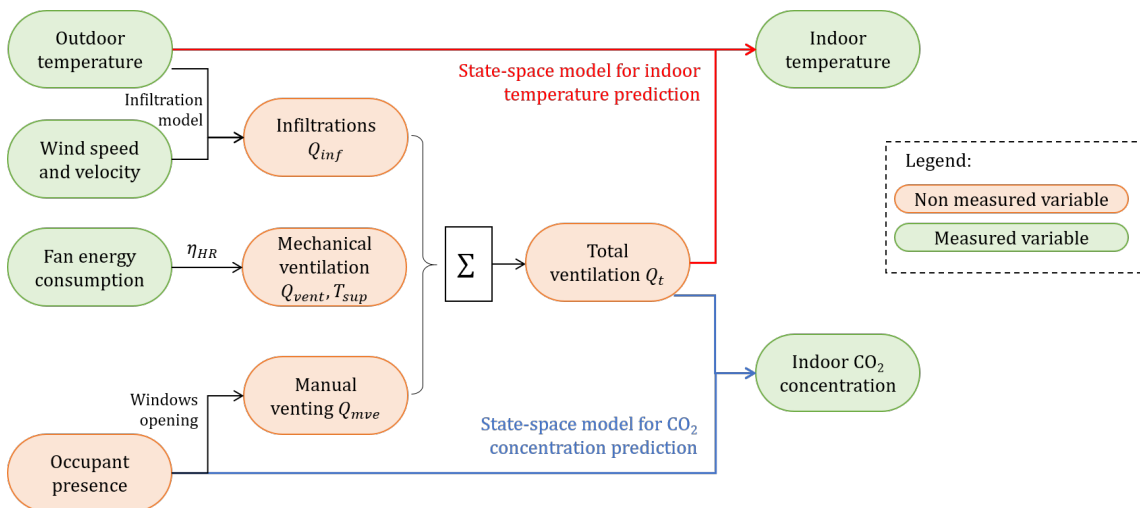


Figure 4.18: From what measured variables may air infiltration be estimated from?

The right side of Fig. 4.18 illustrates where the state-space models for heat transfer, shown by the red lines, stand in the relationship between measurable variables: they may predict the evolution of indoor temperature, given outdoor conditions and a ventilation rate. The total ventilation Q_t is the sum, or a sub-additive function, of infiltrations Q_{inf} , mechanical ventilation Q_{vent} and occupant-induced manual venting Q_{mve} .

- Infiltration models predict Q_{inf} as a function of weather conditions and unknown empirical variables, which should be estimated
- Mechanical ventilation flow rate Q_{vent} and supply temperature T_{sup} can either be measured, or estimated from the characteristics of the system: fan power and heat recovery efficiency η_{HR} .
- Occupant-induced manual venting Q_{mve} is difficult to predict. Either observation periods without occupant influence should be selected, or a way to detect sudden changes in air change rate should be proposed.

Fig. 4.19 shows an RC state-space model that includes terms for ventilation and infiltration heat transfer. The same decomposition of influences can be used with other model types, such as linear regression models. In addition to the identifiability issues that were raised earlier, it is clear that evaluating the magnitude of infiltration heat exchange demands that the mechanical ventilation component is known.

Fig. 4.18 displays another variable that is impacted by ventilation: the evolution of the indoor CO₂ concentration. This measurement is often used either to detect occupancy in a room, or to

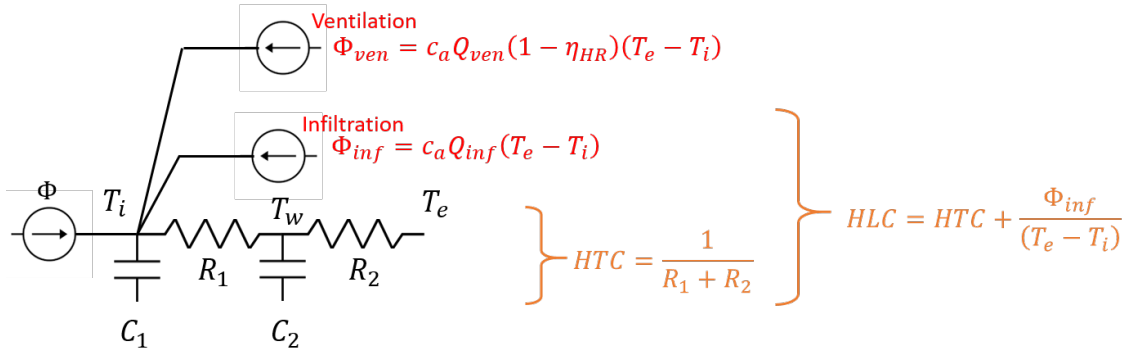


Figure 4.19: An RC model including ventilation and air infiltration

estimate its air change rate from the CO₂ concentration decay rate. Formulating the indoor CO₂ concentration as the output of a state-space model may allow estimating the parameters that drive its evolution by the same methods as with heat transfer.

The following two sections show the first results on the two approaches that are illustrated by Fig. 4.18:

- Including wind measurements as an input of a heat transfer SSM, in order to estimate the magnitude of air infiltration induced heat loss: Sec. 4.6.3
- Using a SSM for CO₂ concentration, in order to estimate the total air change rate from which infiltrations are inferred: Sec. 4.6.4

4.6.2 Case study: Gainsborough house

The case study is an end-terrace dwelling of four social houses built in Gainsborough, UK (53.4°N, 0.77°W). The house under consideration is used by 1 adult and 2 children, and has been monitored from March 2013 until November 2015. A detailed description of the houses and monitoring campaign can be found in [SS16b]. Ventilation is provided using a 'Lo-Carbon Astra' mechanical ventilation system with heat recovery (MVHR) from Vent-Axia. The system is equipped with a monitoring system that registers temperature and relative humidity of supply and return air, as well as the electricity consumption of the ventilation unit. In addition to an extensive monitoring of energy systems and envelope performance, the dataset includes time series data with 5 min intervals of the CO₂ concentration in the living room.

4.6.3 Using wind data to separate HTR from H_{inf}

The first approach to estimate H_{inf} is to include the wind speed as an input variable in a heat transfer SSM. Supposing air infiltration occurs at the ambient temperature T_e with a total mass flow rate Q_{inf} , the related heat flow is:

$$\Phi_{inf} = c_a \dot{m}_{inf} (\theta_e - \theta_i) \quad (4.31)$$

and the H_{inf} coefficient (W/K) is simply $H_{inf} = \Phi_{inf} / (T_e - T_i) = c_a Q_{inf}$

A model for infiltration flow rate is shown by Eq. 4.28. In order to accomodate this formula for linear model structure, we are making some restrictive assumptions: stack effects is neglected, and wind effects have a known exponent. These hypothesis, while optimistic, let us perform a quick assessment on this influence of wind on the heat balance of the building.

$$Q_{inf} \propto U \quad (4.32)$$

This simplified relationship is included in two model structures:

- One is a state-space model with the indoor temperature as output, shown by Fig. 4.19.
- One is a linear regression model,

$$\Phi_h + \Phi_{int} + \Phi_{vent} = HTC(T_i - T_e) - A_i I_{sol} + a_v U(T_i - T_e) \quad (4.33)$$

Both methods estimate a constant a_v coefficient from which the average infiltration flow rate and H_{inf} can be inferred.

Two months of data from the Gainsborough house (see Sec. 4.6.2) with a hourly time step size are used, between January and March 2014. Results of the estimations are shown on Tab. 4.6. The last week of measurements were used as validation data to check the accuracy of the SSM predictions: this comparison is shown by Fig. 4.20.

	Linear regression		State-space model	
	mean	std	mean	std
HLC	45.53	9.76	54.23	13.47
HTC	37.45	7.69	49.72	4.22
H_{inf}	8.08	6.01	4.51	12.8

Table 4.6: Decomposition of HLC into HTC and H_{inf} using wind data

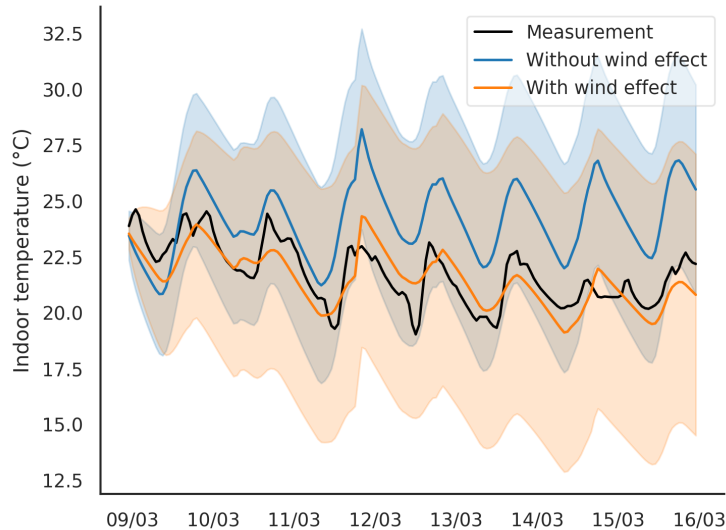


Figure 4.20: An RC model including ventilation and air infiltration

The infiltration heat transfer coefficient H_{inf} has a mean estimated value in the same magnitude as its standard deviation, or even lower in the case of the SSM estimation. This suggests either a very small influence of wind on the energy balance, or insufficient data. Data was indeed sampled at hourly time steps, which might be insufficient for the SSM to assess faster effects. Moreover, the expression of the infiltration flow rate Eq. 4.32 is an excessive simplification of more comprehensive models such as AIM-2: H_{inf} is likely underestimated.

Despite this result, the prediction performance of the SSM seems significantly improved when wind effects are taken into account (see Fig. 4.20). Moreover, we can observe a significant cross-correlation coefficient between the wind speed and the prediction residuals of the model from Fig. 4.19 if wind were not included in the inputs. There are therefore reasons to believe that this approach is promising.

4.6.4 Using CO₂ data to estimate occupancy and air change rates

Detailed coupled heat and air flow modelling in buildings is a time-consuming process that often requires the coupling of several simulation tools and is prone to user errors. Additionally, its outcome is very sensitive to non-controllable and uncertain conditions: occupant behaviour, windows opening schedule, weather... Instead of traditional modelling practices, which translate the knowledge of all physical phenomena of a system into equations, data-driven modelling refers to the use of measurements, rather than a priori knowledge, to build predictive models through statistical learning.

Estimating air flow rates from non-intrusive ambient measurements is a particularly complex problem, especially under real conditions of building use: infiltration and ventilation rates are very sensitive to the openings of doors and windows, and to outdoor conditions. The estimation of ventilation rates is therefore closely linked in the literature to that of the presence and habits of the occupants, by monitoring the evolution of CO₂ concentration in indoor air. From these measurements, a stochastic state space model can estimate the ventilation air change rate if the occupancy is known [Cal+15; Mac+18]. The same type of stochastic differential equation models for CO₂ are used by [Wol+19] to estimate the variable number of persons present in a dwelling, if the air change is known. [CJX18] give a more complete overview of occupancy estimation techniques, with the use of a wide variety of sensor and statistical learning methodologies.

As a first step towards data-driven air flow predictions, the present work uses CO₂ concentration measurements to simultaneously learn the air change rate and occupancy in a room. Based on a simple CO₂ balance equation, two algorithms (Interacting Multiple Models and Particle Swarm Optimisation) are used to find the fixed or time-varying parameters that best explain the evolution of CO₂ concentration. The outcome is an estimation of the ventilation rate, that can be comparatively analysed with other time series such as outdoor measurements (temperature, wind) or occupancy patterns.

Modelling and learning methodology

The case study is described in Sec. 4.6.2. The method starts by selecting a CO₂ balance equation for the lounge. This model should be kept as simple as possible, due to the limited available sensor information: only one CO₂ time series will be used, and no other sensor is available to detect occupancy. We suppose that air is supplied to the lounge at a variable rate $n(t)$ (1/s or 1/h) with outdoor CO₂ concentration c_e (ppm). CO₂ is produced by a number of occupants $p(t)$ with a production rate \dot{c}_0 (ppm/s or ppm/h) per person. Assuming that the living room is ideally mixed, the evolution of its CO₂ concentration c (ppm) reads:

$$\frac{\partial c}{\partial t} = n(t)(c_e - c) + \dot{c}_0 p(t) \quad (4.34)$$

The target of the study is the estimation of the time-varying air change rate n and number of occupants p in a room, using measurements of the CO₂ concentration. An assumption is made in order to make this estimation feasible: at any time coordinate t , n and p can only take values among a finite number of values. $\forall t, p_t \in \{0, 1, 2, 3\}$: there can be up to three people in the living room. $n_t \in \{n_1, n_2\}$: the air change rate may either take a low value n_1 (baseline ventilation) or a higher value n_2 (open windows), to be determined. We will show below how the averaged calculated n_t will then be able to take any value between these two bounds.

These parameters are assembled into a vector $\theta_t = \{n_t, p_t\}$, which is a finite state Markov chain taking a finite number of values N according to a transition probability matrix \mathbf{H} . Other parameters, denoted global parameters $\theta_g = \{n_1, n_2, \dot{c}_0, \mathbf{H}\}$ are constant but unknown: the two air change rate bounds, the CO₂ production rate per occupant and the components of the transition matrix. After time discretization, Eq. 4.34 can be reformulated as a discrete stochastic state-space model:

$$c_t = \mathbf{A}(\theta_g, \theta_t) c_{t-1} + \mathbf{B}(\theta_g, \theta_t) u_t + w_t \quad (4.35)$$

$$y_t = \mathbf{C}(\theta_g, \theta_t) c_t + v_t \quad (4.36)$$

where u_t are input data influencing the balance equation, such as the outdoor CO₂ concentration c_e ; y_t is the measured indoor concentration, w_t and v_t are mutually independent white Gaussian processes which respectively represent the modelling and measurement uncertainties. \mathbf{A} , \mathbf{B} and \mathbf{C} are the matrices of the system, functions of the global and temporal parameters θ_g and θ_t .

If θ_g and θ_t were known, this system of equations is solvable by Kalman filtering, which is common practice for the calibration of heat transfer models in buildings [RRO18]. The point of the study is however to estimate them, which is done by two algorithms: θ_t is estimated by the Interacting Multiple Models (IMM) method [BB88], and θ_g is estimated by Particle Swarm Optimization (PSO). This workflow is shown on Fig. 4.21.

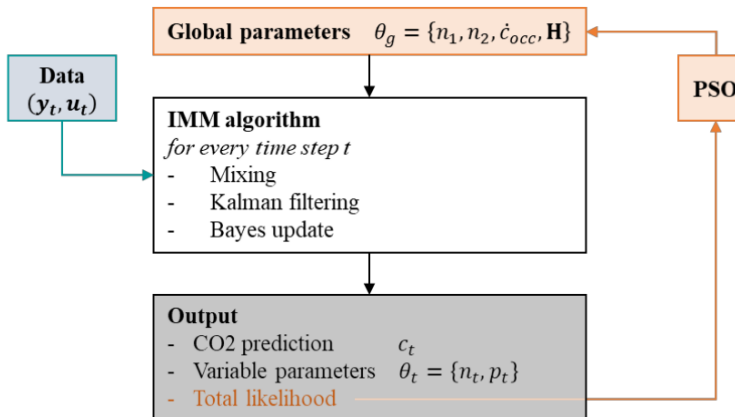


Figure 4.21: Workflow for the simultaneous estimation of occupancy and air change rate

Supposing fixed values for θ_g , the IMM algorithm consists at every time step of a Kalman filter prediction for all N possible values of θ_t . These N "hypotheses" are then weighted by the prediction likelihoods calculated by the Kalman filters. The next time step then starts by a mixing step which computes the initial condition for the filter, according to these weights and the transition probability matrix \mathbf{H} . Although this description is quite concise, the IMM algorithm is more clearly explained by [BB88].

Along with a prediction of the indoor CO₂ concentration and an estimation of the variable air change rate and occupancy, IMM returns the total prediction likelihood, which indicates the fit of predictions with measurements. This indicator is used as objective by a PSO algorithm that computes the optimal values of the global parameters θ_g .

Results

Due to the computational load of the PSO algorithm, the procedure described above was applied on the data in two steps: (1) Global parameter tuning: using one month of data (April 2013), the entire workflow shown on Fig. 4.21 was implemented so that the optimal value of θ_g was found by PSO. (2) The IMM algorithm was then run on the entire dataset (March 2013 to November 2015), using this predetermined value for θ_g . Results are shown on Fig. 4.22 and 4.23 below.

Fig. 4.22 shows the predictions of the fitted model over a short period (2 days): CO₂ concentration in the living room, air change rate and occupancy. The model described above is hereby called Model 2, and compared to an alternative model (Model 1) where the air change rate is constant and part of the global parameters, fitted separately every day. Model 2 (variable air change rate) shows

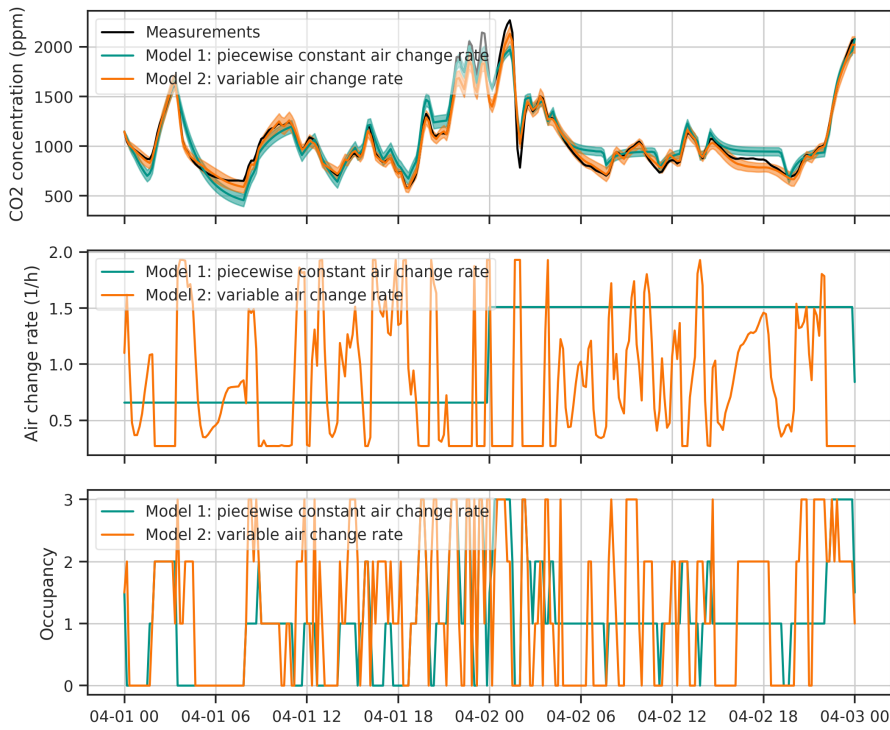


Figure 4.22: Predictions of the fitted CO₂ prediction model

a better agreement with the data, and allows observing the fluctuations of n between a lower value $n_1 = 0.272$ (vol/h) and an upper value $n_2 = 1.93$ (vol/h): this suggests a detection of windows and doors opening, and an estimation of the baseline ventilation rate.

On Fig. 4.23, predictions over the entire dataset (March 2013 to November 2015) were averaged to daily values, in order to detect relationships between n , occupancy and weather trends. Fig 4.23(a) shows averages of ventilation rates sorted by the detected number of occupants in the room at the same time. When at least 1 occupant is present, there is a significant probability that n takes higher values, suggesting that these values denote windows and doors opening. This trend increases with the number of occupants. When the lounge is empty, the probability distribution of n is much more concentrated near its baseline value.

Fig. 4.23(b) compares daily averages of n , sorted by occupancy, with the measured temperature difference ΔT between the living room and outdoor. Although no significant correlation between n and ΔT is visible when the room is empty, there is a stronger one when someone is present. This trend suggests that a behaviour model may be obtained from this method. No significant correlation was found with wind speed measurements yet, from which it may be possible to calibrate air infiltration models.

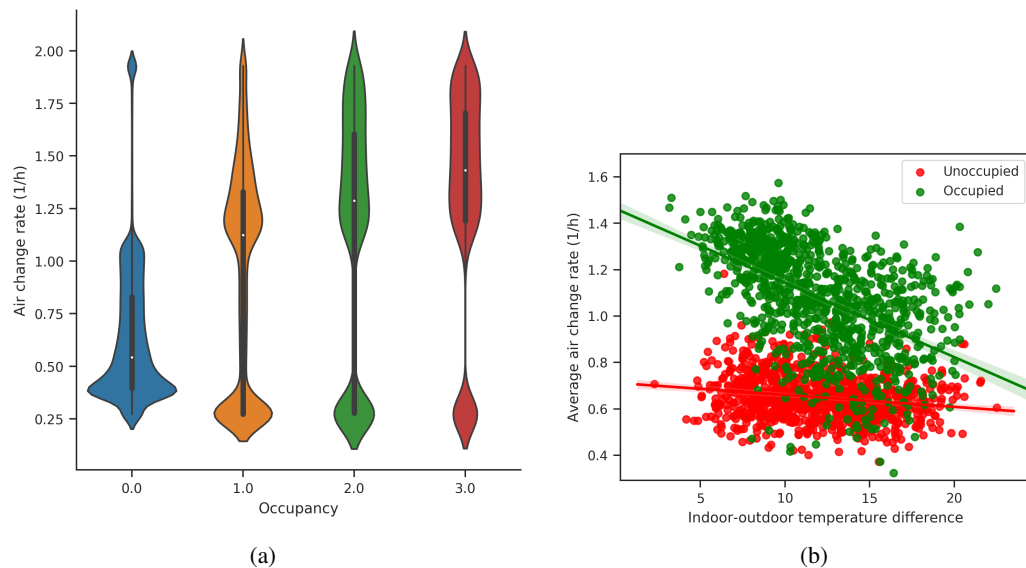


Figure 4.23: Distribution of daily averaged ventilation rates related to occupancy (a), and indoor-outdoor temperature difference (b)

5. Summary and prospects of the project

5.1 Summary of the BAYREB project

The contribution of the project to the area of building energy performance assessment can be described into three main parts.

Background literature review on inverse problems and how to solve them

First, a state of the art of the common practices in building energy performance assessment was attempted. Chap. 1 reviewed some existing practices for estimating energy performance indicators from in-situ measurements, and showed that most of them are not applicable in occupied buildings. The project was indeed motivated by the need for a method that would yield interpretable performance indicators from a monitored building in normal operating conditions, in order to provide incentive for refurbishment. Ideally, these indicators should *disaggregate* the building performance into separate heat loss terms (transmission through the envelope, windows, thermal bridges, heat loss from air infiltration...) as to prioritize energy conservation measures. Chap. 2 then formalizes the problem and presents the mathematical and numerical tools that were used in the project. Some elements of model calibration and statistical learning are presented. We especially emphasize the necessary steps for proper model specification, and for model checking and validation once optimal parameters have been estimated. A special focus is then made on linear stochastic state-space models, a category of models used to learn from time-series energy and temperature readings. The popular RC models belong to this category. All steps of the solving process are described: model specification, discretization, Kalman filtering, and parameter estimation with Maximum Likelihood Estimation or Markov Chain Monte Carlo. The main elements of this chapter were also published in [Rou18].

Identifiability, interpretability, and how to assess them

The second main part of this report, and the first essential contribution of the project to the state of the art, is the question of parameter interpretability. Once a numerical model has been trained by fitting its parameters so that its output best matches observed data, we want to ensure that these parameters may be interpreted as representative of real physical properties. This question goes

beyond the concept of model identifiability, which asks whether model parameters may be uniquely estimated from data: we wish to know about *physical meaning*. Chap. 3 describes the methodology of interpretability assessment. It is based on a numerical benchmark: a simulated building in which all envelope properties (insulation thickness, air change rate, transmission of glazing...) may be changed. The question is whether variations of the properties of the reference building result in variations of the expected performance indicators estimated from reduced-order models, and only the expected indicators. Through sensitivity analysis, we can find the origin of the variance of estimated parameters, and point out the phenomena that were not appropriately explained by the reduced-order models. Two applications of the numerical benchmark were then proposed: finding the minimal monitoring duration so that estimates of the global heat loss coefficient are robust regarding variable weather conditions; finding whether a minimal set of measurements is enough to disaggregate heat loss from air infiltration and envelope transmission. Chap. 3 is thus a theoretical study of the limitations and potential of building energy performance assessment based on in-situ measurements.

In a nutshell, this part of the work aimed at establishing to what extent stochastic RC models were able to estimate the thermal performance of a building envelope from weather, indoor temperatures and heating power designed as to not disturb occupants. The overall thermal resistance can be robustly estimated from minimally 11 days training data and achieves very satisfactory interpretability. Finer decomposition of the heat losses has however not been found possible from poorly informative data. Finally, regardless of the conditions of data collection, the good practice workflow for meaningful calibration remains valid and in any case necessary for any thermal characterisation.

Case studies

Finally, Chap. 4 illustrates the methods proposed by the project by showing a collection of independent practical applications. Several methods are illustrated, each of which aims to answer a question related to building energy performance assessment:

- The energy signature method is used on commercial buildings data. Although this method is very simple and relies on strong assumptions, it allows a coarse decomposition of energy use and a comparison of performance before and after energy conservation measures were applied.
- Ordinary linear regression demonstrates how to easily identify which phenomena have a significant impact on the energy balance of a building, and which measurements do not need to be taken into account.
- In Sec. 4.3, the main methodology of the project is demonstrated: using a state-space model, i.e. a resistor-capacitor network written in stochastic form, to analyse time-series readings of energy use and temperatures, and estimate physical properties of the building envelope. The methodology comes with criteria for model checking and validation, which allow some confidence in the interpretation of results.
- In Sec. 4.4, these physically-based state-space model structures are extended in a hybrid form called latent force models. LFM are a state-space model including an uncertain influence modelled by a temporal Gaussian Process: this is a way to include unobserved phenomena that may have an impact on the model output, and thus improve its predictive accuracy. GPs are however non-parametric models that are difficult to relate to physical concepts: the result is that the estimated parameters of an LFM may not be physically interpretable.
- Sec. 4.5 shows online parameter estimation with the Sequential Monte Carlo algorithm. A similar RC model structure as in the previous sections is trained sequentially: its parameters are updated with every new data point, so that the evolution of their posterior distribution can be seen as a function of the available data.

- Finally, Sec. 4.6 shows an attempt at decomposing the global heat loss coefficient of the envelope into a heat transfer coefficient, and a separate term for heat loss related to air infiltration. We have seen in Sec. 3.3 that such a disaggregation was not possible on the sole basis of indoor temperature measurements: instead, Sec. 4.6 uses more diversified data, such as wind speed and direction and indoor CO₂ concentration measurements, in order to estimate infiltration air flow and the induced heat loss. While results come with a very high uncertainty, this is considered a promising prospect of the work.

5.2 Prospects

In a close future, the results could be supplemented by extending the methodology to other building typologies as to examine how thermal inertia and architectural specificities influence the estimation of the thermal performance. Other typologies would indeed widen the issues to tackle, just to name a few:

- Thermal stratification and temperature differences in the different rooms become all the more problematic in large buildings, notably with several storeys. It implies that some part of the information on the thermal behaviour of the building will be missing. These temperature discrepancies seem indeed to have an impact on the estimation's accuracy and invite to further research on the subject. The issue of measurement representativeness actually also apply to the measurement of wind speed and solar irradiation, as well as measurement of the heating power when it is derived from overall energy use data. A quantification of the effect on accuracy of measurement discrepancy would be valuable and would help understanding the extent of the issue. This would help concentrate the effort on tackling on the most influential measurement discrepancies. It could be done by design of appropriate sensor placement in order to reduce uncertainty, although extensive measurements would certainly be more intrusive. At least, acknowledgement of the measurement discrepancy in the modelling process is necessary to reflect the associated uncertainty in the estimation results.
- Measurement of heating power delivered in a single room for centralized heating systems also pushes further the issue of measurement discrepancy;
- Thermal characterisation of the envelope in apartment blocks, large office buildings, or hospitals questions the measurements representativeness. In particular, it cannot be expected at all that all zones follow identical temperature set point schedules and deploying sensors in all rooms is most probably cost prohibitive. This implies that a model would be trained for each measured zone. But then, sampling of zones to measure raises the issue of a compromise between efficiency and representativeness. Then, while sampling may be an option, the question of the accuracy of RC model training in a single zone remains, when there are more heated neighbouring zones than surfaces towards the exterior.
- The question of buildings bound by large surfaces towards heated neighbouring spaces, such as in offices and hospitals but also in terraced houses, is also left to tackle with RC models trained from non intrusive data.
- There remains questions on the most informative indoor temperature set point schedule. If there were significantly more informative and yet occupant-friendly schedules, it becomes relevant to control such schedules when the experiments are performed, in order to lower uncertainties.

In the prospect of assessing the suitability of retrofit strategies, this work could also be applied to the identifiability of the dynamic characteristics of the envelope. Indeed, energy performance is not only influenced by a static thermal resistance but also by the dynamic response of the envelope. This work suggests that the dynamic nature of stochastic RC models would then be adequate for such estimation, although identifiability and interpretability will have to be assessed on basis of data collected in uncontrolled non intrusive conditions.

Next, in the wider prospect of achieving thermal characterisation of a building envelope from data collection under occupancy, the results of this thesis are believed to enlighten the extent of the scientific problem thus defined. Very basically, measurements in an occupied space imply issues with first data collection which will be aggregated and possibly biased and secondly with unpredictable and barely measurable heat and moisture production as well as unpredictable occupancy related activity such as open doors and windows.

In a non intrusive and uncontrolled experimental framework, data exploitation will first necessarily rely on disaggregation of the energy consumptions to distinguish energy use for heating from energy use for electrical appliances. If it cannot be done, it constitutes an additional measurement discrepancy error with most probably a large effect on accuracy of a thermal characterisation.

Regarding interaction of the occupants on the envelope and on the heat and moisture balance, it implies major model discrepancy as the building envelope has multiple states unaccounted for in a usual RC model. Accuracy and uncertainty are therefore not guaranteed to be to the least satisfactory. The question of repeatability under the variability of the actions of occupants is also questioned, which calls for further research on a Bayesian based indicator for convergence of the estimation.

These occupancy related issues invite to at least account for uncertainties either in the form of a global model discrepancy term as in Bayesian calibration in the sense of [CM18; HCA12], although physical interpretability has been found to be an issue [CM18], or use Gaussian Latent Force Models [SAL18] that account for unmeasured influential input variables directly in the state space equations.

Both propositions are also arguments in favour of a Bayesian approach. Indeed, introduction of unknown, unmeasurable and systematic uncertainties will certainly have an impact on practical identifiability and all the more on the algorithmic ease to make estimations. As a consequence, physical interpretability would even less be within reach. A Bayesian approach through careful prior choices would at least act as regularisation in the inverse problem.

Bibliography

- [ASK12] C. Agbi, Z. Song, and B. Krogh. “Parameter identifiability for multi-zone building models”. In: *2012 IEEE 51st Annual Conference on Decision and Control (CDC)*. Dec. 2012, pages 6951–6956. DOI: 10.1109/CDC.2012.6425995 (cited on page 30).
- [Alz+18] Florent Alzetto et al. “Comparison of whole house heat loss test methods under controlled conditions in six distinct retrofit scenarios”. In: *Energy and Buildings* 168 (June 2018), pages 35–41. DOI: 10.1016/j.enbuild.2018.03.024 (cited on pages 10, 11).
- [AMH00] Klaus Kaae Andersen, Henrik Madsen, and Lars H. Hansen. “Modelling the heat dynamics of a building using stochastic differential equations”. In: *Energy and Buildings* 31.1 (Jan. 2000), pages 13–24. DOI: 10.1016/S0378-7788(98)00069-3 (cited on page 91).
- [And+17] Carlos Andrade-Cabrera et al. “Ensemble Calibration of lumped parameter retrofit building models using Particle Swarm Optimization”. In: *Energy and Buildings* 155 (Nov. 2017), pages 513–532. DOI: 10.1016/j.enbuild.2017.09.035 (cited on page 46).
- [ADH10] Christophe Andrieu, Arnaud Doucet, and Roman Holenstein. “Particle Markov chain Monte Carlo methods”. en. In: *Journal of the Royal Statistical Society: Series B (Statistical Methodology)* 72.3 (June 2010), pages 269–342. DOI: 10.1111/j.1467-9868.2009.00736.x (cited on page 33).
- [Ans+15] F. Anstett-Collin et al. “Sensitivity analysis of complex models: Coping with dynamic and static inputs”. In: *Reliability Engineering and System Safety* 134 (2015), pages 268–275. DOI: 10.1016/j.ress.2014.08.010 (cited on page 51).
- [AAC12] Paul D. Arendt, Daniel W. Apley, and Wei Chen. “Quantification of Model Uncertainty: Calibration, Model Discrepancy, and Identifiability”. In: *Journal of Mechanical Design* 134.10 (Sept. 2012), pages 100908–100908–12. DOI: 10.1115/1.4007390 (cited on pages 14, 15, 91, 101).

- [BM11] Peder Bacher and Henrik Madsen. “Identifying suitable models for the heat dynamics of buildings”. In: *Energy and Buildings* 43.7 (July 2011), pages 1511–1522. DOI: 10.1016/j.enbuild.2011.02.005 (cited on pages 7, 8, 25, 65, 66, 91, 95).
- [BR14] Geert Bauwens and Staf Roels. “Co-heating test: A state-of-the-art”. In: *Energy and Buildings* 82 (Oct. 2014), pages 163–172. DOI: 10.1016/j.enbuild.2014.04.039 (cited on pages 9, 10, 17, 43).
- [BB04] M. J. Bayarri and J. O. Berger. “The Interplay of Bayesian and Frequentist Analysis”. In: *Statistical Science* 19.1 (2004). Publisher: Institute of Mathematical Statistics, pages 58–80 (cited on page 32).
- [Bec85] James V. Beck. *Inverse Heat Conduction: Ill-Posed Problems*. en. James Beck, Oct. 1985 (cited on page 17).
- [BW98] James V. Beck and Keith A. Woodbury. “Inverse problems and parameter estimation: integration of measurements and analysis”. en. In: *Measurement Science and Technology* 9.6 (1998), page 839. DOI: 10.1088/0957-0233/9/6/001 (cited on pages 16, 22).
- [BA⁷⁰] R. Bellman and K. J. Åström. “On structural identifiability”. In: *Mathematical Biosciences* 7.3 (Apr. 1970), pages 329–339. DOI: 10.1016/0025-5564(70)90132-X (cited on pages 29, 30).
- [Bel+07] Giuseppina Bellu et al. “DAISY: A new software tool to test global identifiability of biological and physiological systems”. In: *Computer Methods and Programs in Biomedicine* 88.1 (Oct. 2007), pages 52–61. DOI: 10.1016/j.cmpb.2007.07.002 (cited on page 30).
- [Ber+16] Julien Berger et al. “Bayesian inference for estimating thermal properties of a historic building wall”. In: *Building and Environment* 106 (2016), pages 327–339. DOI: 10.1016/j.buildenv.2016.06.037 (cited on page 17).
- [Bet17] Michael Betancourt. “A Conceptual Introduction to Hamiltonian Monte Carlo”. In: *arXiv:1701.02434 [stat]* (Jan. 2017). arXiv: 1701.02434 (cited on page 36).
- [Bet18] Michael Betancourt. “Calibrating Model-Based Inferences and Decisions”. In: *arXiv:1803.08393 [stat]* (Mar. 2018) (cited on page 32).
- [BB88] H. A. P. Blom and Y. Bar-Shalom. “The interacting multiple model algorithm for systems with Markovian switching coefficients”. In: *IEEE Transactions on Automatic Control* 33.8 (Aug. 1988), pages 780–783. DOI: 10.1109/9.1299 (cited on page 119).
- [BB14] P Boisson and R Bouchié. “ISABELE method: In-Situ Assessment of the Building Envelope Performance”. In: *Proceedings of the Ninth International Conference on System Simulation in Buildings*. 2014 (cited on page 11).
- [BO14] Jenný Brynjarsdóttir and Anthony O’Hagan. “Learning about physical parameters: the importance of model discrepancy”. en. In: *Inverse Problems* 30.11 (Oct. 2014). Publisher: IOP Publishing, page 114007. DOI: 10.1088/0266-5611/30/11/114007 (cited on page 91).
- [Cal+15] Davide Calì et al. “CO₂ based occupancy detection algorithm: Experimental analysis and validation for office and residential buildings”. In: *Building and Environment* 86 (Apr. 2015), pages 39–49. DOI: 10.1016/j.buildenv.2014.12.011 (cited on page 118).
- [CGM07] Olivier Cappé, Simon Godsill, and Eric Moulines. “An overview of existing methods and recent advances in sequential monte carlo”. In: *Proceedings of the IEEE* 95.5 (2007), pages 899–924 (cited on pages 33, 108).

- [CCS15] Manolis N. Chatzis, Eleni N. Chatzi, and Andrew W. Smyth. “On the observability and identifiability of nonlinear structural and mechanical systems”. en. In: *Structural Control and Health Monitoring* 22.3 (Mar. 2015), pages 574–593. DOI: 10.1002/stc.1690 (cited on page 30).
- [CJX18] Zhenghua Chen, Chaoyang Jiang, and Lihua Xie. “Building occupancy estimation and detection: A review”. In: *Energy and Buildings* 169 (June 2018), pages 260–270. DOI: 10.1016/j.enbuild.2018.03.084 (cited on page 118).
- [CM18] Adrian Chong and Kathrin Menberg. “Guidelines for the Bayesian calibration of building energy models”. In: *Energy and Buildings* (July 2018). DOI: 10.1016/j.enbuild.2018.06.028 (cited on pages 15, 43, 101, 126).
- [Cho+17] Adrian Chong et al. “Bayesian calibration of building energy models with large datasets”. In: *Energy and Buildings* 154 (Nov. 2017), pages 343–355. DOI: 10.1016/j.enbuild.2017.08.069 (cited on page 15).
- [CJP13] N. Chopin, P. E. Jacob, and O. Papaspiliopoulos. “SMC2: an efficient algorithm for sequential analysis of state space models”. en. In: *Journal of the Royal Statistical Society: Series B (Statistical Methodology)* 75.3 (June 2013), pages 397–426. DOI: 10.1111/j.1467-9868.2012.01046.x (cited on pages 35, 108).
- [Cho02] Nicolas Chopin. “A sequential particle filter method for static models”. en. In: *Biometrika* 89.3 (Aug. 2002), pages 539–552. DOI: 10.1093/biomet/89.3.539 (cited on pages 33, 35, 108).
- [Cra+01] Drury B. Crawley et al. “EnergyPlus: creating a new-generation building energy simulation program”. In: *Energy and Buildings* 33.4 (Apr. 2001), pages 319–331. DOI: 10.1016/S0378-7788(00)00114-6 (cited on page 46).
- [DH15] Simona D’Oca and Tianzhen Hong. “Occupancy schedules learning process through a data mining framework”. In: *Energy and Buildings* 88 (Feb. 2015), pages 395–408. DOI: 10.1016/j.enbuild.2014.11.065 (cited on page 17).
- [DR17] An-Heleen Deconinck and Staf Roels. “Is stochastic grey-box modelling suited for physical properties estimation of building components from on-site measurements?” en. In: *Journal of Building Physics* 40.5 (Mar. 2017), pages 444–471. DOI: 10.1177/1744259116688384 (cited on pages 38, 43, 50).
- [DA09] Bing Dong and Burton Andrew. “Sensor-based occupancy behavioral pattern recognition for energy and comfort management in intelligent buildings”. In: *Proceedings of 11th IBPSA International Conference*. Glasgow, UK, 2009 (cited on page 17).
- [DL14] Bing Dong and Khee Poh Lam. “A real-time model predictive control for building heating and cooling systems based on the occupancy behavior pattern detection and local weather forecasting”. en. In: *Building Simulation* 7.1 (Feb. 2014), pages 89–106. DOI: 10.1007/s12273-013-0142-7 (cited on page 17).
- [DGA00] Arnaud Doucet, Simon Godsill, and Christophe Andrieu. “On sequential Monte Carlo sampling methods for Bayesian filtering”. en. In: *Statistics and Computing* 10.3 (July 2000), pages 197–208. DOI: 10.1023/A:1008935410038 (cited on page 105).
- [Fel86] Margaret F. Fels. “PRISM: An introduction”. In: *Energy and Buildings* 9.1-2 (Feb. 1986), pages 5–18. DOI: 10.1016/0378-7788(86)90003-4 (cited on pages 13, 17).
- [FS71] J. M. Finkelstein and R. E. Schafer. “Improved goodness-of-fit tests”. In: *Biometrika* 58.3 (1971), pages 641–645. DOI: 10.1093/biomet/58.3.641 (cited on page 51).

- [FK16] Graeme Flett and Nick Kelly. “An occupant-differentiated, higher-order Markov Chain method for prediction of domestic occupancy”. en. In: *Energy and Buildings* 125 (Aug. 2016), pages 219–230. DOI: 10.1016/j.enbuild.2016.05.015 (cited on page 102).
- [FK17] Graeme Flett and Nick Kelly. “A disaggregated, probabilistic, high resolution method for assessment of domestic occupancy and electrical demand”. en. In: *Energy and Buildings* 140 (Apr. 2017), pages 171–187. DOI: 10.1016/j.enbuild.2017.01.069 (cited on page 102).
- [Flo92] F. Flouquet. “Local weather correlations and bias in building parameter estimates from energy-signature models”. In: *Energy and Buildings* 19.2 (1992), pages 113–123. DOI: 10.1016/0378-7788(92)90005-2 (cited on page 13).
- [Fou+13] Aurélie Foucquier et al. “Effect of wall merging on a simplified building energy model: accuracy versus number of equations”. In: *13th International Conference of the International Building Performance Simulation Association* (2013), pages 3161–3168 (cited on page 46).
- [Gar+13] James Gareth et al. *An Introduction to Statistical Learning*. Springer, 2013 (cited on page 100).
- [GCG18] Katia Gaspar, Miquel Casals, and Marta Gangolells. “Review of criteria for determining HFM minimum test duration”. In: *Energy and Buildings* 176 (Oct. 2018), pages 360–370. DOI: 10.1016/j.enbuild.2018.07.049 (cited on page 49).
- [Gel+13] Andrew Gelman et al. *Bayesian Data Analysis, Third Edition*. en. CRC Press, Nov. 2013 (cited on page 36).
- [GA19] Christian Ghiaus and Florent Alzetto. “Design of experiments for Quick U-building method for building energy performance measurement”. In: *Journal of Building Performance Simulation* 12 (2019), pages 465–479 (cited on page 11).
- [Gho+15] Siddhartha Ghosh et al. “Modeling the thermal dynamics of buildings: a latent-force model-based approach”. In: *ACM Transactions on Intelligent Systems and Technology* 6.1 (2015), page 7 (cited on pages 14, 28, 101).
- [GMW17] Jeanne Goffart, Thierry Mara, and Etienne Wurtz. “Generation of stochastic weather data for uncertainty and sensitivity analysis of a low-energy building”. In: *Journal of Building Physics* 41.1 (2017), pages 41–57. DOI: 10.1177/1744259116668598 (cited on page 51).
- [GRM17] Jeanne Goffart, Mickael Rabouille, and Nathan Mendes. “Uncertainty and sensitivity analysis applied to hygrothermal simulation of a brick building in a hot and humid climate”. In: *Journal of Building Performance Simulation* 10.1 (Jan. 2017), pages 37–57. ISSN: 1940-1493. DOI: 10.1080/19401493.2015.1112430 (cited on page 46).
- [GBE18] Virginia Gori, Phillip Biddulph, and Clifford A. Elwell. “A Bayesian dynamic method to estimate the thermophysical properties of building elements in all seasons, orientations and with reduced error”. In: *Energies* 11.4 (2018). DOI: 10.3390/en11040802 (cited on page 49).
- [GE18] Virginia Gori and Clifford A. Elwell. “Estimation of thermophysical properties from in-situ measurements in all seasons: Quantifying and reducing errors using dynamic grey-box methods”. In: *Energy and Buildings* 167 (2018), pages 290–300. DOI: 10.1016/j.enbuild.2018.02.048 (cited on page 49).

- [GMJ17] Thomas R. B. Grandjean, Andrew McGordon, and Paul A. Jennings. “Structural Identifiability of Equivalent Circuit Models for Li-Ion Batteries”. en. In: *Energies* 10.1 (Jan. 2017), page 90. DOI: 10.3390/en10010090 (cited on page 30).
- [GG76] M. Grewal and K. Glover. “Identifiability of linear and nonlinear dynamical systems”. In: *IEEE Transactions on Automatic Control* 21.6 (Dec. 1976). Conference Name: IEEE Transactions on Automatic Control, pages 833–837. DOI: 10.1109/TAC.1976.1101375 (cited on pages 29, 30).
- [Ham87] Stig Hammarsten. “A critical appraisal of energy-signature models”. In: *Applied Energy* 26.2 (1987), pages 97–110. DOI: 10.1016/0306-2619(87)90012-2 (cited on page 13).
- [Han70] J. E. Handschin. “Monte Carlo techniques for prediction and filtering of non-linear stochastic processes”. In: *Automatica* 6.4 (July 1970), pages 555–563. DOI: 10.1016/0005-1098(70)90010-5 (cited on page 105).
- [HTF01] Trevor Hastie, Robert Tibshirani, and Jerome Friedman. *Elements of Statistical Learning: data mining, inference, and prediction. 2nd Edition*. Springer series in statistics. Springer, 2001 (cited on pages 23, 30, 40, 41, 82).
- [HGP12] Ion Hazyuk, Christian Ghiaus, and David Penhouet. “Optimal temperature control of intermittently heated buildings using Model Predictive Control: Part I - Building modeling”. In: *Building and Environment* 51 (May 2012), pages 379–387. DOI: 10.1016/j.buildenv.2011.11.009 (cited on page 17).
- [HCA12] Y. Heo, R. Choudhary, and G. A. Augenbroe. “Calibration of building energy models for retrofit analysis under uncertainty”. In: *Energy and Buildings* 47 (Apr. 2012), pages 550–560. DOI: 10.1016/j.enbuild.2011.12.029 (cited on pages 14, 17, 101, 126).
- [HZ12] Yeonsook Heo and Victor M. Zavala. “Gaussian process modeling for measurement and verification of building energy savings”. In: *Energy and Buildings* 53 (Oct. 2012), pages 7–18. DOI: 10.1016/j.enbuild.2012.06.024 (cited on page 17).
- [Hur16] Nolwenn Hurel. “Impact des infiltrations d’air sur les performances des bâtiments : focus sur l’étude expérimentale dans les parois ossature bois”. Publication Title: <http://www.theses.fr/thesis.Grenoble.Alpes>, Nov. 2016 (cited on page 114).
- [HSW16] Nolwenn Hurel, Max H. Sherman, and Iain S. Walker. “Sub-additivity in combining infiltration with mechanical ventilation for single zone buildings”. en. In: *Building and Environment* 98 (Mar. 2016), pages 89–97. DOI: 10.1016/j.buildenv.2015.12.020 (cited on pages 113, 114).
- [ISO17] ISO 13789. *Thermal performance of buildings - Transmission and ventilation heat transfer coefficients - Calculation method*. 2017 (cited on page 61).
- [ISO14] ISO 9869-1. *ISO 9869 Thermal insulation — Building elements — In-situ measurement of thermal resistance and thermal transmittance — Part 1: Heat flow meter method*. 2014 (cited on page 49).
- [Jan16a] Arnold Janssens. “Report of subtask 1a: Inventory of full scale facilities for evaluation of building energy performance”. In: *IEA EBC Annex 58 - Reliable building energy performance characterisation based on full scale dynamic measurements*. 2016 (cited on pages 7, 91, 102).
- [Jan16b] Arnold Janssens. “Report of Subtask 1b: Overview of methods to analyse dynamic data”. In: *IEA EBC Annex 58 - Reliable building energy performance characterisation based on full scale dynamic measurements*. 2016 (cited on page 8).

- [JMA08] M. J. Jiménez, H. Madsen, and K. K. Andersen. “Identification of the main thermal characteristics of building components using MATLAB”. In: *Building and Environment*. Outdoor Testing, Analysis and Modelling of Building Components 43.2 (Feb. 2008), pages 170–180. DOI: 10.1016/j.buildenv.2006.10.030 (cited on page 40).
- [JPH08] M. J. Jiménez, B. Porcar, and M. R. Heras. “Estimation of building component UA and gA from outdoor tests in warm and moderate weather conditions”. In: *Solar Energy* 82.7 (July 2008), pages 573–587. DOI: 10.1016/j.solener.2008.02.013 (cited on page 25).
- [Jim16] Maria Jose Jiménez. “Reliable building energy performance characterisation based on full scale dynamic measurements. Report of subtask 3, part 1: Thermal performance characterization based on full scale testing - description of the common exercises and physical guidelines”. In: *International Energy Agency, EBC Annex 58*. 2016 (cited on pages 7, 105, 106, 110).
- [JK17] Jaewan Joe and Panagiota Karava. “Agent-based system identification for control-oriented building models”. In: *Journal of Building Performance Simulation* 10.2 (Mar. 2017), pages 183–204. DOI: 10.1080/19401493.2016.1212272 (cited on page 40).
- [Jos17] Rozenn Josse. “Méthode et outils pour l’identification de défauts des bâtiments connectés performants”. PhD thesis. Université Grenoble Alpes, 2017, page 253 (cited on page 61).
- [Jur+18] Sarah Juricic et al. “Evaluation of the physical interpretability of calibrated building model parameters”. In: *7th International Building Physics Conference*. Syracuse (NY), 2018, pages 1199–1204 (cited on page 47).
- [Jur+19] Sarah Juricic et al. “Identifiability of the heat transfer coefficient in buildings with unheated spaces”. In: *Proceedings of the 16th IBPSA Building Simulation Conference*. Rome, 2019 (cited on page 47).
- [KS07] Jari Kaipio and Erkki Somersalo. “Statistical inverse problems: Discretization, model reduction and inverse crimes”. In: *Journal of Computational and Applied Mathematics*. Special Issue: Applied Computational Inverse Problems 198.2 (Jan. 2007), pages 493–504. ISSN: 0377-0427. DOI: 10.1016/j.cam.2005.09.027. URL: <http://www.sciencedirect.com/science/article/pii/S0377042705007296> (visited on 05/12/2017) (cited on pages 44, 45).
- [Kan+15] Nikolas Kantas et al. “On Particle Methods for Parameter Estimation in State-Space Models”. EN. In: *Statistical Science* 30.3 (Aug. 2015), pages 328–351. DOI: 10.1214/14-STS511 (cited on pages 33, 105, 108).
- [KAJ12] Johan Karlsson, Milena Anguelova, and Mats Jirstrand. “An Efficient Method for Structural Identifiability Analysis of Large Dynamic Systems*”. en. In: *IFAC Proceedings Volumes*. 16th IFAC Symposium on System Identification 45.16 (July 2012), pages 941–946. DOI: 10.3182/20120711-3-BE-2027.00381 (cited on page 30).
- [KO01] Marc C. Kennedy and Anthony O’Hagan. “Bayesian calibration of computer models”. en. In: *Journal of the Royal Statistical Society: Series B (Statistical Methodology)* 63.3 (Jan. 2001), pages 425–464. DOI: 10.1111/1467-9868.00294 (cited on pages 14, 91, 101).
- [Ker+20] M Kersken et al. “Whole building validation for simulation programs including synthetic users and heating systems: experimental design”. In: *Proceedings of the Nordic Symposium on Building physic*. Tallinn, 2020 (cited on page 102).

- [KW87] D. E. Kiel and D. J. Wilson. “Influence of natural infiltration on total building ventilation dominated by strong fan exhaust”. English. In: *ASHRAE Trans.; (United States)* 93:2 (June 1987). Institution: Dept. of Mechanical Engineering, Univ. of Alberta, Edmonton, Alberta T6G 2G8 (CA) Number: CONF-870620- (cited on page 114).
- [KSS13] Rick Kramer, Jos van Schijndel, and Henk Schellen. “Inverse modeling of simplified hygrothermal building models to predict and characterize indoor climates”. In: *Building and Environment* 68 (2013), pages 87–99. DOI: 10.1016/j.buildenv.2013.06.001 (cited on page 39).
- [Kre19] Clemens Kreutz. “Guidelines for benchmarking of optimization approaches for fitting mathematical models”. In: *arXiv preprint* (July 2019), pages 1–13 (cited on page 44).
- [KCP17] Martin Heine Kristensen, Ruchi Choudhary, and Steffen Petersen. “Bayesian calibration of building energy models: Comparison of predictive accuracy using metered utility data of different temporal resolution”. In: *Energy Procedia*. CISBAT 2017 International Conference Future Buildings & Districts – Energy Efficiency from Nano to Urban Scale 122 (Sept. 2017), pages 277–282. DOI: 10.1016/j.egypro.2017.07.322 (cited on page 15).
- [KMJ04] Niels Rode Kristensen, Henrik Madsen, and Sten Bay Jørgensen. “Parameter estimation in stochastic grey-box models”. In: *Automatica* 40.2 (Feb. 2004), pages 225–237. DOI: 10.1016/j.automatica.2003.10.001 (cited on pages 25, 27, 91).
- [KK96] Hartwig M. Künzel and Kurt Kiessl. “Calculation of heat and moisture transfer in exposed building components”. In: *International Journal of Heat and Mass Transfer* 40.1 (Oct. 1996), pages 159–167. DOI: 10.1016/S0017-9310(96)00084-1 (cited on page 17).
- [LHS19] Han Li, Tianzhen Hong, and Marina Sofos. “An Inverse Approach to Solving Zone Air Infiltration Rate and People Count using Indoor Environmental Sensor Data”. In: *Energy and Buildings* (June 2019). DOI: 10.1016/j.enbuild.2019.06.008 (cited on page 46).
- [LC98] Jun S. Liu and Rong Chen. “Sequential Monte Carlo Methods for Dynamic Systems”. In: *Journal of the American Statistical Association* 93.443 (Sept. 1998), pages 1032–1044. DOI: 10.1080/01621459.1998.10473765 (cited on page 105).
- [Lju98] Lennart Ljung. *System Identification: Theory for the User, 2nd Edition*. 2nd. Prentice Hall., Dec. 1998 (cited on pages 37, 40).
- [Mac+18] Marcel Macarulla et al. “Estimation of a room ventilation air change rate using a stochastic grey-box modelling approach”. en. In: *Measurement* 124 (Aug. 2018), pages 539–548. DOI: 10.1016/j.measurement.2018.04.029 (cited on page 118).
- [MH95] H. Madsen and J. Holst. “Estimation of continuous-time models for the heat dynamics of a building”. In: *Energy and Buildings* 22.1 (Mar. 1995), pages 67–79. DOI: 10.1016/0378-7788(94)00904-X (cited on pages 25–27, 91, 107).
- [Mad07] Henrik Madsen. *Time Series Analysis*. en. CRC Press, Nov. 2007 (cited on pages 37, 39).
- [Mad16] Henrik Madsen. “Report of subtask 3b: Thermal performance characterisation using time series data - statistical guidelines”. In: *IEA EBC Annex 58 - Reliable building energy performance characterisation based on full scale dynamic measurements*. 2016 (cited on pages 8, 36, 38).

- [MJP11a] Denis Maillet, Yvon Jarny, and Daniel Petit. “Problèmes inverses en diffusion thermique - Formulation et résolution du problème des moindres carrés”. In: *Techniques de l'ingénieur Transferts thermiques* (2011), be8266 (cited on page 24).
- [MJP11b] Denis Maillet, Yvon Jarny, and Daniel Petit. “Problèmes inverses en diffusion thermique - Outils spécifiques de conduction inverse et de régularisation”. In: *Techniques de l'ingénieur Transferts thermiques* (2011), be8267 (cited on pages 22, 91).
- [MPR12] Eric Mangematin, Guillaume Pandraud, and Didier Roux. “Quick measurements of energy efficiency of buildings”. In: *Comptes Rendus Physique*. Science of nuclear safety post-Fukushima 13.4 (May 2012), pages 383–390. DOI: 10.1016/j.crhy.2012.04.001 (cited on pages 10, 93).
- [MS18] Francesco Massa Gray and Michael Schmidt. “A hybrid approach to thermal building modelling using a combination of Gaussian processes and grey-box models”. In: *Energy and Buildings* 165 (2018), pages 56–63 (cited on page 15).
- [ME95] William Q. Meeker and Luis A. Escobar. “Teaching about Approximate Confidence Regions Based on Maximum Likelihood Estimation”. In: *The American Statistician* 49.1 (Feb. 1995), pages 48–53. DOI: 10.2307/2684811 (cited on page 38).
- [Meu+17] Johann Meulemans et al. “QUB/e: A Novel Transient Experimental Method for in situ Measurements of the Thermal Performance of Building Fabrics”. In: *Building Information Modelling, Building Performance, Design and Smart Construction*. Edited by Mohammad Dastbaz, Chris Gorse, and Alice Moncaster. Cham: Springer International Publishing, 2017, pages 115–127. DOI: 10.1007/978-3-319-50346-2_9 (cited on page 11).
- [Mur13] Lawrence M. Murray. “Bayesian State-Space Modelling on High-Performance Hardware Using LibBi”. In: *arXiv:1306.3277 [stat]* (June 2013). arXiv: 1306.3277 (cited on pages 35, 108).
- [NRE16] NREL. *Energy Plus - Testing and Validation reports on https://energyplus.net/testing*. 2016 (cited on page 46).
- [Old+12] Frauke Oldewurtel et al. “Use of model predictive control and weather forecasts for energy efficient building climate control”. In: *Energy and Buildings* 45 (Feb. 2012), pages 15–27. DOI: 10.1016/j.enbuild.2011.09.022 (cited on page 17).
- [Orm99] Malcolm Orme. *Applicable models for air infiltration and ventilation calculations*. Technical report. Coventry: Air Infiltration and Ventilation Centre, 1999 (cited on page 114).
- [PG03] Elena Palomo Del Barrio and Gilles Guyon. “Theoretical basis for empirical model validation using parameters space analysis tools”. In: *Energy and Buildings* 35.10 (Nov. 2003), pages 985–996. DOI: 10.1016/S0378-7788(03)00038-0 (cited on pages 38, 39).
- [PMM91] Elena Palomo Del Barrio, J. Marco, and Henrik Madsen. “Methods to compare measurements and simulations”. In: *Proceedings of the conference on Building Simulation IBPSA*. Nice, France, 1991 (cited on page 39).
- [Per+14] Giovanni Pernigotto et al. “Analysis and improvement of the representativeness of EN ISO 15927-4 reference years for building energy simulation”. In: *Journal of Building Performance Simulation* 7.6 (2014), pages 391–410. DOI: 10.1080/19401493.2013.853840 (cited on page 51).

- [PGT18] Zorana Petojević, Radovan Gospavić, and Goran Todorović. “Estimation of thermal impulse response of a multi-layer building wall through in-situ experimental measurements in a dynamic regime with applications”. In: *Applied Energy* 228.June (2018), pages 468–486. DOI: 10.1016/j.apenergy.2018.06.083 (cited on page 49).
- [PAD03] Maria Pia Saccomani, Stefania Audoly, and Leontina D’Angiò. “Parameter identifiability of nonlinear systems: the role of initial conditions”. In: *Automatica* 39.4 (Apr. 2003), pages 619–632. DOI: 10.1016/S0005-1098(02)00302-3 (cited on page 30).
- [Poh78] H. Pohjanpalo. “System identifiability based on the power series expansion of the solution”. In: *Mathematical Biosciences* 41.1 (Sept. 1978), pages 21–33. DOI: 10.1016/0025-5564(78)90063-9 (cited on page 30).
- [RR92] A. Rabl and A. Rialhe. “Energy signature models for commercial buildings: test with measured data and interpretation”. In: *Energy and Buildings* 19.2 (1992), pages 143–154. DOI: 10.1016/0378-7788(92)90008-5 (cited on pages 13, 17).
- [Rad12] Neal Radford. “MCMC using Hamiltonian dynamics”. en. In: *arXiv:1206.1901 [physics, stat]* (June 2012). arXiv: 1206.1901 (cited on page 36).
- [RG18] L. Raillon and C. Ghiaus. “An efficient Bayesian experimental calibration of dynamic thermal models”. In: *Energy* 152 (June 2018), pages 818–833. DOI: 10.1016/j.energy.2018.03.168 (cited on page 33).
- [RG17] Loïc Raillon and Christian Ghiaus. “Sequential Monte Carlo for states and parameters estimation in dynamic thermal models”. In: San Francisco, USA, 2017 (cited on page 105).
- [RR19] Loïc Raillon and Simon Rouchier. “pySIP: an open-source tool for Bayesian inference and prediction of heat transfer in buildings”. In: Nantes, 2019 (cited on page 32).
- [Ras04] Carl Edward Rasmussen. *Gaussian Processes in Machine Learning*. en. Edited by Olivier Bousquet, Ulrike von Luxburg, and Gunnar Rätsch. Lecture Notes in Computer Science. Berlin, Heidelberg: Springer Berlin Heidelberg, 2004. DOI: 10.1007/978-3-540-28650-9_4 (cited on pages 14, 28, 101).
- [RI18] Arash Rasooli and Laure Itard. “In-situ characterization of walls’ thermal resistance: An extension to the ISO 9869 standard method”. In: *Energy and Buildings* 179 (Nov. 2018), pages 374–383. DOI: 10.1016/j.enbuild.2018.09.004 (cited on page 49).
- [Rau+09] A. Raue et al. “Structural and practical identifiability analysis of partially observed dynamical models by exploiting the profile likelihood”. en. In: *Bioinformatics* 25.15 (Jan. 2009), pages 1923–1929. DOI: 10.1093/bioinformatics/btp358 (cited on pages 38, 39).
- [Rau+14] Andreas Raue et al. “Comparison of approaches for parameter identifiability analysis of biological systems”. In: *Bioinformatics* 30.10 (May 2014), pages 1440–1448. DOI: 10.1093/bioinformatics/btu006 (cited on page 30).
- [RDC99] T. A. Reddy, S. Deng, and D. E. Claridge. “Development of an Inverse Method to Estimate Overall Building and Ventilation Parameters of Large Commercial Buildings”. In: *Journal of Solar Energy Engineering* 121.1 (Feb. 1999), pages 40–46. DOI: 10.1115/1.2888141 (cited on page 50).
- [RDS14] G. Reynders, J. Diriken, and D. Saelens. “Quality of grey-box models and identified parameters as function of the accuracy of input and observation signals”. In: *Energy and Buildings* 82 (Oct. 2014), pages 263–274. DOI: 10.1016/j.enbuild.2014.07.025 (cited on page 40).

- [RGM19] Auline Rodler, Sihem Guernouti, and Marjorie Musy. “Bayesian inference method for in situ thermal conductivity and heat capacity identification: Comparison to ISO standard”. In: *Construction and Building Materials* 196 (Jan. 2019), pages 574–593. DOI: 10.1016/j.conbuildmat.2018.11.110 (cited on page 50).
- [Rou18] Simon Rouchier. “Solving inverse problems in building physics: an overview of guidelines for a careful and optimal use of data”. In: *Energy and Buildings* 166 (2018), pages 178–195. DOI: 10.1016/j.enbuild.2018.02.009 (cited on pages 17, 24, 26, 27, 30, 36, 123).
- [RJC19] Simon Rouchier, Maria José Jiménez, and Sergio Castaño. “Sequential Monte Carlo for on-line parameter estimation of a lumped building energy model”. In: *Energy and Buildings* 187 (Mar. 2019), pages 86–94. DOI: 10.1016/j.enbuild.2019.01.045 (cited on pages 104, 110).
- [RRO18] Simon Rouchier, Mickaël Rabouille, and Pierre Oberlé. “Calibration of simplified building energy models for parameter estimation and forecasting: Stochastic versus deterministic modelling”. In: *Building and Environment* 134 (Apr. 2018), pages 181–190. DOI: 10.1016/j.buildenv.2018.02.043 (cited on pages 25, 26, 33, 91, 107, 119).
- [Rou+15] Simon Rouchier et al. “Identification of the hygrothermal properties of a building envelope material by the covariance matrix adaptation evolution strategy”. In: *Journal of Building Performance Simulation* 9.0 (2015), pages 101–114. DOI: 10.1080/19401493.2014.996608 (cited on page 17).
- [Rou+17] Simon Rouchier et al. “Hygric characterization of wood fiber insulation under uncertainty with dynamic measurements and Markov Chain Monte-Carlo algorithm”. In: *Building and Environment* 114 (Mar. 2017), pages 129–139. DOI: 10.1016/j.buildenv.2016.12.012 (cited on page 17).
- [SAL18] S. Sarkka, M. A. Alvarez, and N. D. Lawrence. “Gaussian Process Latent Force Models for Learning and Stochastic Control of Physical Systems”. In: *IEEE Transactions on Automatic Control* (2018), pages 1–1. DOI: 10.1109/TAC.2018.2874749 (cited on pages 14, 28, 101, 126).
- [SB14] P Schetelat and R Bouchié. “ISABELE: a Method for Performance Assessment at Acceptance Stage using Bayesian Calibration”. In: *9th international conference on system simulation in buildings*. 2014 (cited on page 11).
- [Sed01] Alexandre Sedoglavic. “A Probabilistic Algorithm to Test Local Algebraic Observability in Polynomial Time”. In: *Proceedings of the 2001 International Symposium on Symbolic and Algebraic Computation*. ISSAC ’01. New York, NY, USA: ACM, 2001, pages 309–317. DOI: 10.1145/384101.384143 (cited on page 30).
- [Sen+19] Marieline Senave et al. “Towards the Characterization of the Heat Loss Coefficient via On-Board Monitoring: Physical Interpretation of ARX Model Coefficients”. In: *Energy and Buildings* (May 2019). DOI: 10.1016/j.enbuild.2019.05.001 (cited on page 50).
- [Sen+20] Marieline Senave et al. “Assessment of data analysis methods to identify the heat loss coefficient from on-board monitoring data”. en. In: *Energy and Buildings* 209 (Feb. 2020), page 109706. ISSN: 0378-7788. DOI: 10.1016/j.enbuild.2019.109706. URL: <http://www.sciencedirect.com/science/article/pii/S0378778819319747> (visited on 04/23/2020) (cited on pages 43, 46).

- [SG80] M. H. Sherman and D. T. Grimsrud. “Measurement of infiltration using fan pressurization and weather data”. In: *NASA STI/Recon Technical Report N 81* (Oct. 1980) (cited on page 114).
- [SS16a] Robert Shumway and David Stoffer. *Time series analysis and its applications*. Springer, 2016 (cited on pages 27, 91).
- [SAO09] J. -U. Sjögren, S. Andersson, and T. Olofsson. “Sensitivity of the total heat loss coefficient determined by the energy signature approach to different time periods and gained energy”. In: *Energy and Buildings* 41.7 (July 2009), pages 801–808. DOI: 10.1016/j.enbuild.2009.03.001 (cited on page 13).
- [SS16b] Behzad Sodagar and Diane Starkey. “The monitored performance of four social houses certified to the Code for Sustainable Homes Level 5”. en. In: *Energy and Buildings* 110 (Jan. 2016), pages 245–256. DOI: 10.1016/j.enbuild.2015.11.016 (cited on page 116).
- [Sol16] Arno Solin. *Stochastic Differential Equation Methods for Spatio-Temporal Gaussian Process Regression*. en. Aalto University, 2016 (cited on pages 14, 28, 101).
- [Sou+17] Vasileos Sougkakis et al. “An assessment of the QUB method for predicting the whole building thermal performance under actual operating conditions”. In: *International SEEDS Conference 2017: Sustainable Ecological Engineering Design for Society*. Leeds, United Kingdom: Leeds Beckett University, Sept. 2017 (cited on page 11).
- [Str93] Paul Strachan. “Model Validation using the PASSYS Test Cells”. In: *Building and Environment* 28.2 (1993), pages 53–165 (cited on page 61).
- [Sub+88] K. Subbarao et al. *Short-Term Energy Monitoring (STEM): Application of the PSTAR method to a residence in Fredericksburg, Virginia*. English. Technical report SERI/TR-254-3356. Solar Energy Research Inst., Golden, CO (USA), Sept. 1988. DOI: 10.2172/6734885 (cited on pages 7, 9).
- [Tar05] Albert Tarantola. *Inverse Problem Theory and Methods for Model Parameter Estimation*. en. SIAM, 2005 (cited on page 32).
- [Tia+18] Wei Tian et al. “A review of uncertainty analysis in building energy assessment”. In: *Renewable and Sustainable Energy Reviews* 93.May (2018), pages 285–301. DOI: 10.1016/j.rser.2018.05.029 (cited on page 46).
- [WP97] Eric Walter and Luc Pronzato. “Identification of parametric models”. In: *Communications and Control Engineering* 8 (1997) (cited on pages 29, 32).
- [WM00] E. A. Wan and R. Van Der Merwe. “The unscented Kalman filter for nonlinear estimation”. In: *Proceedings of the IEEE 2000 Adaptive Systems for Signal Processing, Communications, and Control Symposium (Cat. No.00EX373)*. 2000, pages 153–158. DOI: 10.1109/ASSPCC.2000.882463 (cited on page 27).
- [Wol+19] Sebastian Wolf et al. “Carbon dioxide-based occupancy estimation using stochastic differential equations”. In: *Applied Energy* 236 (Feb. 2019), pages 32–41. DOI: 10.1016/j.apenergy.2018.11.078 (cited on page 118).
- [Zha+15] Yuna Zhang et al. “Comparisons of inverse modeling approaches for predicting building energy performance”. In: *Building and Environment* 86 (Apr. 2015), pages 177–190. DOI: 10.1016/j.buildenv.2014.12.023 (cited on page 17).